

# **Design and Evaluation of a Lower Limb Orthoprosthesis for Toddlers with Fibular Hemimelia Using Additive Manufacturing**

**Lilli Josephine Anders**

Thesis to obtain the Master of Science Degree in

**Biomedical Engineering**

Supervisors: Prof. Hugo Humberto Plácido da Silva  
Prof. Cláudia Regina Pereira Quaresma

**Examination Committee**

Chairperson: Prof. Rita Homem de Gouveia Costanzo Nunes  
Supervisor: Prof. Hugo Humberto Plácido da Silva  
Member of the Committee: Prof. Bruno Alexandre Rodrigues Simoes Soares

**July 2025**



# Preface

This work was conducted at Instituto de Telecomunicações (IT) (Lisbon, Portugal) and at the Departamento de Biomedica of Instituto Superior Técnico (IST) (Lisbon, Portugal), in collaboration with Nova School of Science and Technology (NOVA-FCT), the 3D Printing Center for Health and Hospital Dona Estefânia (Lisbon, Portugal), under the supervision of Professors Hugo Plácido da Silva of IT and IST, and the co-supervision of Professor Cláudia Quaresma of NOVA-FCT and REAL. It was partially funded by FCT/MECI through national funds and, when applicable, co-funded EU funds under project UID/50008: Instituto de Telecomunicações. This work was also funded by Fundação para a Ciência e Tecnologia (FCT, Portugal) through national funds UI/BD/151321/2021 (LIBPhys-UNL) and LA/P/0117/2020.

# Declaration

I declare that this document is an original work of my own authorship and that it fulfills all the requirements of the Code of Conduct and Good Practices of the Universidade de Lisboa.



# Acknowledgments

Seeing Bryan clapping, dancing, and taking his very first steps will forever remain an unforgettable moment — a reminder that every long night, every frustration, every doubt, and every up and down was completely worth it.

Reaching the goal of this master's thesis would not have been possible without the incredible support I received along the way. The biggest thanks:

To my supervisors, Professor Cláudia and Professor Hugo, for believing in me since the beginning to face this challenge. For the good relationship and all the encouraging words.

To Mr. Bruno, for the hands-on support in the mechanical lab.

To Paula, for the kindness and the medical expertise.

To the parents of Bryan, for the trust and patients.

And to Bryan, for always smiling.

To my boyfriend Ben for the endless support and love.

To my special friend Matte, for many brainstorming session & for always motivating me to keep pushing.

To Ricci, for the help, whenever I got stuck with the software.

To Bia, Liina & Bernie, for all the good days in uni, the biggest laughs and the project we smashed together.

To all my surf friends, for every wave we surfed together, the surf trips, and for cooling my head in between working.

To my grandma, for the weekly phone calls and the endless curiosity.

To my parents, for making it possible for me to study in Lisbon and for always supporting me in every way possible.

Throughout this project, I not only learned a lot, but also found clarity about the academic path I want to pursue. I could not have asked for better two years here in Lisbon. Thank you!



# Abstract

This thesis presents the design, fabrication, and clinical evaluation of a modular, low-cost 3D-printed orthoprostheses tailored for a toddler aged 1–2 years with fibular hemimelia. Current commercial and research-based solutions for pediatric lower-limb prosthetics rarely address the unique anatomical and developmental needs of toddlers, particularly in cases requiring integrated orthotic and prosthetic support. To fill this gap, a novel device was developed using additive manufacturing an iterative design process, informed by direct clinical feedback and real-world testing.

Three materials, including PLA, PETG-CF, and TPU, were selected based on recent literature due to their printability, mechanical performance, and safety. A total of five prototypes were produced using FDM printing, gradually optimizing shell geometry, joint design, and strapping for improved stability, wearability, and alignment. The final device was evaluated in a clinical setting using both observational assessments and sensor-based analysis, including EMG, FSR, and force plate data. Functional evaluations demonstrated significant improvements, including correction of a 4.5 cm leg length discrepancy, reduction of pelvic tilt from 15° to 0°, and initiation of unassisted gait with controlled knee flexion up to 45°.

This study demonstrates that affordable, patient-specific orthoprosthetic devices can be rapidly developed using 3D printing and clinically validated in real use. The findings lay the foundation for future scalable designs adaptable to broader pediatric populations with congenital limb differences.

# Keywords

Fibular Hemimelia, Gait analysis, Orthoprostheses, Additive manufacturing, User-centered design, Signal processing



# Contents

<b>1</b>	<b>Introduction</b>	<b>1</b>
1.1	Problem Statement . . . . .	2
1.2	Motivation . . . . .	3
1.3	Objectives . . . . .	3
1.4	Document Structure . . . . .	4
<b>2</b>	<b>Theoretical Background</b>	<b>5</b>
2.1	Anatomy of Lower Limb in Early Childhood . . . . .	6
2.2	Biomechanics of Lower Limb in Early Childhood . . . . .	8
2.3	Daily Leg-Based Activities in Toddlers . . . . .	12
2.4	Congenital Malfunction of Lower Limb . . . . .	13
2.4.1	Fibular Hemimelia . . . . .	13
2.4.2	Knee Flexion Contracture . . . . .	15
2.5	Additive Manufacturing . . . . .	15
2.5.1	Base Principles . . . . .	15
2.5.2	Materials for 3D-Printed Orthoses and Prostheses . . . . .	16
2.6	Sensor Technologies for Lower Limb Activity Monitoring . . . . .	18
2.6.1	Surface Electromyography (sEMG) Sensors . . . . .	18
2.6.2	Force Sensing Resistors (FSRs) . . . . .	19
<b>3</b>	<b>State of the Art</b>	<b>21</b>
3.1	Commercial Products . . . . .	22
3.1.1	Orthoses . . . . .	22
3.1.2	Prosthetic Feet . . . . .	23
3.2	3D-Printed Solutions for Pediatric Use . . . . .	24
<b>4</b>	<b>Proposed Approach</b>	<b>27</b>
4.1	Clinical Case Assessment . . . . .	28
4.2	Design Requirements . . . . .	29
4.3	Measurement Protocol . . . . .	30

4.4	Material and 3D-Printing Parameters Selection . . . . .	31
<b>5</b>	<b>Device Development</b>	<b>35</b>
5.1	Co-Creation Methodology and Workflow . . . . .	36
5.2	Prototypes Overview . . . . .	37
5.3	Initial Fitting . . . . .	37
5.4	Knee Joint Mechanism and Shell Geometry . . . . .	40
5.5	Functional Redesign of Knee Joint, Shells, and Foot . . . . .	42
5.6	Limb Length Adaptation and Final Material Selection . . . . .	44
5.7	Reinforced Structure and Enhanced Comfort Features . . . . .	50
5.8	Final Device . . . . .	52
5.9	Discussion . . . . .	53
<b>6</b>	<b>Experimental Evaluation</b>	<b>57</b>
6.1	Observational Findings . . . . .	58
6.1.1	Static Alignment and Pelvic Correction . . . . .	58
6.1.2	Early Unassisted Walking Behavior . . . . .	59
6.1.3	Controlled Gait Cycle on a Treadmill . . . . .	61
6.2	Data-Driven Validation . . . . .	62
6.2.1	Preliminary Work for Data Acquisition . . . . .	62
6.2.2	CoP Assessment with Force Plates . . . . .	64
6.2.3	EMG & FSR Analysis . . . . .	67
6.3	Discussion . . . . .	71
<b>7</b>	<b>Conclusion</b>	<b>73</b>
7.1	Summary . . . . .	74
7.2	Regulatory Outlook . . . . .	75
7.3	Future Work . . . . .	75
<b>Bibliography</b>		<b>76</b>
<b>A Preliminary Design Attempts</b>		<b>85</b>
<b>B Clinical Evaluation</b>		<b>89</b>

# List of Figures

1.1 Child with fibular hemimelia and knee flexion contracture.	2
1.2 WHO growth chart.	3
2.1 Schematic representation of the lower leg muscles.	7
2.2 Development of human foot in different ages.	8
2.3 Toddlers gait patterns	9
2.4 CoM and CoP displacement patterns in early walking.	10
2.5 Joint kinematics of hip, knee, ankle, and pelvis during gait.	11
2.6 Toddlers vs. older children joint motion	11
2.7 The Paley Classification system for Fibular Hemimelia (FH)	14
2.8 EMG setup and electrodes	18
2.9 FSR structure and response	20
3.1 Commercial Orthoses.	23
3.2 Foot Prosthesis.	23
4.1 Clinical condition and provisional devices.	28
4.2 Early mobility challenges.	29
4.3 Anthropometric measurement protocol used to guide the orthoprosthetic design.	31
4.4 Additional orthoprosthetic materials.	34
5.1 Co-creation methodology used for this study.	36
5.2 Digital design and fabrication workflow for the orthoprosthetic device.	37
5.3 Overview of all Prototypes.	37
5.4 Foot measurements for shell design.	38
5.5 Components of first prototype.	39
5.6 First assembled prototype printed.	39
5.7 Device fitting and early use.	40

5.8	Mechanical failure points on the first prototype. . . . .	41
5.9	Knee joint flexion mechanics. . . . .	42
5.10	Second prototype model and print. . . . .	43
5.11	Mechanical failure of second prototype. . . . .	43
5.12	Third prototype model and print. . . . .	44
5.13	Third prototype evaluation. . . . .	44
5.14	Fourth prototype height adapter designs. . . . .	45
5.15	FEA analysis with vertical static loading and inclined 45° load. . . . .	47
5.16	Fourth prototype: clinical testing results. . . . .	49
5.17	PETG-CF prototype mechanical failure. . . . .	50
5.18	Fifth prototype model and print. . . . .	51
5.19	Fifth prototype evaluation. . . . .	51
5.20	Final device model and print. . . . .	52
5.21	Final design hospital testing. . . . .	53
6.1	Postural alignment with and without orthoprostheses. . . . .	58
6.2	Early unassisted walking with orthoprostheses. . . . .	59
6.3	Fall due to missing sensory feedback. . . . .	60
6.4	Recovery using prosthetic knee. . . . .	61
6.5	Healthy vs. orthoprosthetic gait. . . . .	62
6.6	Sensor placement on TA and GC. . . . .	63
6.7	Sensor setup with EMG and FSR. . . . .	64
6.8	Plantar pressure assessment with force platform. . . . .	64
6.9	Ground reaction force during early standing. . . . .	65
6.10	CoP trajectory during standing. . . . .	66
6.11	Gait Comparison across three gait cycles. . . . .	67
6.12	Gait phases of both legs. . . . .	68
6.13	Normalized EMG – left leg. . . . .	70
6.14	Normalized EMG – right leg. . . . .	70
A.1	Preliminary ideas. . . . .	85
A.2	Preliminary shell design. . . . .	86
A.3	Preliminary knee design. . . . .	86
A.4	Preliminary foot design. . . . .	86
B.1	Sensor placement on subject's own legs . . . . .	90
B.2	Preliminary analysis of EMG and FSR. . . . .	90

B.3	Four cycles of the Gastrocnemius (GC) left leg.	91
B.4	Four cycles of the GC right leg.	91
B.5	Four cycles of the Tibialis Anterior (TA) left leg.	92
B.6	Four cycles of the TA right leg.	92

**x**

# List of Tables

2.1 Comparison of knee flexion ranges in toddler activities . . . . .	12
2.2 3D-printing parameters and properties . . . . .	17
3.1 Comparison of existing pediatric solutions. . . . .	24
4.1 Key functional requirements and associated KPIs. . . . .	30
4.2 Mechanical properties of 3D-printed materials used in FEA simulation. . . . .	32
4.3 3D-printing parameters used for orthotic device fabrication. . . . .	32
5.1 Final device material use and cost . . . . .	53
5.2 Functional requirements and KPI fulfillment . . . . .	54
A.1 Key parameters across prototypes. . . . .	87



# Acronyms

<b>ABS</b>	Acrylonitrile Butadiene Styrene
<b>ACL</b>	Anterior Cruciate Ligament
<b>AFO</b>	Ankle-Foot Orthoses
<b>ASTM</b>	American Society for Testing and Materials
<b>AM</b>	Additive Manufacturing
<b>CAD</b>	Computer-Aided Design
<b>CF</b>	Carbon Fiber
<b>CLRD</b>	Congenital Limb Reduction Defects
<b>CoM</b>	Center of Mass
<b>CoP</b>	Center of Pressure
<b>CT</b>	Computerized Tomography
<b>DED</b>	Directed Energy Deposition
<b>EMG</b>	Electromyography
<b>FDM</b>	Fused Deposition Modeling
<b>FEA</b>	Finite Element Analysis
<b>FH</b>	Fibular Hemimelia
<b>FSR</b>	Force-Sensitive Resistor
<b>GC</b>	Gastrocnemius
<b>GRF</b>	Ground Reaction Force
<b>KAFO</b>	Knee-Ankle-Foot Orthoses
<b>KFC</b>	Knee Flexion Contracture
<b>KPI</b>	Key Performance Indicator

<b>LOM</b>	Laminated Object Manufacturing
<b>MJF</b>	Multi Jet Fusion
<b>MRI</b>	Magnetic Resonance Imaging
<b>MVC</b>	Maximum Voluntary Contraction
<b>PETG</b>	Polyethylene Terephthalate Glycol
<b>PETG-CF</b>	Carbon Fiber Reinforced PETG
<b>PLA</b>	Polylactic Acid
<b>PLA-CF</b>	Carbon Fiber Reinforced PLA
<b>RMS</b>	Root Mean Square
<b>SACH</b>	Solid Ankle Cushion Heel
<b>SLA</b>	Stereolithography
<b>SLS</b>	Selective Laser Sintering
<b>STL</b>	Standard Tessellation Language
<b>TA</b>	Tibialis Anterior
<b>TPU</b>	Thermoplastic Polyurethane
<b>Velcro</b>	Velvet Crochet Hook-and-Loop Fastener

# 1

## Introduction

### Contents

---

1.1	Problem Statement . . . . .	2
1.2	Motivation . . . . .	3
1.3	Objectives . . . . .	3
1.4	Document Structure . . . . .	4

---

This chapter outlines the problem (Sec.1.1), motivation (Sec.1.2), and objectives (Sec.1.3) of the thesis. It outlines the lack of suitable orthotic solutions for toddlers with congenital lower limb deficiencies and sets the base for a personalized, 3D-printed orthoprosthetic to support early walking development. Lastly, section 1.4 provides an outline of the document.

## 1.1 Problem Statement

Most children start to walk between 18 and 24 months of age. This is a big step in their motor development, autonomy, and social interaction [1, 2]. For toddlers with congenital lower limb deficiencies, such as Fibular Hemimelia (FH), tibial hemimelia, or congenital femoral deficiency, this milestone is often delayed or disrupted. Although individually rare, these conditions collectively impact a significant number of children globally. The occurrence of Congenital Limb Reduction Defects (CLRD) is about 4.48 for every 10,000 live births; and in the U.S., these congenital issues make up around 84% of major lower limb loss in children [3, 4]. Early intervention is very important for encouraging neuromuscular development and preventing long-term damage [5].

However, most orthotic and prosthetic devices are designed for older children or adults and do not address the unique biomechanical, ergonomic, and developmental needs of toddlers [4, 6]. These solutions are often unevolutive, heavy, and uncomfortable for toddlers. Furthermore, they offer limited adjustability and are poorly suited to the rapid physical changes that occur during early childhood, placing both functional and financial strain on families [7, 8].

Additive Manufacturing (AM) has emerged as a viable alternative, however only few devices exist for this age group. For lower limb impairments, AM has not yet reached its full potential in improving mobility for young children.



**Figure 1.1:** Child diagnosed with fibular hemimelia and knee flexion contracture.

## 1.2 Motivation

The motivation for this project stems from the need to support walking in a child with FH, using an approach prone to contribute to allow other children with congenital lower limb deficiency in learning to walk at the right stage of their development. As outlined in the problem statement, early mobility is essential not only for physical growth but also for social, emotional, and cognitive development [9]. This work is motivated by the fact that personalized orthoprosthetic solutions can make a critical difference during early childhood. Children facing structural challenges should not be overlooked simply because their needs fall outside conventional commercial focus. There is also a strong motivation to explore the potential of AM for lower limb devices. To date, most research has focused on upper limb applications, largely because lower limb devices must withstand significantly higher loads, posing greater challenges for AM and 3D-printed materials. AM provides a flexible, cost-effective approach to addressing the anatomical needs of pediatric patients; using these technologies for young, underserved children can promote more inclusive and flexible pediatric care.

## 1.3 Objectives

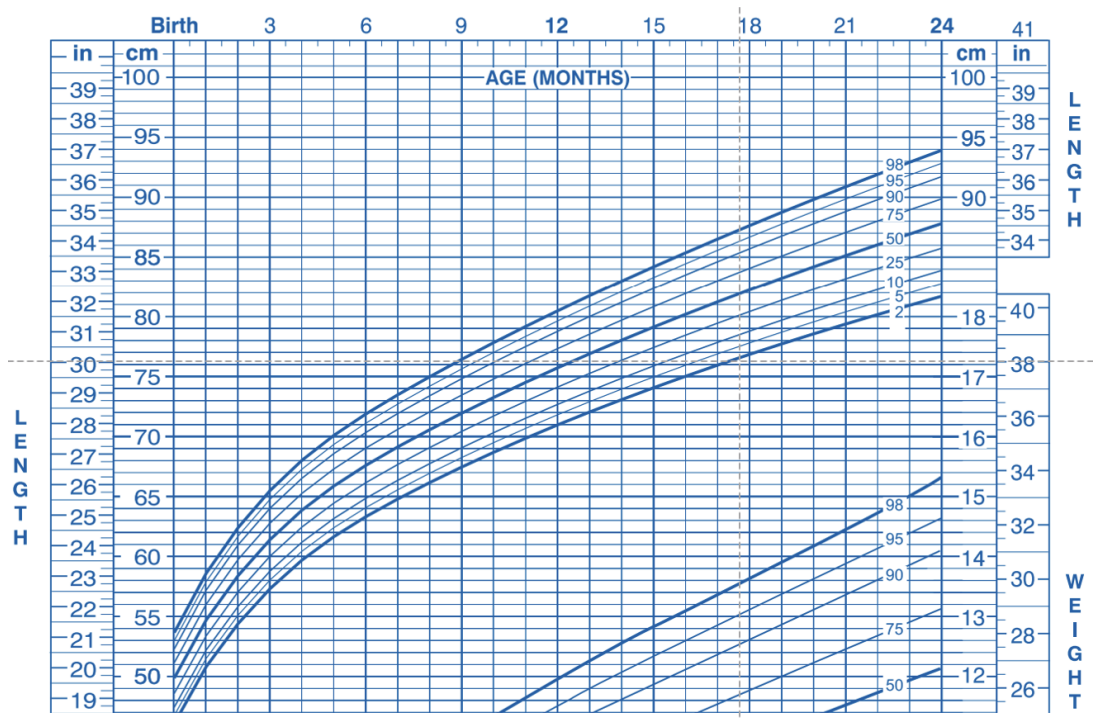


**Figure 1.2:** WHO growth chart<sup>1</sup> for boys aged 0–24 months, showing standard growth percentiles for monitoring early childhood development.

The primary goal of this thesis is to enable independent walking in a toddler with FH, through the development of a personalized 3D-printed orthoprosthetic. This work takes a step toward closing a critical research gap, where current commercial orthotic solutions, as well as AM approaches, fall short in addressing very young children, characterized by their rapid growth (Fig.1.2). This goal is achieved by answering, the project seeks to answer three key research questions (RQ's):

**RQ 1:** Can a low-cost, 3D-printed orthoprosthetic be effectively tailored to the anatomical and developmental needs of toddlers with FH?

**RQ 2:** What are the material and design considerations for ensuring durability and functionality of a 3D-printed pediatric lower limb orthoprostheses under real-world conditions?

**RQ 3:** Can a modular, 3D-printed orthoprosthetic improve stability and gait symmetry in toddlers with fibular hemimelia, while ensuring comfort and user satisfaction?

By answering these questions, the thesis aims to evaluate that a custom, 3D-printed orthoprosthetic can successfully support a toddler in achieving independent gait, paving the way for broader use in early pediatric rehabilitation.

## 1.4 Document Structure

This master thesis is organized into six chapters. The current chapter provided an introduction to the problem and motivation. Chapter 2 provides an overview of the anatomy and biomechanics of the lower limb, with particular attention to congenital conditions such as FH and Knee Flexion Contracture (KFC). Chapter 3 presents a state-of-the-art analysis, including market research on commercial products, a review of 3D-printed solutions, and the used materials in this context. Chapter 4 outlines the proposed approach and case study, detailing the design requirements, the co-creation methodology, and the materials used. Chapter 5 documents the prototype development process, showing the initial to the final design. Chapter 6 presents the clinical testing and results, including assessments of static alignment, pelvic tilt correction, assisted and unassisted walking, as well as data collection and analysis using Electromyography (EMG), Force-Sensitive Resistor (FSR), and a force plate system. Finally, Chapter 7 summarizes the main conclusions and outlines directions for future work.

---

<sup>1</sup><https://www.who.int/tools/child-growth-standards/standards/weight-for-age>

# 2

## Theoretical Background

### Contents

---

2.1 Anatomy of Lower Limb in Early Childhood . . . . .	6
2.2 Biomechanics of Lower Limb in Early Childhood . . . . .	8
2.3 Daily Leg-Based Activities in Toddlers . . . . .	12
2.4 Congenital Malfunction of Lower Limb . . . . .	13
2.5 Additive Manufacturing . . . . .	15
2.6 Sensor Technologies for Lower Limb Activity Monitoring . . . . .	18

---

This chapter provides the theoretical background necessary for developing a 3D-printed orthoprosthetic for toddlers with lower limb deficiencies. It covers the anatomy (Sec.2.1) and biomechanics of the developing leg (Sec.2.2), daily movement needs (Sec.2.3), relevant congenital conditions (Sec.2.4), additive manufacturing techniques and suitable printing materials (Sec.2.5), and sensor technologies (Sec.2.6) used for evaluating mobility and muscle function.

## 2.1 Anatomy of Lower Limb in Early Childhood

In early childhood, a child's leg goes through considerable changes in its bones, muscles, and connective tissues. These changes enable the leg to support weight, facilitate movement, and adapt to the increasing demands of mobility.

The thighbone, or femur, is the longest and strongest bone in the body and it supports the upper leg structurally [10]. During childhood, the femur grows at its epiphyseal plates, which are areas of cartilage near the ends of the bone, where new bone cells are produced. These growth areas are still soft and flexible compared to the rest of the bone, allowing for elongation while reducing the risk of fractures [10, 11]. The muscles in the thigh, particularly the quadriceps femoris, develop significantly; this group of muscles, located at the front of the thigh, is responsible for straightening the knee and stabilizing the leg. The vastus lateralis, one of the quadriceps muscles, is very important for giving the child strength and stability when they start to do weight-bearing tasks like standing and walking [10, 12].

The knee, a hinge joint, connects the femur to the tibia and facilitating bending and straightening of the leg. At young ages, the patella, or kneecap, is primarily cartilaginous and begins to ossify as the child grows; this cartilage provides flexibility and protects the developing joint [13]. The ligaments around the knee, such as the Anterior Cruciate Ligament (ACL), are elastic and allow for a wide range of motion while maintaining stability. The surrounding muscles, including the hamstrings at the back of the thigh and the popliteus at the back of the knee, contribute to knee flexion and stabilization. Together, these structures support the developing joint as the child progresses in mobility [10, 11]. The lower leg consists of two long bones, the tibia and fibula, which support weight transfer from the knee to the foot. The tibia, being the larger and stronger of the two, bears most of the body's weight, while the fibula provides additional stability. Similarly to the femur, both bones grow at their epiphyseal plates, making the leg longer overall [10, 11].

The muscles in the lower leg develop asynchronously, meaning that different muscles grow and build strength at different rates to fit the child's needs [12]. This reflects the body's prioritization of certain movements, such as those required for standing, walking, and maintaining balance. Among the most important muscle groups in this region are the gastrocnemius and soleus, which together form the calf muscles (Fig. 2.1). These muscles grow rapidly during this stage, as they are essential for plantar

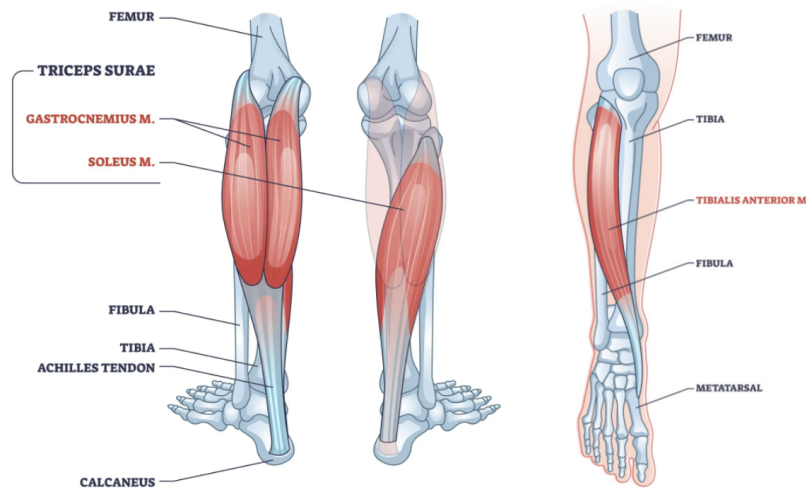


**Figure 2.1:** Schematic representation of the lower leg muscles.<sup>1</sup>

flexion, i.e., the movement of pointing the toes downward. This action is critical for enabling children to stand upright, push off the ground during walking, and maintain stability when transitioning between movements. The Gastrocnemius (GC), a two-joint muscle, also plays a role in knee flexion, further contributing to the child's ability to perform complex motions such as crouching or shifting weight from one foot to the other [11, 12].

In contrast, the Tibialis Anterior (TA), a muscle located at the front of the lower leg, grows more gradually (Fig. 2.1). This muscle is primarily responsible for dorsiflexion, i.e., the motion of lifting the foot upward, which is not used as much in the early stages of movement. At this age, dorsiflexion is mainly involved in activities like clearing the toes during the swing phase of walking or maintaining a stable foot position while standing. Since children at this stage are still developing their balance and walking, they don't need as much strength for dorsiflexion as they do for plantar flexion. This slower development of the TA reflects a change as their walking improves and they start trying more complex movements [11, 12].

The leg axis, which refers to the alignment of the femur and tibia, undergoes significant changes during early childhood as part of normal physiological growth. At birth and during the first year of life, children naturally exhibit genu varum, where the knees remain apart even when the feet are together. This alignment is due to the fetal position in the womb and the natural curvature of the bones [11]. The bowing in the legs starts to improve by the age of 1 to 2 years, as standing and walking put pressure on them, helping the legs straighten over time [11, 14]. Around 18–24 months, the alignment typically becomes neutral or straight. After 24 month, many children exhibit genu valgum (knock-knees), where

<sup>1</sup>Certified Foot, "Unveiling the mysteries of the muscles of the shin bone," <https://certifiedfoot.com/unveiling-mysteries-muscles-shin-bone/>, 2025, accessed: 2025-01-14.

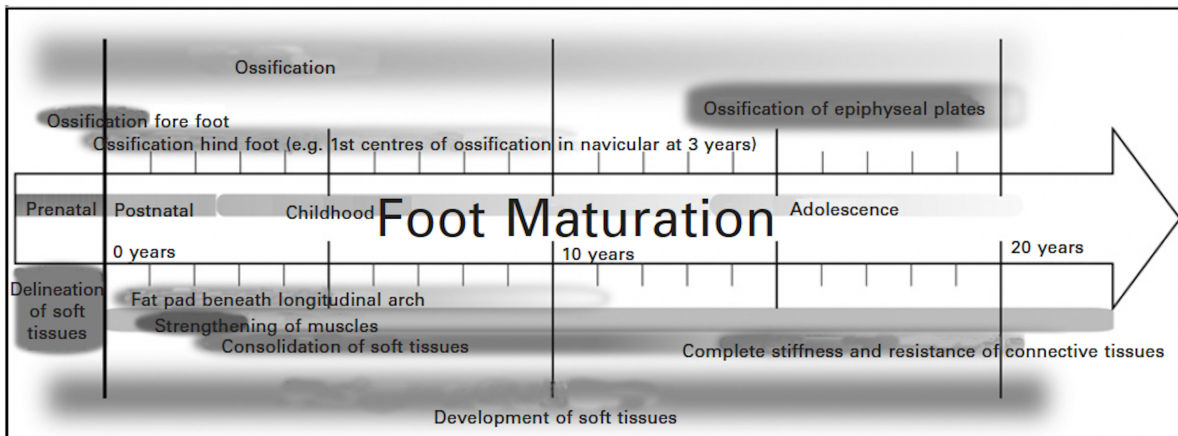


**Figure 2.2:** Development of human foot in different ages [15].

the knees angle slightly inward. This stage peaks around 3–4 years of age and transitions to the stable, straight alignment of older children by approximately 6 years [11, 14].

The foot, composed of 26 bones, numerous muscles, and connective tissues, adapts significantly during this period. At birth, many of the foot's bones are cartilaginous and ossify gradually. [15] Key bones, such as the navicular, begin to harden around 2–3 years of age, reflecting the progression of the foot's structural maturity [11, 14].

The foot often appears flat due to a fat pad beneath the arch and the immaturity of arch-supporting ligaments; flat feet are normal at this stage and improve as foot muscles like the flexor digitorum brevis get stronger (Fig. 2.2). These muscles, located within the foot, work alongside extrinsic muscles like the tibialis posterior, which controls foot movements and supports balance [12, 14]. The foot's flexibility allows it to adapt to uneven surfaces, while its broad shape provides a stable base for standing and walking, essential for supporting a child's weight and maintaining balance during this developmental period [12, 14]. Additionally, their forefoot is proportionally larger than in adults [15, 16].

## 2.2 Biomechanics of Lower Limb in Early Childhood

Toddlers undergo rapid development in the movement and function of their lower limbs. This period marks the transition from early, unsteady steps to more stable walking patterns as their musculoskeletal and neuromuscular systems mature. [17, 18].

The gait cycle in toddlers comprises two primary phases: the stance phase, when the foot is in contact with the ground; and the swing phase, when the foot moves forward to prepare for the next step. The stance phase occupies over 60% of the gait cycle in toddlers due to extended periods of double support, where both feet are simultaneously on the ground. This prolonged double support helps

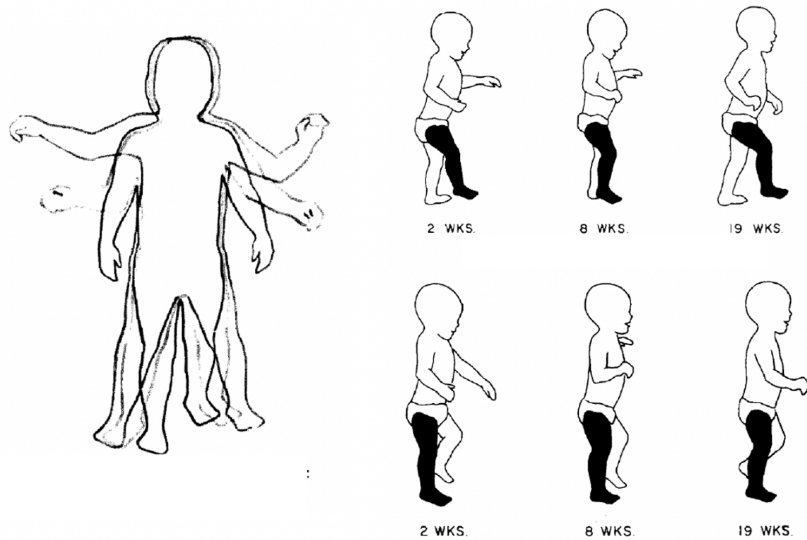


**Figure 2.3:** Toddlers gait patterns. Modified from [19].

the child to stabilize, but limits the speed and fluidity of movement [15]. As mentioned in the previous section, unlike adults, toddlers walk flat-footed, with minimal or no heel strike and limited toe-off. These characteristics particularly reflect the immaturity of their musculoskeletal and neuromuscular systems, which are still adapting to the demands of upright locomotion [17, 18].

Toddlers' steps are typically shorter and more frequent than those of adults, so they walk with a wide base of support to enhance balance. Their arms are often outstretched or swing exaggeratedly to counterbalance the body's movements. These adaptations, while necessary for maintaining stability, also make toddler gait less energy-efficient.

Ground Reaction Force (GRF)s, which show the forces from the ground on the body during movement, also vary noticeably. Vertical GRFs, which are responsible for supporting body weight, are proportionally higher in toddlers due to their stamping, unsteady steps. This reflects their need to exert greater force to maintain balance and propel themselves forward. Additionally, mediolateral forces, those acting side-to-side, are more pronounced because of their wide base of support and lateral sway during walking. The transition from braking forces to propulsive forces occurs earlier in their gait cycle. [17, 18].

Accordingly, the weight distribution in toddlers also differs notably; as they are not striking the ground with the heel and transitioning weight smoothly to the forefoot during push-off, toddlers rely more on their midfoot and forefoot regions throughout the stance phase.

This even weight distribution compensates for their limited balance capabilities and helps prevent falls. However, it reduces the efficiency of their steps since they lack the well-defined weight shift that enables efficient energy transfer.

Adults use an inverted pendulum mechanism when walking, where the body pivots over the stance

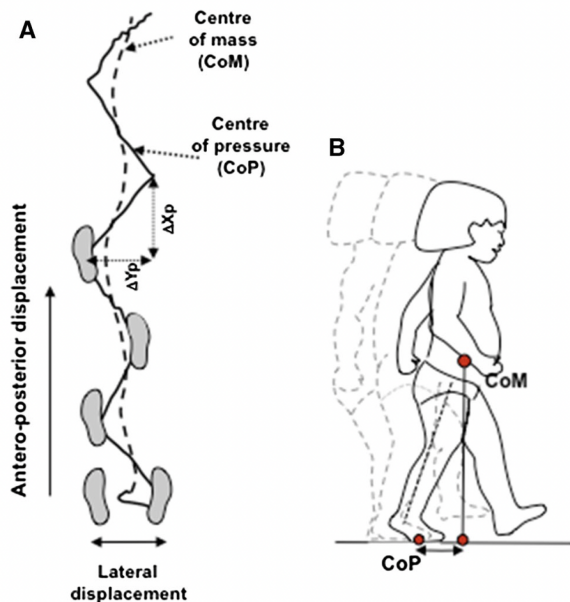


**Figure 2.4:** CoM and CoP displacement patterns in early walking [22].

leg like an inverted pendulum. In this system, potential energy (linked to height), changes as the body moves up and down, and kinetic energy (linked to forward motion), oscillate out of phase. When potential energy decreases kinetic energy increases, and vice versa, enabling energy to be conserved and efficiently reused during movement. This natural energy exchange reduces the effort required for walking [20, 21].

In toddlers, however, this mechanism is still underdeveloped. Their center of mass is relatively high due to the short legs and larger torsos. They recover only about 40% of the energy used during walking, compared to 70% in adults. This inefficiency stems not only from their shorter stride lengths but also from greater vertical oscillations of the body and immature joint coordination [17].

To better understand this, Figure 2.4 illustrates the Center of Mass (CoM) and Center of Pressure (CoP) during toddler gait. The solid line represents the CoP displacement, while the dotted line reflects the CoM displacement. In toddlers, the CoM-CoP dynamics are less coordinated, with limited displacement between the two. This, contributing to the "toddler wobble" [23]. Over time the CoM and CoP trajectories become more aligned [17, 22]; as the arch of the foot begins to form and balance improves, weight distribution becomes more focused and energy transfer during each step becomes more effective [14, 15]. As neural pathways mature, coordination and stability becomes easier, enabling toddlers to perform more complex movements, such as turning, stopping abruptly, and navigating uneven surfaces [22, 24]. Figure 2.5 illustrates the fundamental joint angles involved in toddler gait, including hip flexion/extension, knee flexion/extension, ankle dorsiflexion/plantarflexion, and pelvic tilt.

These kinematic variables are critical for understanding how toddlers adapt their movements for

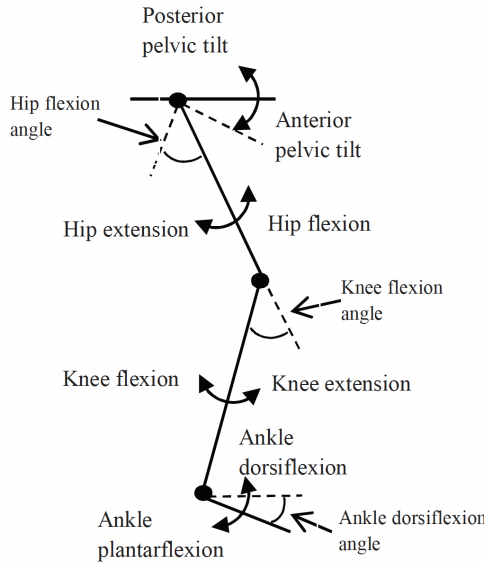


**Figure 2.5:** Joint kinematics of hip, knee, ankle, and pelvis during gait [25].

balance and propulsion. Hip flexion during the stance phase ranges from  $20^\circ$  to  $40^\circ$ , while during the swing phase it transitions to extension at approximately  $10^\circ$ . At the knee, flexion reaches up to  $60^\circ$  during the swing phase to facilitate foot clearance, while during stance the knee maintains a mild flexion angle ( $10^\circ$  to  $20^\circ$ ) to support weight-bearing [25, 26]. At the ankle, dorsiflexion peaks at  $10^\circ$  to  $20^\circ$  during mid-stance to stabilize the foot, transitioning to plantarflexion ( $15^\circ$  to  $20^\circ$ ) during push-off for propulsion [18, 26] (Fig. 2.6) shows the comparison of different aspects of the gait cycle between toddlers and older children, who already show a difference. Additionally, toddlers exhibit a pronounced anterior pelvic tilt, reflecting underdeveloped hip and abdominal musculature, which contributes to their "crouched gait" posture. Later the base of support narrows, arm movements become more controlled, and steps lengthen, leading to a smoother and more coordinated walking pattern [18, 27].

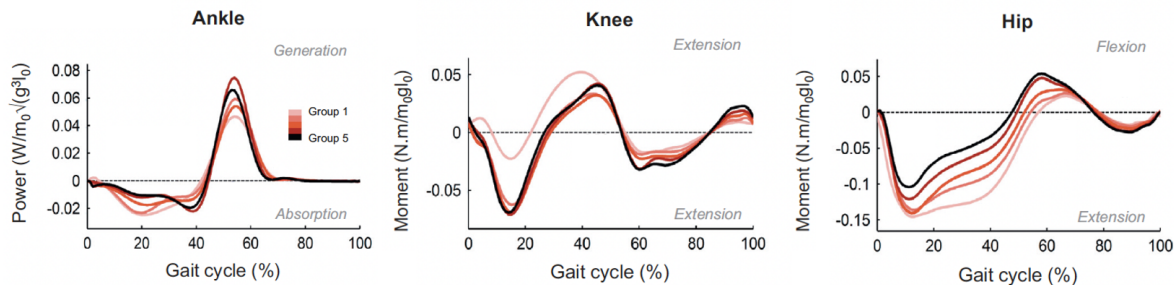


**Figure 2.6:** Toddlers (Group 1) vs. older children (Group 5) ankle, knee, and hip motion. Adapted from [28].

## 2.3 Daily Leg-Based Activities in Toddlers

Between 12 and 24 months, children transition from crawling to independent walking, engaging in various leg-based activities essential for physical and cognitive growth [29]. Few studies report exact knee angles in toddlers during functional tasks. However, gait research shows that from around 24 month of age, children's joint movements are similar to those of older children and adults [30]. Therefore, the estimated knee flexion angles referenced in this section are approximated from studies on older children or adults, and are used as guidance to describe the general range of movement likely required in toddlers. In addition, these values were reviewed and discussed with medical professionals at the hospital to ensure they are suitable for clinical use.

Walking requires knee flexion between 0-60° depending on the gait phase [28]. Toddlers frequently climb furniture, stairs, or playground structures; this activity strengthens lower limb muscles and helps children understand where their body is in space. Climbing stairs, in particular, requires knee flexion of approximately 83-105° to lift the leg adequately [31]. Kicking objects, such as balls, typically begins to emerge around 18 months of age, although early attempts often involve simply walking into the ball rather than executing a coordinated kick. By age two years old, most children can perform a more recognizable kicking action, however, the backswing part of the kick doesn't fully develop until around age four; as a result, toddlers usually show less knee flexion during kicking [32]. Toddlers begin stepping over objects as they develop proprioception and depth perception; these skills help them move safely through their environment. Research shows that obstacle crossing increases knee flexion compared to regular walking with higher obstacles requiring more knee bending [33]. Table 2.1 presents key daily leg-based activities relevant to toddlers during early walking development.

**Table 2.1:** Comparison of knee flexion ranges in toddler activities [24,29-33]

Activity	Knee Flexion Range (Degrees)
Walking	0–60°
Standing up after fall	deep knee flexion above 90°, decreasing over time
Climbing stairs	83–105°
Kicking	10°-30°
Standing up	0° (full extension)
Stepping over obstacles	60–90°

## 2.4 Congenital Malfunction of Lower Limb

### 2.4.1 Fibular Hemimelia

FH is a rare congenital condition characterized by a deficiency or absence of the fibula, the smaller of the two bones in the lower leg. It is the most common congenital longitudinal deficiency of the lower limb, with an estimated prevalence of 5.7 to 20 cases per million births, occurring more frequently in males than females [34]. FH typically affects one leg, with the right leg more commonly involved, though bilateral cases also occur [34,35]. The condition arises due to disruptions during limb development in the embryonic period, particularly affecting the apical ectodermal ridge, a critical structure for limb growth and differentiation [34].

Other proposed mechanisms include vascular anomalies, such as the absence of the anterior tibial artery, and genetic influences, including autosomal dominant or recessive inheritance patterns [34]. Environmental factors, such as exposure to teratogens during pregnancy, have also been implicated [36]. To guide diagnosis and treatment, FH is classified into distinct types that differ significantly in clinical and radiographic characteristics. The Paley Classification is widely used, offering a comprehensive framework for understanding the structural and functional abnormalities of the tibia, ankle, and foot, which are central to decision-making.

- **Type 1** represents the mildest form of FH. It is characterized by a stable ankle and minimal deformities. These cases typically require minimal interventions, such as orthotic management or minor surgical corrections, prior to limb lengthening [34,35].
- **Type 2** is defined by a dynamic valgus deformity of the ankle, primarily caused by soft tissue imbalances. Treatment focuses on tendon balancing and stabilization techniques to correct the deformity and restore ankle stability [35–37].
- **Type 3** includes more severe fixed quino-valgus deformities, which often require complex surgical interventions; advanced imaging and functional assessment are critical in pre-operative planning [34,36]. This class of deformities can be further divided into subtypes:
  - **Type 3A:** Deformity isolated to the ankle.
  - **Type 3B:** Deformity involving the subtalar joint.
  - **Type 3C:** Deformity affecting both the ankle and subtalar joints.
- **Type 4** is the most severe form of FH, characterized by fixed equino-varus deformities with significant soft tissue and bony abnormalities.

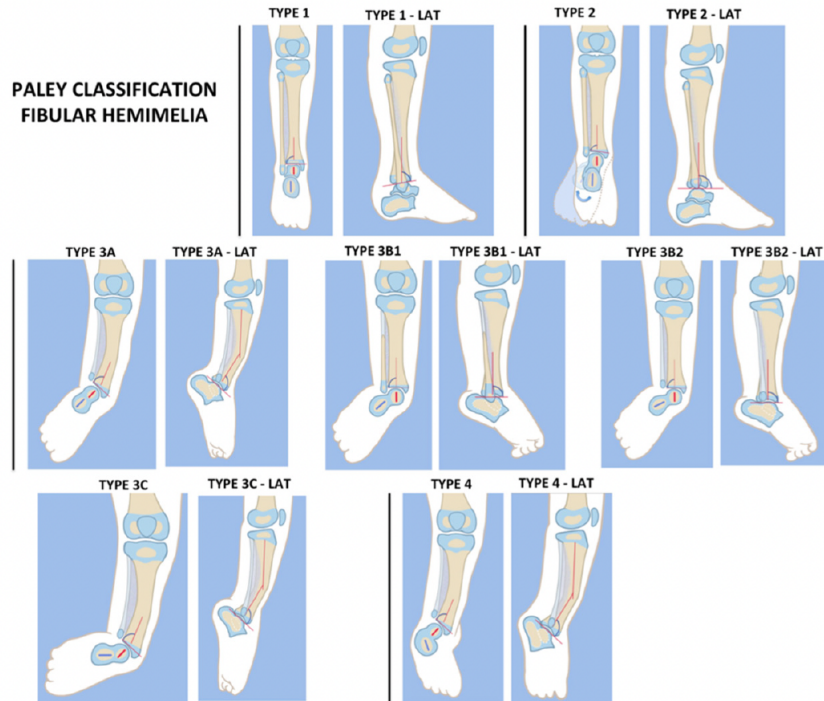


**Figure 2.7:** The Paley Classification system for FH, illustrating the four main types and their subtypes based on tibial, ankle, and foot deformities. Extracted from [37].

- Treatment aims to achieve a functional, stable, and plantigrade foot. However, amputation followed by prosthetic fitting may be considered when extensive reconstruction is not feasible [35–37].

FH is often accompanied by other abnormalities, including: Bowing or shortening of the tibia; Valgus deformity of the knee (outward angulation); Ankle instability due to ligamentous deficiencies; or Foot deformities such as equino-valgus (downward and outward positioning) or absent toes. These associated deformities highlight the need for comprehensive evaluation and individualized treatment [34, 35, 37]. FH is typically diagnosed through clinical examination and imaging studies; X-rays are used to assess bone alignment and development, while Magnetic Resonance Imaging (MRI) can provide detailed visualization of soft tissue abnormalities, including ligament and vascular structures. In older children, Computerized Tomography (CT) scans may be used to evaluate bony deformities while ultrasound can also assist in detecting vascular anomalies in infancy. Early diagnosis is critical to planning timely interventions that optimize outcomes [35, 36].

Despite advancements in surgical approaches, managing FH remains challenging, especially for severe cases with extensive deformities. Complications, such as joint stiffness or infection during lengthening procedures, are common. Nevertheless, with early diagnosis, individualized treatment plans, and proper rehabilitation, most patients can attain functional mobility and a high quality of life [35, 36].

### **2.4.2 Knee Flexion Contracture**

In toddlers with FH, KFC can significantly impact early developmental milestones, particularly walking and standing balance. KFC is a condition where the knee cannot fully straighten, leading to functional and biomechanical challenges in young children. It often arises in toddlers due to congenital or developmental disorders such as cerebral palsy, FH, or arthrogryposis. This condition stems from lower limb misalignment, compensatory adaptations from fibular deficiencies, and structural abnormalities like ACL hypoplasia, valgus knee deformity, and tibial or femoral misalignment. These factors weaken knee stability, promoting KFC progression over time [38, 39]. KFC disrupts muscle growth, ligament function, or skeletal alignment and can worsen rapidly during early musculoskeletal development if left untreated [40, 41]. The flexed knee position in a toddler's gait increases energy expenditure and worsens the naturally shorter stride lengths characteristic of this developmental stage [19]. This combination results in inefficient movement patterns and impairs forward propulsion, leading to substantial challenges in mobility. The crouched posture associated with KFC further heightens energy demands and limits stride length, compounding the functional impact on young children [40, 42]. Additionally, the inability to fully extend the knee shifts the child's center of gravity forward, making it challenging to maintain standing balance or transition smoothly between sitting and standing positions. [38, 40]. Management of KFC in toddlers with FH focuses on early intervention to improve joint mobility and support functional development, including:

- *Physical Therapy:* Stretching and strengthening exercises targeting the quadriceps and hamstring muscles are fundamental in preventing progression of the contracture [42].
- *Orthotic Devices:* Bracing can help maintain knee extension during early standing and walking activities [42].
- *Surgical Interventions:* In severe cases, procedures like soft tissue releases or guided growth techniques may be necessary to correct angular deformities and restore knee alignment [39, 42].

Over time, many toddlers achieve functional improvement, including independent walking and better balance. However, untreated or severe contractures can lead to long-term complications [39, 42].

## **2.5 Additive Manufacturing**

### **2.5.1 Base Principles**

AM, commonly known as 3D-printing, refers to a group of technologies that create physical objects by building them layer by layer from digital 3D models. This approach allows for the fabrication of complex geometries with minimal material waste and enhanced design flexibility [43].

The origins of AM trace back to the early 1980s with the development of Stereolithography (SLA), which used ultraviolet lasers to solidify photopolymer resins layer by layer. This breakthrough paved the way for various AM technologies, including Fused Deposition Modeling (FDM), Selective Laser Sintering (SLS), Laminated Object Manufacturing (LOM), and Directed Energy Deposition (DED) [44]. While these techniques share foundational principles, they differ in materials, energy sources, and application domains.

This thesis focuses on FDM, an extrusion-based AM method in which a thermoplastic filament is heated to a semi-molten state and extruded in a predefined pattern to build a 3D-structure layer by layer [45, 46]. FDM has become the most widely used 3D-printing technology due to its cost-effectiveness, ease of use, and adaptability for both prototyping and manufacturing [46]. To achieve optimal mechanical properties key parameters such as material selection, print orientation, raster angle, air gap, and layer height must be carefully controlled [46].

The standard AM workflow begins with designing a 3D-model using Computer-Aided Design (CAD) software. Afterwards the model is exported as a file format like Standard Tessellation Language (STL), which approximates its geometry with a mesh of triangles. This file is then sliced into layers and interpreted by the AM machine, which deposits or solidifies material accordingly [47].

One of AM's most impactful advantages is its capacity for high customization and complexity, particularly valuable in fields like biomedical engineering. Here, AM enables digital modeling to produce custom and low cost orthotic and prosthetic devices tailored to individual patients, leading to improved fit, reduced lead times, and better clinical outcomes [48].

### 2.5.2 Materials for 3D-Printed Orthoses and Prostheses

The use of 3D-printing in orthoses and prostheses is still relatively limited, especially for load-bearing applications. One of the key challenges lies in the ability of printed materials to reliably support body weight and withstand repeated dynamic stresses. As a result, recent research has focused on improving the mechanical performance of 3D-printed materials through the optimization of print settings, infill geometries, and structural design parameters for load-bearing devices [49].

Devices must be lightweight to accommodate children's mobility, yet robust enough to withstand irregular and dynamic movements. In addition, they must be safe for prolonged skin contact and capable of enduring daily wear. Notably, even minor variations in stiffness or brittleness can significantly impact gait development and overall wearability in children [50, 51].

Among the materials most commonly used in pediatric orthotic designs is Polylactic Acid (PLA). PLA is favored for its accessibility, low cost, and ease of printing. It offers high stiffness and excellent dimensional accuracy, making it ideal for early prototyping. However, PLA has been shown to be brittle and prone to failure under cyclic or impact loads in adult devices. [51–53].

**Table 2.2:** Optimized 3D-printing parameters and mechanical properties for PLA, PLA-CF, PETG, and PETG-CF [49, 55–59].

Property	PLA	PLA-CF	PETG	PETG-CF
Nozzle Diameter (mm)	0.4	0.4	0.6	0.6
Layer Height (mm)	0.2	0.2	0.2	0.2
Print Temperature (°C)	235	215	240	250
Max Bending Stress (MPa)	112.5	127.0	98.5	135.2
Elastic Modulus (MPa)	3774	4050	3250	4400
Strain at Break (%)	5.7	3.2	8.1	4.5
Energy at Break (mJ)	1300	1100	1650	1500

To overcome PLA's limitations, Carbon Fiber Reinforced PLA (PLA-CF) has been explored, as the addition of carbon fibers increases tensile strength and rigidity. However, this reinforcement comes at the cost of reduced ductility and higher brittleness; Rybarczyk et al. [50] found that PLA-CF performed poorly in fatigue testing of ankle-foot orthoses, making it less suitable for the high-repetition, load-bearing demands.

An increasingly popular alternative is Polyethylene Terephthalate Glycol (PETG) and its reinforced variant, Carbon Fiber Reinforced PETG (PETG-CF). PETG is more impact-resistant than PLA and offers greater toughness, while PETG-CF enhances mechanical strength even further. Daly et al. [54] reported that PETG-CF showed significantly higher compressive strength than PLA-CF, with improved behavior under complex loading conditions . Rybarczyk et al. [50] similarly found PETG-CF to offer a better strength-to-weight ratio and more predictable failure behavior than PLA-based composites.

Despite its benefits, PETG-CF also presents limitations, in particular, the carbon fiber content can reduce interlayer adhesion, making the material more prone to delamination under stress. Daly et al. [54] noted an increase in brittleness and lower elongation at break, raising concerns about sudden failure in dynamic pediatric use. Furthermore, Carbon Fiber (CF) introduces anisotropic mechanical properties and requires optimized print settings, including hardened nozzles, which can reduce accessibility in low-cost or clinical environments.

Thermoplastic Polyurethane (TPU) serves a complementary role in orthotic design; TPU is a flexible, rubber-like material valued for its elasticity and wear resistance, it is commonly used for padding, contact zones, and non-structural components that require flexibility and comfort. While TPU cannot be used for load-bearing elements, it significantly enhances the comfort and safety of pediatric orthoses by reducing pressure and friction at the user interface [51, 53].

Other engineering materials such as Acrylonitrile Butadiene Styrene (ABS) and nylon are occasionally used in 3D-printed orthotic applications but present several disadvantages, particularly in pediatric contexts. ABS emits toxic fumes during printing and requires ventilated environments [60]; it is also known to warp during printing, resulting in dimensional inaccuracies that compromise device fit and

function [61]. Nylon offers excellent strength and fatigue resistance, but it is highly hygroscopic and absorbs moisture from the environment. Such properties can lead to material degradation unless the filament is carefully stored and dried [62]. Nylon also requires advanced printing systems such as SLS or Multi Jet Fusion (MJF), which are often inaccessible in resource-limited settings [61].

Due to these limitations, PLA, PETG, and TPU remain the most practical and widely used materials, hence being selected in the context of this work as the most suitable for toddler devices. They offer a favorable balance between printability, safety, and mechanical performance.

Since most materials have been tested on adults, it's unclear how they perform for young children, who move differently and weigh less. Real-world testings on the specific design is needed to understand their behavior in pediatric use.

Table 2.2 summarizes the optimized printing parameters and mechanical properties of the most suitable 3D-printing materials for toddlers orthotic and prosthetic applications. These values highlight the trade-offs between printability and mechanical performance [49, 55–59].

## 2.6 Sensor Technologies for Lower Limb Activity Monitoring

### 2.6.1 Surface Electromyography (sEMG) Sensors

Surface EMG is a non-invasive technique that records the electrical activity generated by skeletal muscles during contraction. It is widely used to assess neuromuscular function in clinical and research contexts focused on gait development, postural control, and motor rehabilitation [63, 64].

Accurate EMG acquisition depends heavily on proper sensor setup. As shown in Figure 2.8; A two active electrodes, about 2 cm apart, are placed over the muscle belly, aligned with the muscle fibers, while a reference electrode is placed on a bony, electrically neutral site (e.g., the lateral epicondyle or collarbone). This reference stabilizes the signal baseline and minimizes noise.

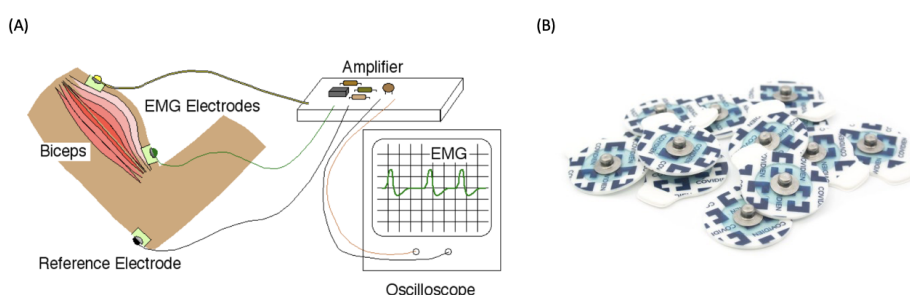


**Figure 2.8:** Overview of typical EMG aspects, namely: (A) EMG setup with electrode placement and signal amplification and (B) Disposable surface EMG electrodes.<sup>2</sup>

Signal preprocessing is essential to extract meaningful information from raw sEMG. Standard procedures include high-pass filtering to eliminate motion artifacts, full-wave rectification to convert the signal to absolute values, and Root Mean Square (RMS) smoothing to estimate signal amplitude over time [65].

In toddlers, it's often not possible to measure Maximum Voluntary Contraction (MVC) because their neuromuscular system is still developing and they have limited control over their movements. As a result, normalization strategies such as temporal normalization to the gait cycle are commonly employed. This approach enables consistent comparisons of muscle activation timing and amplitude across steps or between limbs [64, 65].

In toddlers aged 12–36 months, using sEMG can be difficult because their muscles are small and they have more fat under the skin, which can attenuate the sEMG signal and cause interference from nearby muscles [63]. Furthermore, less coordinated movement in toddlers often leads to more frequent motion artifacts and signal variability [65]. To minimize this problem, specific adhesive electrodes for children can be used, which promote higher signal quality and improved comfort [65] (Fig. 2.8; B).

## 2.6.2 Force Sensing Resistors (FSRs)

FSRs are thin, flexible sensors that change their electrical resistance in response to mechanical force. Typically, FSRs consist of a pressure-sensitive conductive polymer layer sandwiched between two flexible substrates. In the commonly used *thru mode* configuration (Fig. 2.9; A), conductive silver traces are printed on opposing layers and separated by the polymer. When pressure is applied, the polymer deforms, increasing electrical contact between the traces and thereby reducing resistance [66].

When no force is applied, FSRs exhibit very high resistance typically in the  $M\Omega$  range. As pressure increases, resistance drops sharply, often into the  $k\Omega$  range. This change allows them to act as variable resistors.

Conductance increases nearly linearly across their functional force range (Fig. 2.9; B), enabling straightforward interpretation of applied pressure. Because of this predictable behavior, FSRs can be calibrated using just two or three known load points, simplifying their use in embedded systems [67].

In most applications, FSRs are connected in a voltage divider circuit. As force changes, so does the sensor's resistance, resulting in a corresponding change in output voltage. Additional filtering or signal processing can be applied to refine the output or detect events like contact onset or release.

FSRs are lightweight, inexpensive, low-power, and easy to embed in both analog and digital systems, making them especially well-suited for pediatric applications. In gait analysis for children with motor impairments such as cerebral palsy, FSRs embedded or attached to shoe soles can reliably detect key

<sup>2</sup>Instructables User. (2019). \*EMG sensing circuit\*. Accessed: 2025-06-02. [Online]. Available: <https://www.instructables.com/EMG-Sensing-Circuit/>

<sup>3</sup>Tekscan. (2016). \*How does a force sensing resistor (FSR) work?\* Accessed: 2025-06-02. [Online]. Available: <https://www.tekscan.com/blog/flexiforce/how-does-force-sensing-resistor-fsr-work>

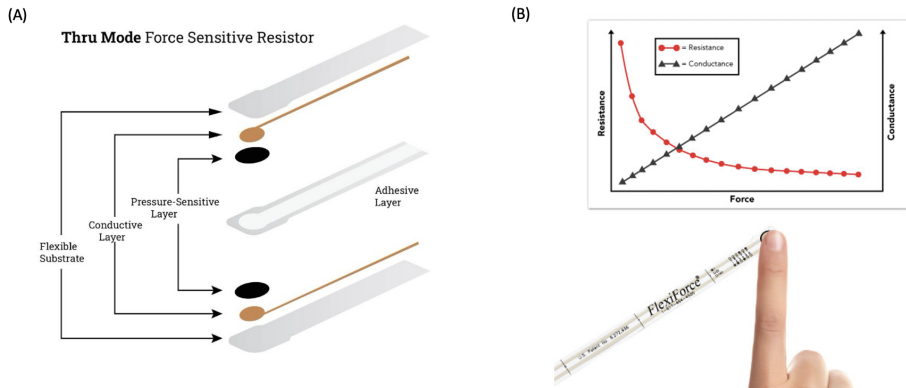


**Figure 2.9:** Typical structure of a thru-mode Force Sensitive Resistor (FSR) (A) and FSR response (B) showing how resistance decreases and conductance increases with applied force.<sup>3</sup>

gait events, such as heel strike, midstance, and toe-off [68].

When used alongside sEMG, FSRs provide precise timing for muscle activation relative to gait phases. This combined sensing approach delivers a detailed picture of neuromuscular coordination and compensatory movement strategies, helping clinicians tailor rehabilitation programs to each child's specific motor profile [68].

# 3

## State of the Art

### Contents

---

3.1 Commercial Products . . . . .	22
3.2 3D-Printed Solutions for Pediatric Use . . . . .	24

---

This chapter reviews commercial products (Sec.3.1) and research studies related to lower limb devices for children (Sec. 3.2). It also discusses how current solutions are not suited for toddlers with conditions like FH and KFC, highlighting the need for personalized, lightweight, and developmentally appropriate designs.

## 3.1 Commercial Products

The commercial review focuses on the European market leaders, Össur and Ottobock.

### 3.1.1 Orthoses

Orthoses, especially Knee-Ankle-Foot Orthoses (KAFO)s, are used to stabilize and align the lower limbs in children with muscle weakness, joint instability, or deformities. These devices support functional walking by redistributing loads and correcting posture.

Ottobock's *C-Brace* is a microprocessor-controlled KAFO that dynamically adjusts knee flexion and extension during walking. It offers excellent support for adults. However, due to its size, weight, and complexity, it is unsuitable for toddlers (Fig. 3.1). Similarly, Össur's *C180™ Rocket* knee brace is designed for children and adolescents with knee instability [69]. Although effective for older users, it is not adapted to the needs of toddlers with congenital deficiencies.

Notably, Össur does not offer KAFOs or orthoprostheses, even for adults. This highlights a significant gap in commercially available comprehensive support systems for toddlers.

Most commercial orthotic and prosthetic products are designed as separate components. These include devices such as Ankle-Foot Orthoses (AFO)s, KAFOs, or prosthetic feet. They are typically targeted for children with conditions such as cerebral palsy or spina bifida. Fully integrated orthoprosthetic solutions for toddlers, which combine limb support and prosthetic extension, are not currently available. The absence of such devices may be due to the complexity of toddler-specific needs and the relatively low clinical demand.

Furthermore, most orthotic devices are simply scaled-down versions of adult or adolescent models, hence they do not accommodate the lower weight, unstable gait, and rapid growth seen in toddlers. Publicly available information on orthoprostheses, or devices that combine orthosis and prosthesis, is extremely limited. KAFOs remain the closest equivalent, but they are designed primarily for stabilization and not for replacing missing limb segments (Tab. 3.1).

---

<sup>1</sup>Image sources: C-Brace Ottobock – <https://www.ottobock.com>, and C180™ Rocket Össur – <https://www.ossur.com>.

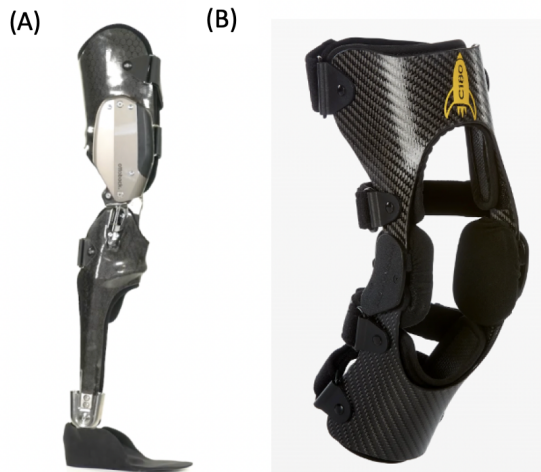


**Figure 3.1:** Example orthoses, namely: A: C-Brace Ottobock and B: C180™ Rocket Össur.<sup>1</sup>

### 3.1.2 Prosthetic Feet

Prosthetic feet help restore functional mobility by replicating foot biomechanics. Essential functions include shock absorption, stability, and push-off during gait. For pediatric users, they must also be lightweight, durable, and flexible. These qualities are necessary to support the development of natural walking patterns.

Prosthetic feet are generally either articulated or non-articulated [70]; articulated feet include ankle joints for terrain adaptability; non-articulated models like the foot are simpler, more durable, and require less maintenance [70, 71].

Ottobock's *Children-Solid Ankle Cushion Heel (SACH)-Foot* is lightweight but often too stiff for toddlers. Taboga and Grabowski [73] note that inappropriate stiffness can disrupt gait and increase energy demands. Many such issues arise when adult designs are simply scaled down without sufficient adjustment. Össur offers the *Flex-Foot Junior*, *Vari-Flex*, and *Flex-Run*. These are intended for active children over 15 kg. They prioritize energy return, which is less relevant for toddlers who are still learning to



**Figure 3.2:** Example prosthetic feet, namely: A: Flex-Foot Junior [69] and B: Children-SACH Foot [72].

**Table 3.1:** Comparison of existing pediatric prosthetic and orthotic solutions needed for toddlers [69, 72].

Factor	Existing Solutions	Toddler-Specific Requirement
<b>Weight</b>	~800g (SACH Foot)	<400g
<b>Cost</b>	~€100 (SACH Foot)	<€100
<b>Delivery Time</b>	Weeks (if custom-made components)	<1 week
<b>Stiffness</b>	Optimized for older children	Scaled to body weight: $k = \frac{F}{\Delta x}$
<b>Growth Adjustability</b>	Fixed-size	Modular, extendable
<b>Energy Return</b>	Designed for active children (15kg+)	Stability-focused, low-energy return
<b>Customization</b>	Limited	High
<b>Orthosis / Knee Braces</b>	Large, heavy, not optimized for toddlers	Lightweight, adaptable to congenital conditions

balance and walk. Table 3.1 highlights the differences between currently available off-the-shelf products and the specific design needs of toddlers for a tailored and not scaled down solution.

## 3.2 3D-Printed Solutions for Pediatric Use

Although research specifically focused on toddlers or fully integrated devices is limited, the literature on 3D-printed solutions highlights a promising approach for developing personalized pediatric orthotic and prosthetic devices. Toddlers require lightweight, adaptable, and personalized devices, all needs that traditional products often fail to meet.

Several recent studies explore 3D-printed lower limb devices for children. Yeung and Subburaj et al. [74] created a patient-specific AFO using 3D-scanning, topology optimization, and SLS printing in PA12 nylon; their single-user case study highlighted excellent anatomical fit. Wojciechowski et al. [75] tested traditional, replica, and redesigned AFOs in twelve children aged 5–16 years old with Charcot-Marie-Tooth disease. Their FDM-printed nylon AFO performed comparably to traditional versions and improved both fit and comfort.

Rochlitz and Pammer et al. [76] proposed a low-cost, 3D-printable prosthetic foot using ABS, PLA, and TPU via FDM; their work focused on mechanical behavior rather than clinical use. Mansilla Navarro et al. [2] developed a soft robotic exosuit to assist pediatric gait. It used textile actuators and 3D-printed shell components. The study included five children and showed improved gait symmetry and step timing. However, the device was not intended to provide structural correction or limb replacement.

Most current studies focus on AFOs, with few exploring prosthetic limbs; full-leg braces like KAFOs

are rare and typically designed for older children with complex needs. Thammakornsuksiri et al [77] presented a clinical case involving a 10-year-old child with congenital fibular and tibial hemimelia. A modular orthoprosthetic device was designed combining a KAFO with a prosthetic foot extension. Over a five-month rehabilitation period, the child achieved measurable improvements in gait and mobility.

Nearly all research involves children aged five and older, with no studies found to address 3D-printed lower limb devices adapted specifically for toddlers. Most studies are single-user case reports; only the study by Wojciechowski et al. [75], involves multiple participants. This reflects both the experimental nature of 3D-printing in pediatric care and the personalized nature of these devices.

This thesis addresses this gap, by presenting the design and evaluation of a modular, 3D-printed orthoprostheses for a toddler aged 1–2 years with FH. The device combines orthotic and prosthetic support in a lightweight, developmentally appropriate form.



# 4

## Proposed Approach

### Contents

---

4.1 Clinical Case Assessment . . . . .	28
4.2 Design Requirements . . . . .	29
4.3 Measurement Protocol . . . . .	30
4.4 Material and 3D-Printing Parameters Selection . . . . .	31

---

This chapter presents the proposed approach for designing and developing a personalized, 3D-printed orthoprosthetic device for a toddler with Fibular FH and KFC. It includes a detailed clinical case assessment (Sec.4.1), defines design and functional requirements (Sec.4.2), outlines the measurement protocol used for anatomical fitting (Sec.4.3), and explains the selection of materials and 3D-printing parameters (Sec.4.4). While focused on a specific clinical case, the methodology and workflow adopted were designed to be adaptable and scalable, making them applicable to other pediatric rehabilitation scenarios requiring customized assistive devices. This chapter lays the groundwork for the prototype development and testing presented in the subsequent chapters.

## 4.1 Clinical Case Assessment

This case study focuses on the development of an orthoprosthetic device for a pediatric patient currently under care at the rehabilitation center of Dona Estefânia Hospital in Lisbon. Born on 1 August 2023, the child was 18 months at the beginning and 22 months old at the end of the work. He has been diagnosed with FH, classified as Type 3C, a severe form of the condition, as described in Section 2.4.1. This classification indicates complete absence of the fibula, a nonfunctional foot with only two toes, and significant shortening of the tibia. Furthermore, the child also exhibits KFC.

The child faces significant physical and functional challenges. A leg length discrepancy of approximately 4.5 cm impairs symmetric standing and walking, while the KFC further limits the potential for achieving a natural gait. The absence of functional toes and the shortened tibia compromise both stability and mobility. Due to the KFC, the child instinctively maintains the affected leg in a flexed position when attempting to stand (Fig. 4.1).

Initially, the child was fitted with a provisional orthosis supplied by the hospital. However, this device had major limitations in fit, adjustability, and function, in particular, it prevented knee flexion, restricting

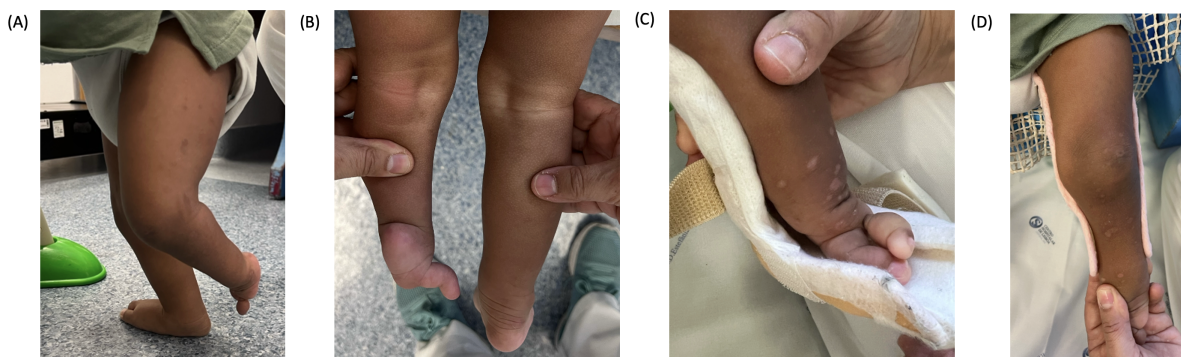


**Figure 4.1:** Main aspects of the clinical case, namely: A: Standing in flexed position; B: Leg length discrepancy; C: Provisional orthosis and D: Night orthosis.

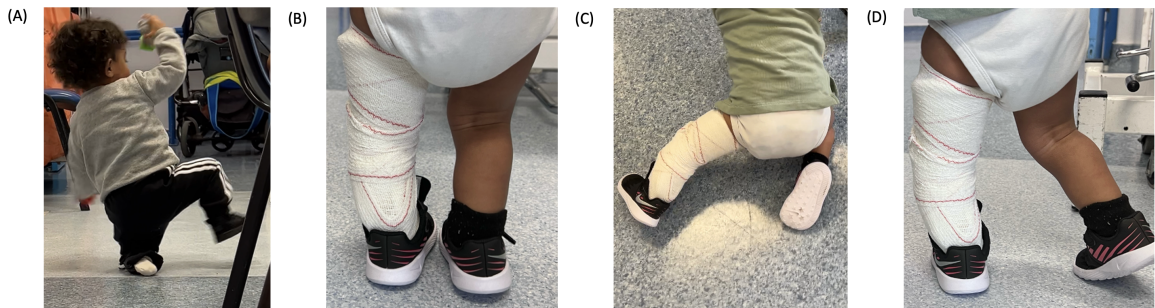


**Figure 4.2:** Illustration of the initial stance and gait abilities of the child, showing: A: Knee walking; B: Standing with provisional orthosis; C: Extended leg position while crawling and D: Inward walking and leg instability.

natural movement (Fig. 4.1; C). Without orthotic support, the child resorted to knee walking, which compromised balance and led to frequent falls (Fig. 4.2; A). The orthosis did not correct for the leg length discrepancy, making it impossible to stand or walk at the same height as the unaffected side. While it provided some stability, independent walking remained difficult. Nevertheless, it enabled the child to bear weight on both legs to some extent (Figs. 4.1 & 4.2). During crawling, the affected leg extended outward in a stiff, straightened posture, hindering fluid movement transitions (Fig. 4.2; C). Additionally, a night brace was used to maintain knee extension and manage the KFC, but it was not designed for daytime use (Fig. 4.1; D).

While it was initially uncertain whether the ligaments and muscles of the affected leg were stable enough to support long-term use, clinical evaluation with the orthoprostheses later confirmed sufficient functional integrity, which will be discussed in Chapter 6. This assessment played a critical role in determining whether limb preservation was feasible or if amputation would eventually be necessary, depending on the limb's performance during weight-bearing and early gait.

## 4.2 Design Requirements

The orthoprostheses was developed based on both the typical gait characteristics of young toddlers, as discussed in Section 2.2, and the child's specific impairments. This approach ensured that the device addressed key functional needs.

Table 4.1 summarizes the main functional requirements and their corresponding Key Performance Indicator (KPI). How each requirement was incorporated into the design and how it was evaluated using the KPIs will be explained and discussed in Chapter 5. Nevertheless, the orthoprostheses was designed as a modular system comprising an upper and lower shell, a knee section, a foot adapter, and a prosthetic foot. The design featured an open area at the foot to accommodate the child's natural equino-valgus foot position without applying compression. Below this, a foot adapter was added to

**Table 4.1:** Key functional requirements and associated KPIs.

ID	Requirement	Metric / KPI
R1	Lightweight construction	< 500g
R2	Modular and adjustable components	Yes/No
R3	Knee joint mobility support	$\geq 0\text{--}120^\circ$
R4	Correction of leg length discrepancy	$\geq 4.5 \text{ cm}$
R5	Stable plantar surface	Yes/No
R6	Comfortable, ergonomic fit	Reaction of child
R7	Breathable, soft materials	Reaction of child
R8	Easy donning and doffing	$\leq 60\text{s}$
R9	Affordability	$\leq 50 \text{ Euro}$
R10	Growth adaptability	Parametrization

compensate for leg length discrepancy and to connect the limb to a prosthetic foot, which provided a stable base for standing and walking. Each component was made adjustable to support the child's anatomy and allowed for adaptation as he grows.

### 4.3 Measurement Protocol

To ensure an anatomically tailored fit and functional performance of the orthoprostheses, anthropometrics from the affected limb were recorded (Fig. 4.3). Measurements were taken using a standard measuring tape, as a 3D-scan of the child's leg was not feasible due to his young age. For the upper shell, measurements included the circumference of the upper thigh (1), the length of the upper thigh (2), and the circumference of the lower thigh (3). These dimensions informed the shaping and sizing of the proximal support section. In the knee section, measurements focused on achieving proper joint alignment and fit. These included the lateral knee bone length (4), the medial-lateral distance between the two knee sides (5), the vertical length of the knee section (6), and the depth of the knee cavity (7). This data enabled accurate placement and articulation of the integrated knee joint. For the lower shell, key values included the circumference of the upper lower leg (8), the length of the lower limb (9), and the circumference near the ankle (10). To accommodate the child's natural foot position, further measurements were taken: the width of the foot (11), length of the foot including toes (12), heel height (13), and heel width (14). These informed the design of an open foot area that allowed the child's foot to rest in its natural equino-valgus position.

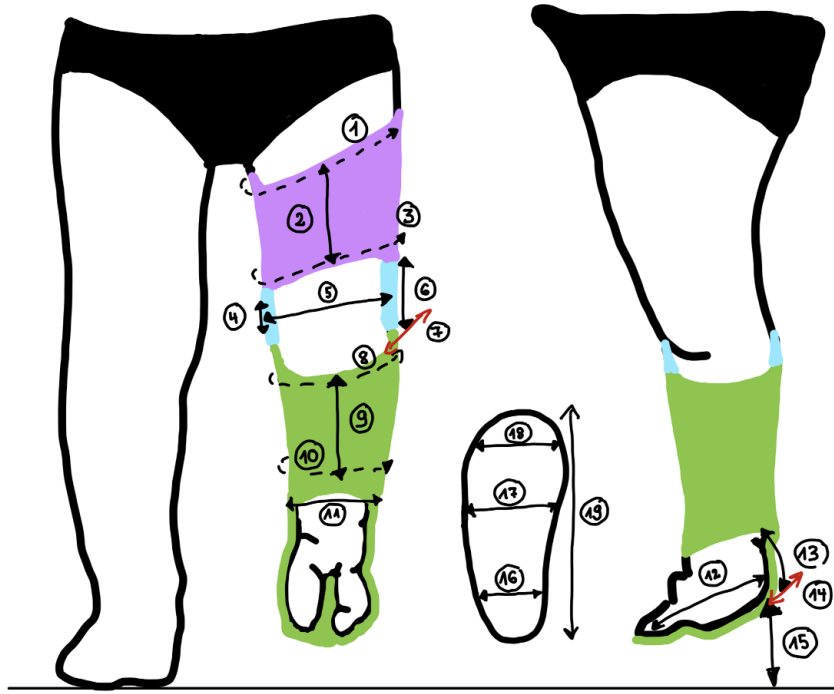


**Figure 4.3:** Anthropometric measurement protocol used to guide the orthoprostheses design.

For the foot adapter and prosthetic foot, key design parameters included the distance from heel to floor (15) to ensure proper height adjustment with an adapter and a prosthetic foot, eliminate pelvic tilt, and promote symmetric standing and walking. To enable seamless integration of the prosthetic foot into standard footwear, additional measurements were taken for the widths at the heel (16), midfoot (17), and toe section (18), as well as the total length of the healthy foot and shoe (19). These values were critical for defining the external geometry of the prosthetic foot module and ensuring compatibility with everyday footwear without compromising gait or stability. The toddler's body weight was also measured to accurately define loading conditions for FEA and mechanical testing.

## 4.4 Material and 3D-Printing Parameters Selection

For material selection, existing literature was reviewed instead of conducting extensive experimental material testing. The focus of this project was on designing and evaluating the device in real-world conditions rather than on fundamental material research. A comparative overview of potentially suitable materials is provided in Section 2.5.2.

Three main materials were selected: PLA, PETG-CF, and TPU. Their key mechanical properties are summarized in Table ?? and served as direct input parameters for the Fusion 360 simulations conducted on the fourth prototype, as described in Section 5.6. Mechanical properties and 3D-printing parameters

**Table 4.2:** Mechanical properties of 3D-printed materials used in FEA simulation.

Property	TPU (95A Shore)	PLA	PETG-CF
Young's modulus (GPa)	0.004	3.500	5.000
Poisson's ratio	0.38	0.39	0.35
Density (g/cm <sup>3</sup> )	1.20	1.300	1.300
Tensile yield strength (MPa)	10.000	49.500	60.000
Tensile ultimate strength (MPa)	12.000	50.000	75.000

can be found in the data sheet and Prusament materials<sup>1</sup>. TPU 95A properties measured under low infill conditions ( $\leq 20\%$ ), not representative of solid samples.

As previously mentioned in Section 2.5.2, PLA-CF was considered a potentially stronger alternative to standard PLA [50]. PETG-CF was selected over PLA-CF because it demonstrated superior mechanical performance in prior studies, particularly in terms of stiffness and strength-to-weight ratio [50, 54]. However, both PLA-CF and PETG-CF have potential drawbacks, such as increased brittleness and reduced interlayer bonding strength, limits that are especially critical in dynamic, load-bearing pediatric applications, compared to non-reinforced materials.

For this study it was therefore decided to compare one reinforced material with a non-reinforced one. PLA was chosen over PETG due to its higher dimensional accuracy, ease of printing, and less flexibility.

Fabrication was performed using FDM. Multiple prototypes were produced to evaluate the influence of print parameters, including infill percentage, internal pattern, and print orientation. PLA was used especially during the development of modular components and for most prototypes, due to its low cost and ease of printing. It showed high print success rates, low risk of cracking, and was ideal for rapid iterative development.

**Table 4.3:** 3D-printing parameters used for orthotic device fabrication.

Parameter	Value	Material	Component
Nozzle diameter	0.4 mm	PLA & TPU	All components
Layer height	0.2 mm	PLA & TPU	All components
Infill density	15% / 50% / 100%	TPU / PLA	Sole / Adapter / Shell
Printing temperature	215°C / 230°C	PLA / TPU	All PLA parts / Sole
Bed temperature	60°C / 50°C	PLA / TPU	All PLA parts / Sole
Print speed	0.20 mm/s (layer) / 40–60 mm/s (travel)	PLA & TPU	All components
Cooling fan speed	100% / Off or low	PLA / TPU	All PLA parts / Sole
Print orientation	Flat / horizontal	PLA & TPU	All components
Printing pattern	Gyroid / Grid / Rectilinear	TPU / PLA	Sole / Adapter / Shell

<sup>1</sup>See Prusament portfolio for technical details: <https://www.prusa3d.com/downloads/press/prusament-portfolio-march-2025.pdf>.

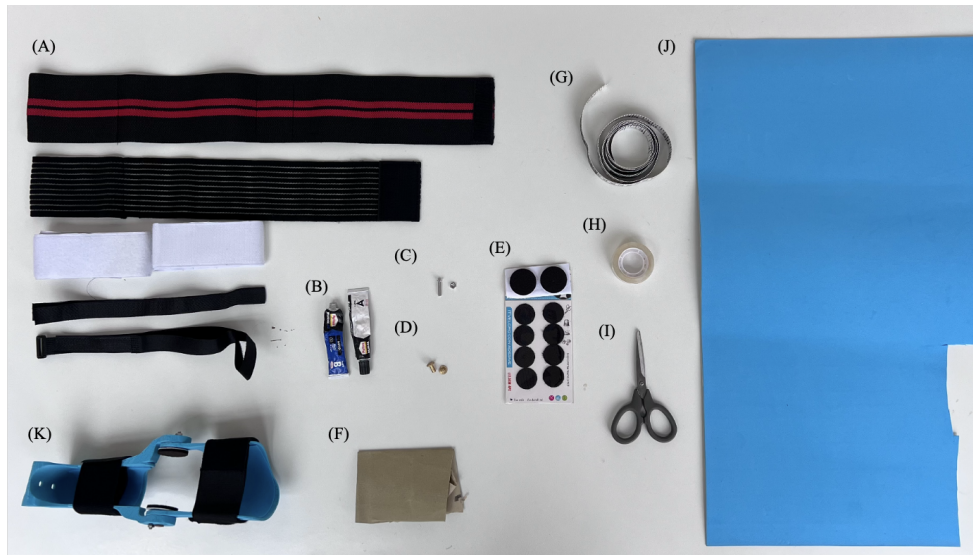
PETG-CF outperformed PLA in preliminary Finite Element Analysis (FEA) simulations (Sec. 5.6). Its carbon fiber reinforcement improved rigidity while reducing density. Although the literature reports issues with brittleness and poor interlayer adhesion, these studies were mostly conducted in the context of adult or heavier patients. It was therefore assumed that the lower impact forces generated by toddlers might reduce the severity of these limitations in practice. However, during prototype testing, PETG-CF still exhibited brittle fracture behavior, particularly at joint interfaces aligned with the print layer direction, as further discussed in Section 5.9. TPU was selected for the sole to mimic soft tissue behavior and shock absorption of the human foot. The final functional device used a combination of PLA and TPU (Sec. 5.8).

Table 4.3 summarizes the optimized parameters used in the final working device. All components were printed with a 0.4 mm nozzle and a 0.2 mm layer height, settings shown to provide a good compromise between detail and mechanical strength [78, 79]. Printing temperatures were set to 215°C for PLA and 230°C for TPU. Bed temperatures were 60°C and 50°C, respectively. Cooling fans were used at 100% for PLA and turned off or set low for TPU to ensure bonding and prevent warping.

Infill density was adjusted based on functional requirements. Load-bearing parts like the knee joint and lower shell used 100% infill. The foot adapter, which was less likely to fail under load, was printed with 50% infill to reduce material use and overall weight without significantly compromising stiffness [80]. The sole, requiring compliance, was printed at 15% infill. These choices were guided by mechanical performance data, including American Society for Testing and Materials (ASTM) D638 tensile tests [78, 81]. Different infill patterns were applied by region: gyroid for flexibility in the sole; grid for the adapter; and rectilinear in rigid structures. All parts were printed in a flat orientation to enhance inter-layer bonding [78] and improve stability against shear forces generated by the child's leg during movement.

Additional materials were selected to ensure the device was stable, functional, and comfortable for daily use (Fig. 4.4). Velcro straps (A), in various widths (2.5–5cm), were used externally to tighten and secure the orthosis around the limb, offering an adjustable and comfortable fit for the child. The upper and lower shell components (K) were connected using two union screws (D), allowing for modular assembly and easy part replacement. At the knee joint, two lateral stop screws (C) were inserted, one on each side, to function as mechanical end stops, controlling flexion within a defined stop-and-go range, and ensuring safe joint movement.

The lower shell, including the natural foot contour, was affixed to the prosthetic foot adapter using two additional screws (C) to ensure proper height alignment and stability during gait. To enhance contact with the ground and provide shock absorption, the flexible TPU sole was bonded to the foot adapter using cyanoacrylate glue (B). For added user protection, foam rubber sheets (J) and knee padding (E) were applied at contact areas in the shells and at the knee joint to create soft interface layers, enhancing comfort and protection during use.



**Figure 4.4:** Additional materials used to complete the orthoprosthesis: (A) Velcro straps; (B) Glue; (C) Screw; (D) Union Screw; (E) Knee padding; (F) Sandpaper; (G) Measurement tape; (H) transparent tape; (I) Scissors; (J) Foam rubber.

The measurement band (G) was used to measure the child's limb. Scissors (I) helped to cut the materials, sandpaper (F) was used to roughen surfaces prior to gluing, and transparent tape (H) supported attachment of FSR sensors and cables to the shoe and limb.

# 5

## Device Development

### Contents

---

5.1 Co-Creation Methodology and Workflow . . . . .	36
5.2 Prototypes Overview . . . . .	37
5.3 Initial Fitting . . . . .	37
5.4 Knee Joint Mechanism and Shell Geometry . . . . .	40
5.5 Functional Redesign of Knee Joint, Shells, and Foot . . . . .	42
5.6 Limb Length Adaptation and Final Material Selection . . . . .	44
5.7 Reinforced Structure and Enhanced Comfort Features . . . . .	50
5.8 Final Device . . . . .	52
5.9 Discussion . . . . .	53

---

This chapter details the development process of the orthoprosthetic device, from early concept to the final working device. It describes an iterative, co-creation methodology (Sec.5.1) involving multiple design iterations, clinical feedback, and real-world testing (Sec.5.3-5.8). The chapter also evaluates material performance through both physical testing and FEA, highlighting key differences between PLA and PETG-CF (Sec.5.6). It concludes with a discussion showing that the final design met most key requirements (Sec.5.9).

## 5.1 Co-Creation Methodology and Workflow

The development of the orthoprosthetic device followed an iterative and modular approach, resulting in five progressively refined prototypes each optimizing one or more components of the device. Each design was digitally modeled, 3D-printed, assembled, and tested to reach the final version presented in this study (Sec.5.8). The process integrated digital simulation with hands-on clinical feedback, as fit optimization was performed directly on the child during in-person hospital visits.

Shell geometry, joint alignment, and interface contours were manually adjusted based on input from therapists and caregivers. This continuous loop of modeling, fabrication, and real-world validation is summarized in Figure 5.2, while preliminary design steps and early test attempts are documented in the Appendix A.

All prototypes were printed using PLA, with the exception of Prototype 4 (Sec. 5.6), which was fabricated using PETG-CF. Detailed print settings and the materials used for each prototype are provided in Section 4.4. Components not explicitly discussed in a given prototype iteration remained unchanged from the previous version.

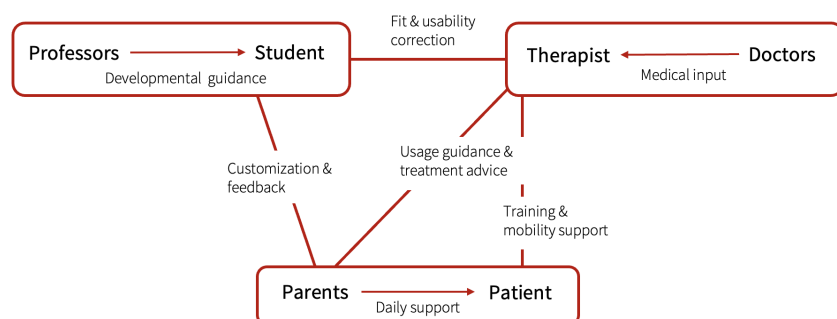


**Figure 5.1:** Co-creation methodology used for this study.

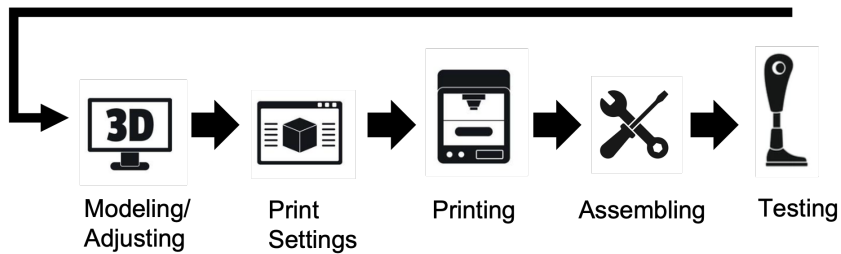


**Figure 5.2:** Digital design and fabrication workflow for the orthoprosthetic device.

## 5.2 Prototypes Overview

Figure 5.3 shows the full set of prototypes developed, starting from the first fully assembled device (Prototype 2) to the final version (Prototype 6). Pink components indicate PLA-printed parts, red indicates PETG-CF-printed components, and light pink represents the TPU sole. Each prototype will be discussed in detail in the following sections.

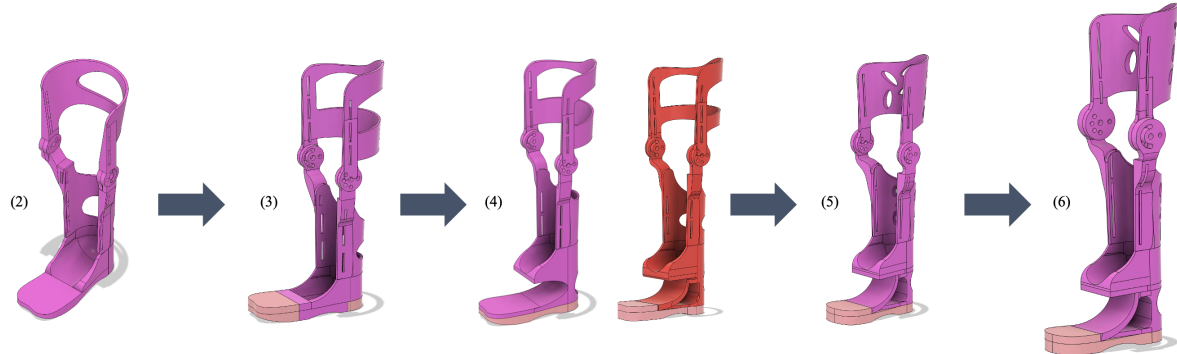


**Figure 5.3:** Progression of fully assembled prototypes, from the first complete version (2) to the final device (6).

## 5.3 Initial Fitting

The first prototype served as an initial test of the complete orthoprosthetic system, consisting of a custom-designed foot module, knee joint, and upper and lower leg shells. It was created to assess the overall fit, alignment, and functionality based on the child's specific posture and anatomy. The following sections describe each component in detail.

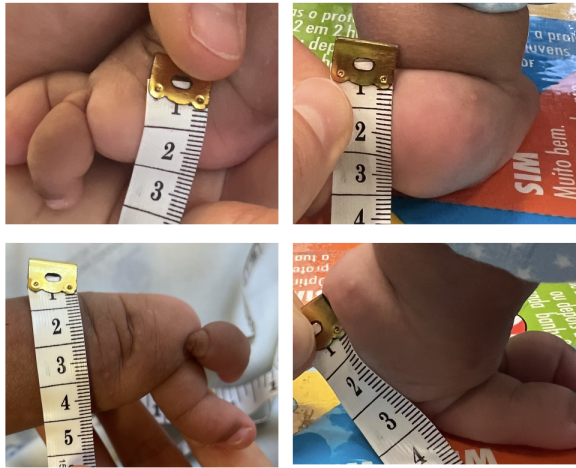


**Figure 5.4:** Required foot measurements for designing the foot shell.

## Design

**Foot.** The foot shell was custom designed to accommodate the specific anatomical dimensions and posture. Detailed anthropometric measurements, including foot width, toe span, and heel height, were recorded directly from the patient using a flexible tape measure, as shown in Figure 5.4.

These measurements were used to define the shape and size of the contoured foot cup, ensuring a precise and comfortable fit that supports the foot in its natural fixed position without compression or forced correction. The inside was shaped to support the sole of the foot, with space to accommodate the fixed toe and angled foot position. A flat forefoot extension was incorporated to match the length of the child's healthy foot, ensuring full-length ground contact and enabling balanced weight distribution during standing and walking (Fig. 5.5; A)

**Knee.** The knee joint consisted of a two-part circular hinge mechanism designed to allow controlled flexion. It was composed of an upper and a lower segment. The lower part of the joint contained a fixed pin, while the upper part featured a curved slot that guided the pin's movement. This slot–pin mechanism restricted flexion to a safe range between  $0^\circ$  and  $45^\circ$ , helping to prevent overmovement at the beginning of gait (Fig. 5.5; B). By limiting the range of motion, the joint provided a controlled and predictable flexion pattern, which is especially important when learning how to develop coordination. Preliminary trials helped determine the appropriate depth and positioning of the knee joint to align with the lateral femoral condyles. Details of this process can be found in the Appendix A. Due to the natural contour of the limb, the lower shell had uneven supporting vertical sockets on either side. As a result, the right joint arm was designed longer to bridge the height difference and maintain even hinge alignment between the upper and lower shells.

**Shells.** The orthoprostheses included an upper and a lower shell. Both had a curved, semi-round

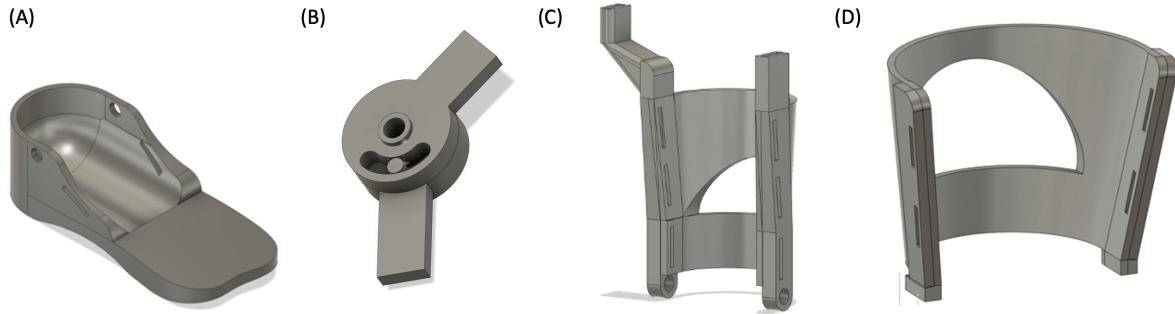


**Figure 5.5:** Prototype 1: (A) Foot (B) Knee Joint (C) Lower Shell (D) Upper Shell.

shape that wrapped around the thigh and lower leg to give the child stability while walking. Both shells had side openings to fit 2.5 cm wide Velcro straps. In addition to that, the shells had a large cut-out in the back, to reduce weight and improve ventilation. In the upper shell the lower end was slightly flared to connect smoothly with the knee joint, which linked the upper and lower shell (Fig.5.5; C;D). At the top of the lower shell, two vertical sockets held the arms of the knee joint. A curved cut-out at the bottom allows for the ankle movement, that should support more natural walking.

### Assembly

After the digital design was completed, the orthoprostheses were 3D-printed in separate parts: the upper shell; lower shell; knee joint; and foot module. Velcro straps were attached through the side slots of the upper and lower shells to secure the device around the limb. The two parts of the knee joint were first screwed together. The completed joint was then slotted into the vertical openings on the upper and lower shells, creating a stable connection between the thigh and lower leg sections. Finally, the foot module was attached to the lower shell using screws, and the entire device was checked for alignment and fit.



**Figure 5.6:** First assembled prototype printed.

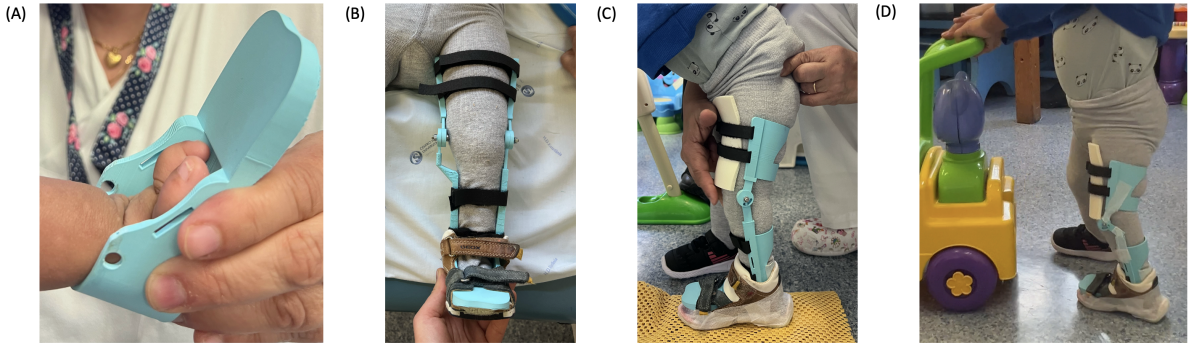


**Figure 5.7:** Initial fitting evaluation highlights showing: (A) Foot shell fitting; (B) Early fitting with all modular components; (C) Standing with final first setup; and (D) Walking with the device.

## Evaluation

The first assembled prototype was primarily developed to assess initial fitting and alignment of the shells and foot cup. The fit on the limb and foot was successful, with the device securely fastened using Velcro straps (Fig. 5.7; A; B). However, several structural issues became apparent during early movement trials. To test the orthoprostheses, the leg with the orthoprostheses was placed inside a sandal and several shoe soles were taped underneath to match the height of the unaffected side (Fig. 5.7; C). The knee joint, which was only slotted into the upper and lower shells without additional reinforcement, repeatedly detached during walking attempts, making functional use impossible, as it would fall out with nearly every step (Fig. 5.7; D). Additionally, the small 3D-printed pin inside the joint could not withstand the force of the toddler's movements and failed under load. As highlighted in red in Figure 5.8, all critical weak points in the knee and ankle joints cracked after only a few steps. The thin knee connection arms detached easily under load, and the open ankle joint, designed to allow some mobility, provided too much movement and breaking under pressure. These issues made it clear that the joint mechanisms lacked the required strength and rigidity for safe use. Reinforcement of the knee and ankle joints, along with stronger materials and more secure attachment methods, were therefore necessary in the next prototype iteration.

## 5.4 Knee Joint Mechanism and Shell Geometry

The second prototype was developed in response to feedback from initial fitting. While the main components, the foot, knee joint, upper shell, and lower shell, remained the same, several important changes were made. Most notably, the knee joint was redesigned to allow more flexibility and to connect more smoothly with the rest of the device. The following sections explain these updates in more detail.

## Design

**Knee.** The updated knee mechanism built on the previous slot–pin concept, but now included a longer slot that allowed guided flexion up to 90°, along with the option to limit movement as needed. The joint consisted of one fixed 3D-printed pin, and a second pin in the form of a removable screw.

By placing the screw in different holes along the curved slot, the range of motion could be adjusted. For example, in the fully extended position (Fig. 5.9; A), the screw pin, locked the joint at 0°. This configuration was included to meet the clinical need for keeping the leg straight at night. By changing the screw's position, the joint could be limited to 45° (Fig. 5.9; B), or opened fully to 90° (Fig. 5.9; C), offering more movement flexibility throughout rehabilitation. One side of the joint was integrated directly into the upper shell (grey), while the other connected to the lower shell (pink). The circular joint component from the upper shell slotted into the corresponding section of the lower shell, which was reinforced with a horizontal support bed beneath the joint, to enhance stability and load distribution.

**Shells.** To allow for up to 90° of knee flexion, both the upper and lower shells were rounded at the back. This cut-out design prevented the shells from colliding during bending and ensured that the joint could move freely without being blocked by the structure behind the knee. The lower shell was printed as a single piece together with the foot section, which retained the same design as in the first prototype.

## Evaluation

During initial lab testing, the new prototype broke under minimal pressure while assembling the upper and lower shell components. The material failed along the 3D-printing layer lines, splitting into multiple pieces (Fig. 5.11). Although the surrounding geometry was designed to add support, it became clear that one of the parts blocked proper joint movement (Fig. 5.10; B). As a result, the knee mechanism could not function as intended. Due to this immediate failure and structural issue, the prototype was not taken to the hospital for further testing and was instead revised for the next iteration.

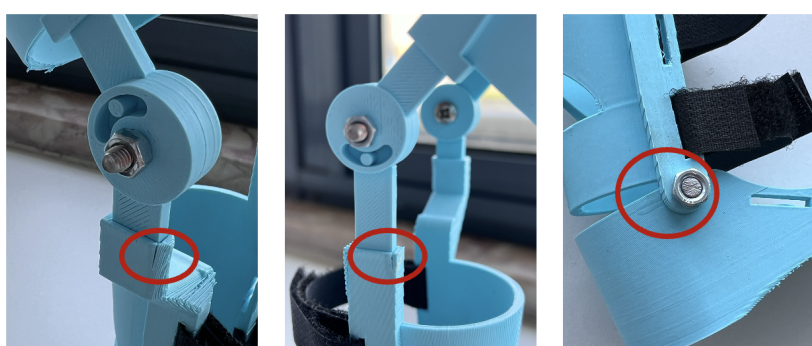


**Figure 5.8:** Mechanical failure points on the first prototype.

## 5.5 Functional Redesign of Knee Joint, Shells, and Foot

The third prototype introduced a series of functional improvements focused on durability, comfort, and movement optimization. Key changes were made to the knee joint, shell geometry, and foot design based on mechanical testing and clinical feedback from earlier versions. The following sections describe the redesigned components and the rationale behind each modification.

### Design

**Knee.** The previous joint design had a horizontal support bed surrounding structure connected to the lower limb shell. This restricted motion and was prone to early mechanical failure. To ensure proper joint rotation, the design was adjusted for smooth, unrestricted movement between the connected parts; as a result, the previously added support bed beneath the joint was removed 5.10. To ensure durability without the support bed, the overall joint surface area was slightly enlarged to withstand mechanical stress. Due to previous failures along the print layer lines, the knee joint was printed at a  $45^\circ$  angle to improve resistance to breakage. This orientation distributes stress more evenly across layers, reducing the risk of fractures. Since the joint is subject to considerable vertical loading during standing and walking, this adjustment was key to improving structural durability. The updated design also replaced the weaker 3D-printed pin with a non-printed pin screw. The range of motion was extended to  $110^\circ$ , allowing the child to potentially perform all everyday activities (see Sec.2.3). The vertical knee supports connecting the joint to the upper and lower shells were redesigned with rounded edges to improve stability and eliminate sharp, potentially harmful corners. Additionally, smoother transitions at the connection points enhanced print reliability and reduced the risk of breakage during use.

**Shells.** Based on more observations and discussions with therapists after fitting Prototype 1 (Sec.5.3), several improvements were made to the shell design, even though the second prototype was not taken to the hospital (Sec.5.4). The back section of the upper shell near the knee was reinforced to provide better posterior support and improve knee stabilization during movement. At the same time, material

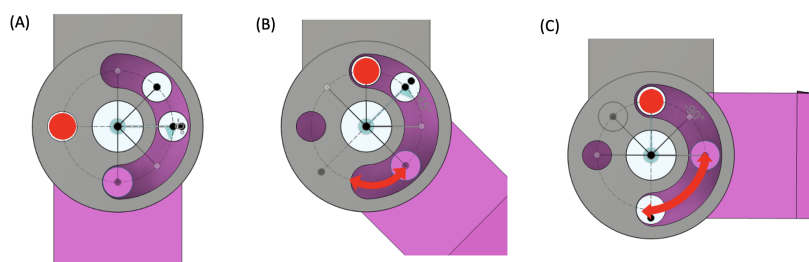


**Figure 5.9:** Knee joint mechanism showing range of motion and rotation path at different flexion angles: (A) initial; (B) mid-flexion; and (C) full flexion.

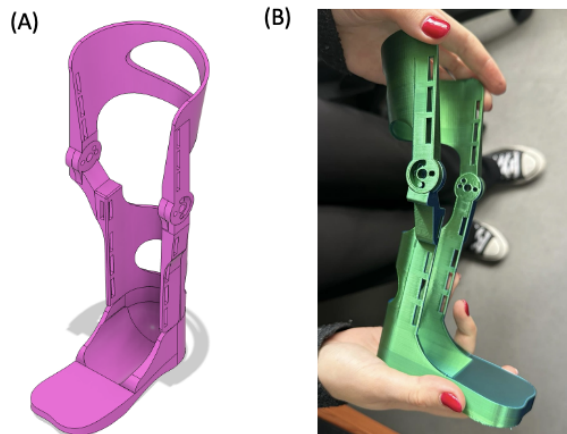


**Figure 5.10:** Second prototype: (A) CAD model; and (B) Printed.

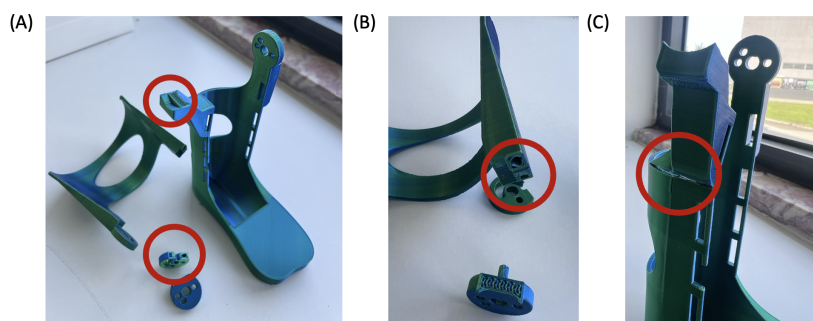


**Figure 5.11:** Mechanical failure of second prototype.

was removed from the inner thigh area to increase comfort, as the diaper was sitting too close to the shell. To allow up to 90° of knee flexion without interference, a rounded cut-out was added to the back of the lower shell.

The strapping system was optimized by replacing several narrow 1.5 cm Velcro straps with fewer, wider 2.5 cm straps. This change was intended to improve overall stability, reduce slippage, and secure the child's leg more effectively within the orthoprosthetic. To improve comfort and protect the skin, the interior of the upper and lower shells was lined with soft foam rubber, preventing skin irritation.

**Foot.** To improve shock absorption and promote a more natural gait, TPU was added to the toe and heel sections of the footplate. This change reduced rigidity and provided better cushioning during walking, which was especially important for the comfort and safety of the child during use. The overall shape of the footplate was kept consistent with the first prototype. However, the integration of softer materials in critical impact zones allowed the orthoprosthetic to absorb ground reaction forces more effectively and minimize pressure on the residual limb.

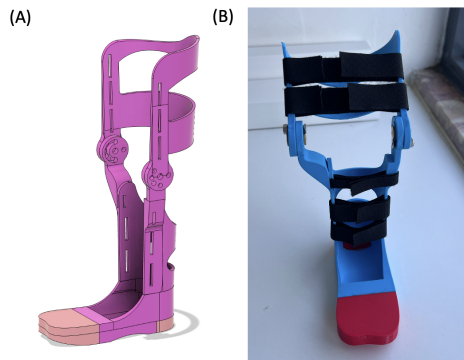


**Figure 5.12:** Third Prototype: (A) CAD model; and (B) Printed.

## Evaluation

Figure 5.13 shows the third prototype testing in the hospital, which marked a significant improvement in functionality. The child fitted the orthoprosthetic well and the foot component was inserted into a standard shoe (A). To address leg length discrepancy, additional shoe soles were taped underneath the unaffected foot (B). The orthoprosthetic was well tolerated by the child, whom was able to take his first independent steps without hand support (C) demonstrating both mechanical stability and comfort.

During testing, the knee joint remained stable and did not experience any mechanical failure. To reduce any flexibility in the upper shell, the Velcro straps were reinforced with clinical tape.

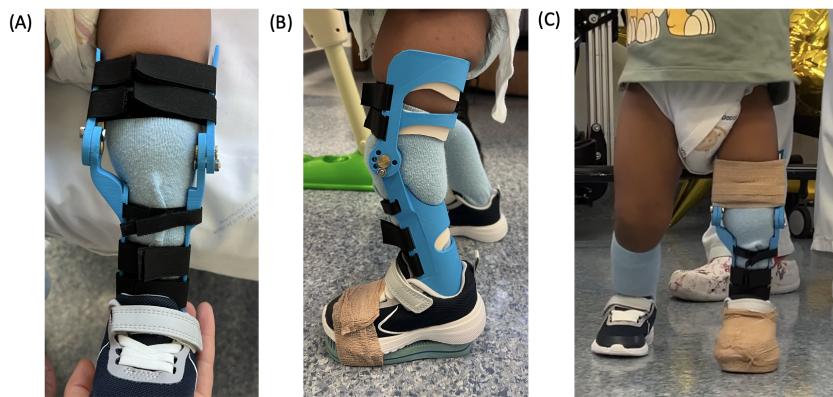


**Figure 5.13:** Evaluation of third prototype: (A) Fitting laying; (B) Fitting standing; and (C) First unassisted steps.

## 5.6 Limb Length Adaptation and Final Material Selection

Building on the success of the third prototype (Sec.5.5), the fourth iteration focused on addressing the child's limb length discrepancy while refining material use and foot functionality. The main changes involved an integrated height adaptation system and improved sole design, with minor adjustments to

the shell for better support. The following sections outline the key modifications and their intended benefits.

## Design

**Foot.** Figure 5.14 illustrates the progression of the third prototype (Sec.5.5), which introduces an integrated height adaptation system to address the limb length discrepancy. The prosthetic foot was extended downward in a continuous structure, smoothly transitioning from the natural foot contour to a lower support base (Fig. 5.14; B). A flexible TPU sole was printed to improve shock absorption during walking. Since young children typically walk with a flat-footed gait, it made sense to extend the previous TPU sections, originally limited to the heel and toe, into a fully integrated TPU sole. To improve shoe compatibility, the heel area was carved out and the toe region was reshaped to be thinner compared to the previous prototype (Fig. 5.14). These adjustments allowed for easier insertion into standard footwear.



**Figure 5.14:** Fourth Prototype including two different design approaches for the height adapter: (A),(C) CAD Design and (B),(D) Printed.

The entire foot section, including the adapter and lower shell, was printed as one piece in the same material as in Prototype 3 (Sec.5.5). The upper shell was not printed again.

Due to concerns about mechanical reliability, the initial integrated height adapter version was revised before clinical testing. Figure 5.14; D shows the refined version of the design, featuring a screw-on modular height adapter integrated with the prosthetic foot. A reinforced central support was added to improve stability, particularly in the midfoot region where most of the load is applied during gait. The component also allowed for adjustable height compensation through removable additional adapter plates, if the child grows. The adapter was attached with screws to the natural foot counter. The screws enabled also control over rotational alignment of the prosthetic foot to the inner or outer shell.

**Shell.** The upper shell design in PLA remained unchanged. However, in the PETG-CF version, the upper shell was slightly enlarged to include an additional opening for a Velcro strap, providing improved

fastening and support.

**Finite Element Analysis.** Two loading scenarios were simulated to assess mechanical performance: vertical static loading; and an inclined 45° load representing the toe-off phase of walking. The justification for the material selection is discussed in Section 2.5.2. In both configurations, the sole and toe section were modeled using TPU, selected for its elastic and cushioning properties to mimic a more natural gait pattern.

The simulations were performed using Autodesk Fusion 360 with a static stress study. A model-based tetrahedral mesh was applied, with automatic element sizing and a refinement level set to approximately 3% of the overall part scale. This resulted in a moderately fine mesh capable of capturing deformation in complex geometries such as the foot shell and joint region. The upper shell of the orthoprosthetic was fully fixed to replicate its attachment to the residual limb.

A load of 200 N was applied vertically to the plantar surface in the static loading scenario. Although the child's body weight was approximately 11 kg, the applied load accounts not only for gravitational force but also for dynamic contributions from muscle action and ground reaction forces during standing and walking. This ensures a sufficient representation of the forces acting on the orthoprosthetic during functional use. For the inclined load case, the same 200 N force was applied at a 45° angle to the toe region to simulate the toe-off phase of gait. All materials were modeled as linear, elastic, and isotropic, with mechanical properties listed in Table 4.2.

In the vertical static displacement analysis (Fig. 5.15; A), the PLA + TPU configuration exhibited a maximum displacement of 13.33 mm, primarily located in the TPU portion of the prosthetic foot adapter, which extends beneath the natural foot shell to compensate for limb length discrepancy. The toe region of the adapter displayed the highest deformation, shown in orange to red tones, while the midfoot area exhibited green to yellow, indicating moderate displacement. Additionally, light green shading extended into the base of the rigid PLA structure, particularly in the lower part of the natural foot shell, suggesting that some of the load-induced movement was transferred beyond the TPU zone into the stiffer material.

In contrast, the PETG-CF + TPU configuration showed a reduced maximum displacement of 10.14 mm. In this case, the deformation remained more tightly localized within the forefoot section of the TPU adapter, with blue to green coloration dominating the rest of the shell, indicating minimal movement. The PETG-CF upper structure remained largely rigid, demonstrating improved load containment and allowing the TPU to function more effectively as a cushioning interface.

The corresponding von Mises stress analysis (Fig. 5.15; B) revealed similar peak stress values for both configurations: 38.35 MPa for PLA; and 38.30 MPa for PETG-CF. However, while the absolute stress values were nearly identical, their significance differs when considered relative to each material's mechanical capacity. PLA typically has a tensile strength of approximately 50 MPa, meaning the observed stress approached its lower failure threshold, especially given PLA's brittle nature and

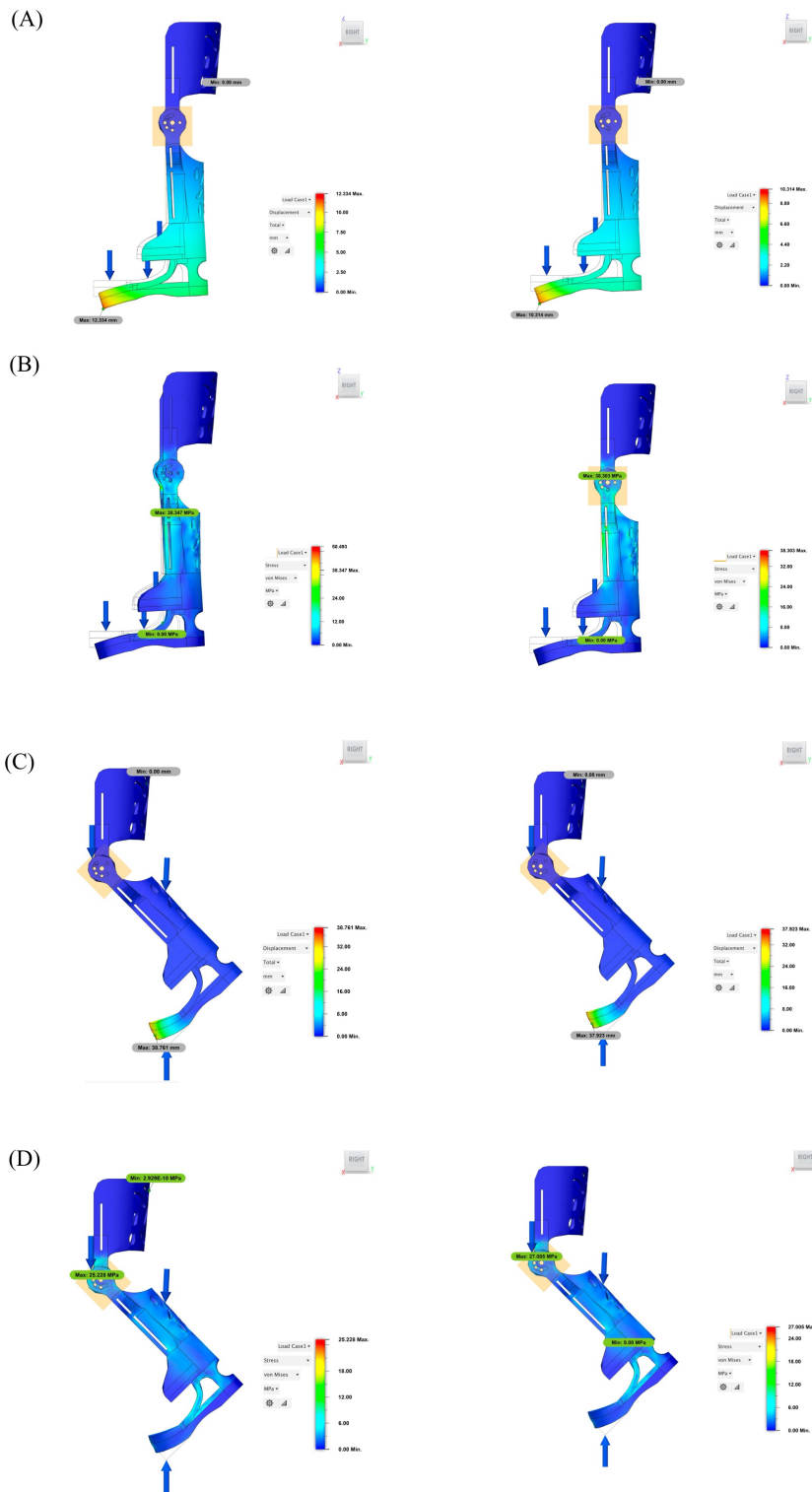


**Figure 5.15:** FEA analysis with vertical static loading and inclined  $45^\circ$  load.

poor fatigue resistance. In contrast, PETG-CF has a higher tensile strength of approximately 70 MPa. Therefore, the PETG-CF configuration remained well within its safe operating limits, offering a greater mechanical buffer and reduced risk of structural failure under repeated loading. Stress was primarily concentrated around the central joint region in both cases, but PETG-CF distributed these forces more evenly, reducing the likelihood of localized failure or fatigue. Under walking conditions simulated with a 45° inclined load (Fig. 5.15; C), both configurations experienced higher total displacements due to the combined axial and bending forces. The PLA + TPU model reached a maximum displacement of 38.76 mm, slightly higher than the 37.92 mm observed for the PETG-CF + TPU setup.

While the overall displacement magnitudes were comparable, the distribution and localization of deformation differed notably between the two materials. In the PETG-CF configuration, displacement was more tightly concentrated in the TPU toe region, indicated by a compact green-to-yellow gradient. In contrast, the PLA model showed more spread-out deformation, with a broader transition of color gradients extending into surrounding regions. This suggests that load was transferred further into the structure in the PLA model, while PETG-CF more effectively contained the deformation within the intended flexible zone.

This behavior reflects the higher stiffness and better structural retention of PETG-CF, which allows the orthoprosthetic to maintain its shape more consistently under load, aligning with its expected mechanical performance. Finally, stress analysis under the walking scenario (Fig. 5.15; D) showed a peak of 25.23 MPa in the PLA model and 27.01 MPa in the PETG-CF model. Despite the slightly higher stress, the PETG-CF configuration remained mechanically safe due to its superior material strength and fatigue resistance. In contrast, the PLA structure approached its performance threshold, posing a higher risk of long-term failure under cyclic loading. Following the mechanical analysis, PETG-CF was selected for printing the fourth prototype.

**Assemble.** Because the third prototype performed successfully, the herein described fourth prototype was intended to be printed using the initially selected final material. The rationale behind this material choice, along with the FEA analysis, was described before (Sec. 5.6). As a result, all components incorporating the updated foot adapter design were fabricated using PETG-CF.

This included the lower shell with the integrated natural foot contour, the foot adapter with the prosthetic foot, and the upper shell. The knee joint and foot adapter components were assembled using screws. Elastic Velcro straps were attached on the lateral and medial sides to secure the orthoprosthetic to the limb, and the inner surfaces were once again lined with foam rubber to enhance comfort and prevent skin irritation (Fig. 5.14; D).

## Evaluation

Both foot adapter designs were brought to the hospital for testing. The PETG-CF printed prototype was tested first but failed within the first few steps due to a fracture in the knee joint, as shown in Figure 5.17; A. The joint broke along the print layer lines, indicating the brittle material behavior and poor interlayer adhesion addressed in Section 2.5.2. This failure suggested that the 45° print orientation, previously effective, was no longer sufficient under the increased flexibility and loading introduced by the new design.

As a temporary solution, the older PLA-based foot adapter from the previous iteration (Fig. 5.14; B) was reused for testing the new PETG-CF upper shell. Fig. 5.16; A shows the internal rotation and movement of the upper thigh during gait. Despite PETG-CF's theoretical strength, the material proved too flexible to provide sufficient stability for a toddler. Additionally, although the Velvet Crochet Hook-and-Loop Fastener (Velcro) straps were redesigned to extend from the medial to the lateral side, covering more of the leg, they still permitted excessive movement. Even supplemental clinical tape was unable to counteract the child's strength or prevent the device from failing (Fig. 5.16; B).

After only a few additional steps, the previously stable lower shell also fractured at both the knee joint and the vertical side support, due to continued excessive lateral loading during gait. Although PETG-CF appeared stronger in simulations, it ultimately proved unsuitable for the final prototype under real-world conditions. While further testing and optimization of the PETG-CF print orientation and parameters may have improved performance, it was decided to return to PLA. This material not only demonstrated greater reliability in practice, but also simplified the production workflow.

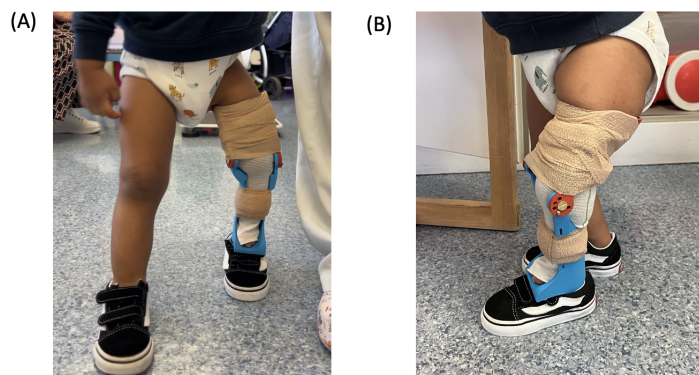


**Figure 5.16:** Clinical testing of the fourth prototype revealed overflexibility in the upper shell, leading to reduced stability during standing (B) and walking (A).

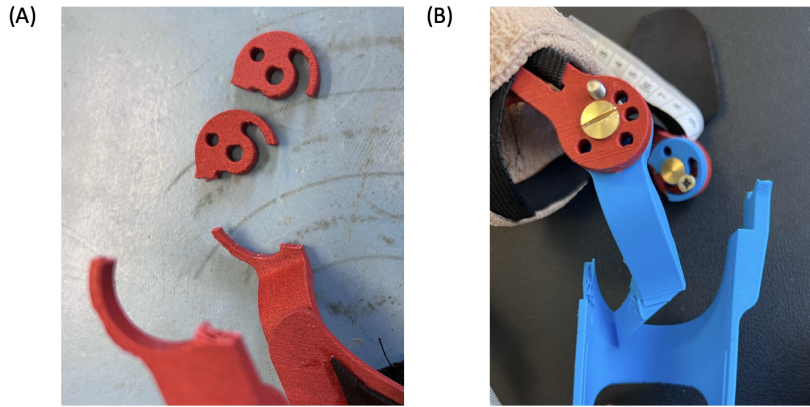


**Figure 5.17:** Mechanical failure of the PETG-CF prototype during clinical testing.

## 5.7 Reinforced Structure and Enhanced Comfort Features

The fifth and final prototype focused on reinforcing structural elements while enhancing the child's comfort and wearability. Improvements addressed previous mechanical failures and material selection, printing strategies, and padding for better performance and fit. The following sections describe the final refinements made to the knee, foot, and shell components.

### Design

**Knee.** As the previous lower shell failed under lateral force, the circular area around the knee joint was again enlarged to enhance durability. Additionally, the inner and outer components of the joint were reversed comparatively to earlier iterations, allowing for smoother sliding during knee movement (Fig.5.18; A) .

**Foot.** The heel section was further reduced, while additional material was added to the forefoot to improve stability in the shoe and weight transfer during walking. Additional TPU material was also applied to the toe area, increasing flexibility and contributing to a more natural and fluid gait.

**Shells.** The upper and lower shells were redesigned to increase surface coverage and provide enhanced support. To maintain user comfort despite the expanded structural areas, ventilation holes were integrated for heat dissipation without compromising rigidity. The lower shell was printed horizontally to reduce lateral forces and prevent structural failure, while the upper shell was printed at a 45-degree angle to balance strength and printability. The strapping system was upgraded with wider 5 cm Velcro straps lined with thick neoprene, improving limb stability. Additional neoprene padding around the knee openings ensured a snug and secure fit at the joint (Fig. 5.18; B).

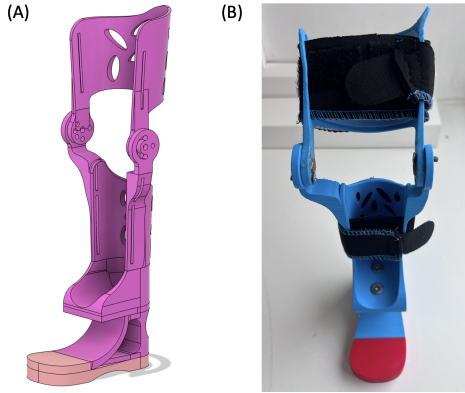


**Figure 5.18:** Fifth prototype: (A) CAD Model; and (B) Printed.

## Evaluation

The design was tested during a clinical visit at the hospital. Figure 5.19 shows the orthoprostheses fitted on the child. All components functioned well throughout the visit, with the knee joint appearing stable and reliable, even during activities such as climbing. The child accepted the orthoprostheses without hesitation and was able to walk independently through the hospital environment.

Following the hospital visit, the device was taken home and used daily over a period of three weeks. During this time, it continued to support mobility until the knee joint eventually failed due to mechanical stress (Fig. 5.19; C).

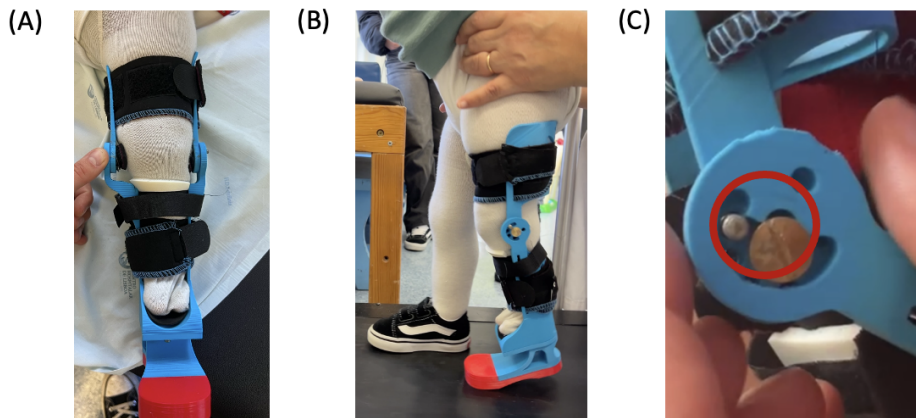


**Figure 5.19:** Evaluation of fifth prototype: (A) Fitting lying down; (B) Walking; and (C) Knee joint failure.

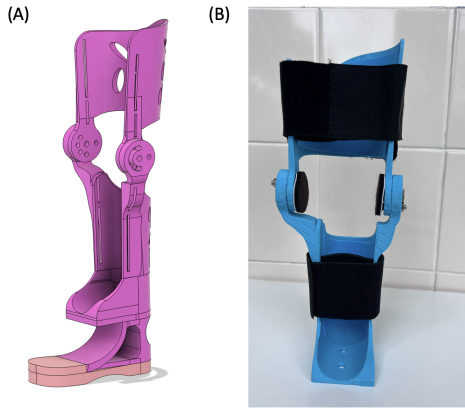


**Figure 5.20:** Final device: (A) CAD Model; and (B) Printed

## 5.8 Final Device

The final device included only minor refinements, focusing on reinforcing the knee joint and adapting to the child's growth. The following sections describe the final changes made to the knee, shells, and assembly process.

### Design

**Knee.** To improve joint durability, the surface area of the knee joint was enlarged again, and the material around critical stress points, particularly between the screw holes and along the guiding slot, was reinforced by increasing its width. Additionally, the entire enlarged surface of the joint was thickened (Fig. 5.20). These modifications increased the overall volume and significantly enhanced the structural stability of the joint interface.

**Shells.** The upper shell was reprinted with increased height to accommodate the child's growth over the past month. The lower shell remained unchanged, except for the localized thickening around the knee joint, as previously described.

**Assembly.** In this iteration, only the upper and lower shells were reprinted. The foot section from earlier prototypes was reused and attached in the hospital. New Velcro straps were introduced, offering similar performance to the previous ones, but with slightly stronger adhesion and more uniform stickiness across the surface. To improve comfort around the joint area, the knee was additionally cushioned with soft padding (Fig. 5.20; B).

### Evaluation

At the hospital, the fitting process proceeded smoothly. The child was able to walk around and climb onto small objects with relative ease (Fig. 5.21).

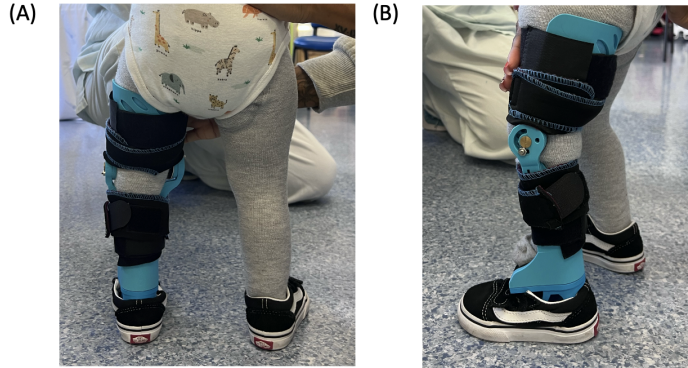


**Figure 5.21:** Testing the final design in the hospital.

While playing and throwing a ball, he occasionally lost balance and fell. However, he was able to stand up independently and continue walking, demonstrating that the device maintained stability even during frequent falls and uncontrolled movements. In Chapter 6 this will be further discussed. The orthoprosthetic was then taken home for extended use, during which it continued to perform reliably and remained structurally stable over a four week on going period.

## 5.9 Discussion

The development of the final orthoprosthetic device demonstrated that AM was able to provide a lightweight, modular, and affordable solution tailored to the specific anatomical and functional needs of the toddler.

Achieving the final prototype required several redesigns and prototypes, with each iteration targeting a particular limitation observed in real-world testing. The most difficult challenge encountered was the development of a stable and reliable knee joint. Early versions frequently failed under dynamic and unpredictable load (see Fig. 5.11 & 5.17).

Despite these challenges, the final device met or exceeded nearly all KPIs, as summarized in Table 5.2. The total weight of all four components was only 266.68g, well under the 500g limit defined in requirement R1. A full breakdown is presented in Table 5.1, which lists the material weight, print time, and cost per component.

**Table 5.1:** Material usage, cost, and print time per component for the final device.

Component	Weight (g)	Cost (€)	Print Time (h:min)
Upper Shell	69.41	1.76	5:38
Lower Shell	110.23	2.80	7:00
Foot Adapter	61.08	1.55	3:04
Foot Sole	25.96	2.13	2:05
<b>Total</b>	<b>266.68</b>	<b>8.24</b>	<b>17:47</b>

The lightweight construction, along with a modular and stackable design, enabled both ergonomic usability and adaptability for future growth. The design supported up to 120° of knee motion (R3), matching the flexion range required for activities such as stair climbing and kicking, as detailed in Chapter 2.3. However, until now, the knee joint range was intentionally restricted to 45°, as full flexion proved too challenging for the child to control at this stage, particularly due to the limited stability and muscle strength associated with his KFC. The orthoprosthetic also successfully corrected the 4.5 cm leg length discrepancy (R4) and was adaptable for further growth via 0.5 cm modular stacking plates (R10). Clinical testing confirmed a stable plantar surface (R5), and the child has now worn the prosthesis for a month, exhibiting improved balance and early unassisted walking.

The child and caregivers reported a positive reaction to comfort and usability (R6). Donning and doffing were quick and intuitive (R8). However, ventilation remained a partially fulfilled requirement (R7). Although the design included ventilation holes, these were blocked by foam rubber used to enhance comfort on the child's leg, reducing breathability.

One of the most revealing findings was the discrepancy between simulated and real-world material performance. Initial FEA simulations identified PETG-CF as a favorable material due to its high stiffness and low deformation predictions. However, PETG-CF prototypes fractured during early testing due to weak interlayer adhesion, highlighting the material's anisotropic and brittle nature in FDM printing. This outcome reflects known issues in literature and underscored the need for application-specific validation (Sec. 2.5.2).

In contrast, PLA demonstrated superior mechanical performance in clinical use. Its good layer bonding and sufficient flexibility enabled the device to survive the three-week clinical trial and an additional month with only a small refinement, without structural failure. TPU, used selectively in the sole and toe region, played an important role in sufficient flexibility for the gait.

Economically, the device exceeded expectations. The final material cost remained under €15, significantly lower than commercial solutions, where even the most affordable option costs around €100

**Table 5.2:** Key functional requirements, associated KPIs, and fulfillment status.

Requirement	ID	Metric / KPI	Fulfilled
Lightweight construction	R1	< 500g	✓
Modular and adjustable components	R2	Yes/No	✓
Knee joint mobility support	R3	≥ 0–120°	✓
Correction of leg length discrepancy	R4	≥ 4.5 cm	✓
Stable plantar surface	R5	Yes/No	✓
Comfortable, ergonomic fit	R6	Reaction of child	✓
Breathable, soft materials	R7	Reaction of child	Partially
Easy donning and doffing	R8	≤ 60s	✓
Affordability	R9	≤ 50 Euro	✓
Growth adaptability	R10	Parametrization	Partially

for the foot alone, excluding the rest of the device. Total print time was under 18 hours, and while not yet fully parametrized, the device could be adapted to other children in less than a week, assuming access to design knowledge.



# 6

## Experimental Evaluation

### Contents

---

6.1 Observational Findings . . . . .	58
6.2 Data-Driven Validation . . . . .	62
6.3 Discussion . . . . .	71

---

This chapter presents the experimental evaluation of the developed orthoprostheses through clinical observation (Sec.6.1) and data-driven analysis (Sec.6.2). It assesses the device's impact on posture, early gait, and muscle activity, showing that the orthoprostheses enables functional standing and walking while revealing neuromuscular engagement in the affected limb.

## 6.1 Observational Findings

### 6.1.1 Static Alignment and Pelvic Correction

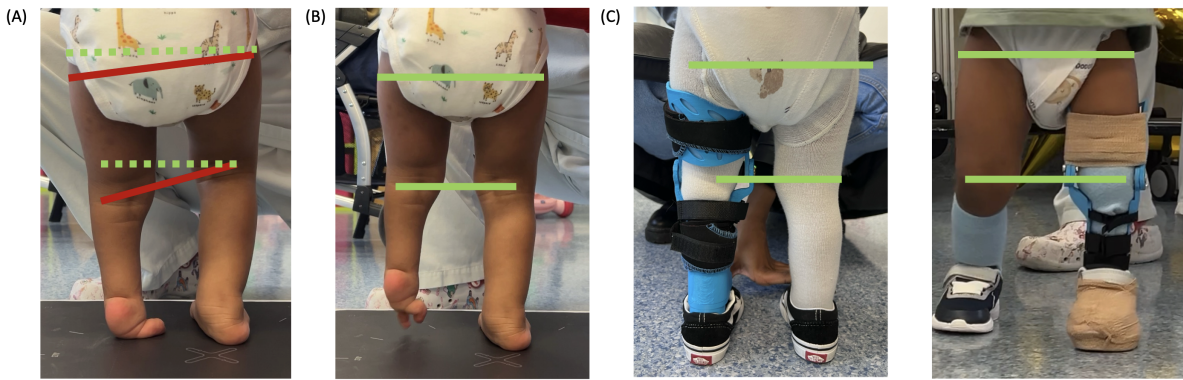


**Figure 6.1:** Postural alignment while: (A) Standing without orthoprostheses; (B) Child being manually supported into an upright position without any assistive device; and (C) Fitted orthoprostheses. Dotted lines indicate the intended or ideal alignment, while solid lines represent the observed orientation of body segments.

When not using the orthoprostheses (Fig. 6.1; A), the child had a clear leg length difference of about 4.5 cm, resulting in significant pelvic tilt of around 15° toward the deseaeed leg. This unevenness caused the hip to shift to the side, showing reduced pelvic control and uneven weight on the legs. The affected limb showed valgus deviation and medial rotation, contributing to visible misalignment of the lower limb. Without proper support under the foot, most of the weight was placed on the outside and top parts of the foot, leading to further destabilization. A compensatory shift in the CoP toward the unaffected limb was evident, which made it harder to put stable weight on the shorter leg. This postural imbalance likely increases the risk of secondary complications such as asymmetric gait development or spinal curvature. Support by the therapist (Fig. 6.1; B) enabled the child to achieve a more upright posture, but it did not correct the underlying biomechanical asymmetries. Pelvic tilt and limb misalignment persisted, and independent stable standing or walking was not possible without external support.

When fitted with the 3D-printed orthoprostheses, several key postural improvements were observed (Fig. 6.1; C). Firstly, the device effectively compensated for the leg length discrepancy, restoring pelvic symmetry as indicated by the leveling of the iliac crest. The hip axis appeared re-centralized, contributing to improved axial alignment and upright stance. Furthermore the affected limb followed a straighter

mechanical axis, reducing angular deviation and improving load-bearing alignment with the body's centerline. The prosthetic foot provided a stable and flat plantar surface, facilitating full-foot contact and more equal load distribution between limbs. Notably, the CoP was observed in a more central position when the orthoprosthesis was worn, suggesting enhanced postural stability and greater readiness for bipedal gait initiation.

### 6.1.2 Early Unassisted Walking Behavior

After completing the postural assessment, the orthoprosthesis was tested during early walking trials. Remarkably, the child was able to initiate walking almost immediately without external support and adapted comfortably to the device.

Figure 6.2 shows early unassisted walking with the orthoprosthesis in a clinical hallway. The child is making firm, flat-footed contact with the ground, especially visible in the first and middle frames. There's no clear heel strike, supporting the description of stamping movement and higher vertical GRFs. The prosthetic foot and healthy foot both land flatly, with no rolling seen from heel to toe, which supports the idea of a midfoot-dominant contact pattern. As compensatory strategies the child used wide arm movements, forward trunk sway, and cautious weight shifts; these patterns help maintain balance by widening the base of support and adjusting step timing. In addition the child appears to be wobbling side-to-side, especially as weight shifts from one leg to another, visually reflecting the immature CoM-CoP relationship. All these observations align well with findings in the literature, confirming that the child is going through a typical developmental stage for a toddler (Sec.2.2).

Tests further revealed, it can be shown that, while precise control of the prosthetic knee had not yet been established, the child was able to take the first steps, shift weight onto the prosthetic side, and maintain upright posture.



**Figure 6.2:** Sequential images showing early, unassisted walking attempts with the 3D-printed orthoprosthesis. The child demonstrates forward trunk sway, wide arm movements, and cautious weight shifting.



**Figure 6.3:** Falling due to missing sensory control.

During walking, the affected leg tended to move outward, reflecting the child's early use and incomplete understanding of how to actively control knee flexion and extension. The timing and control of the bending were inconsistent, which is expected for someone who has never used the mechanism before.

In addition, it was interesting to see that the child experienced a lack of sensory feedback from the prosthetic foot. As the device does not provide real-time proprioceptive or tactile input, the child was unable to accurately sense the position of the foot during walking. This resulted in incidents where the child unintentionally walked into obstacles, as there was no feedback to help guide or adjust foot placement.

Figure 6.3 shows an example where the child fell after colliding with a chair leg. The child did not recognize that the prosthetic foot was in contact with the object and continued the motion, leading to a loss of balance. Although the child showed limited active control of the knee joint during walking, with a tendency to rotate the leg outward and rely more on hip movement, an important observation was made during a fall, namely, as illustrated in Figure 6.4. The child demonstrated the ability to bend the knee and use it effectively to rise from the ground.

After falling forward, the child flexed the knee to approximately 45°, which corresponds to the mechanical limit built into the orthoprostheses. This controlled flexion indicates that, despite not actively using the knee during normal gait, the child was capable of engaging the joint in specific functional situations, such as standing up after a fall. This behavior suggests that the child possesses underlying motor capacity and coordination that may not yet be apparent during structured walking tasks. The orthoprostheses provided a balanced design by limiting excessive motion for safety, while still allowing enough range to support independent recovery and movement initiation.



**Figure 6.4:** Child pushing up after a fall, actively engaging the prosthetic knee joint for support.

### 6.1.3 Controlled Gait Cycle on a Treadmill

To validate and extend the findings from unassisted walking trials, a controlled treadmill assessment was conducted under therapist supervision using the final orthoprosthetic. This evaluation focused on the repeatability and coordination of gait patterns, with particular attention to prosthetic knee function.

Figure 6.5 presents a time-sequenced image series of the treadmill trial. The upper sequence (A) illustrates the motion of the healthy limb during a complete gait cycle, while the lower sequence (B) shows the orthoprosthetic side. Both limbs demonstrate consistent and comparable phase transitions, including initial contact, stance, toe-off, and swing. This picture is showing that the child understood the basic motor pattern for gait and is able to actively coordinate the orthotic knee with the natural limb, however he lacks the experience of walking in a controlled setting; overall, the movements on the treadmill appeared more rhythmic. Section 2.2 described the kinematics of the hip, knee, ankle and pelvic; the healthy leg closely aligns with toddler gait norms, however, the orthoprosthetic leg shows less knee flexion than the typical  $60^\circ$ . Nevertheless, but the child consistently achieved approximately  $45^\circ$  of controlled knee flexion during swing and the norm of  $10-20^\circ$  in stance, which matches the prosthetic joint's mechanical limit and reflects successful adaptation. In both Figure 6.5; A,B, hip flexion is seen at the start of the gait cycle; while in (A), the hip extends more during swing, in (B) the hip stays more flexed, likely due to limited movement or compensation.

Also, the TPU outsole and reinforced toe helped the foot make flexible contact with the ground and roll smoothly during stance. This flexibility appeared to support mid-stance progression and effective weight transfer, suggesting that the prosthetic foot was not overly stiff and allowed for a more natural gait pattern.

Taken together, these findings show that the orthoprosthetic is working well and closely matches typical toddler movement. It helps the child start walking on their own and supports steady, repeatable movements in a safe setting. To strengthen these findings a data-driven validation was also conducted.

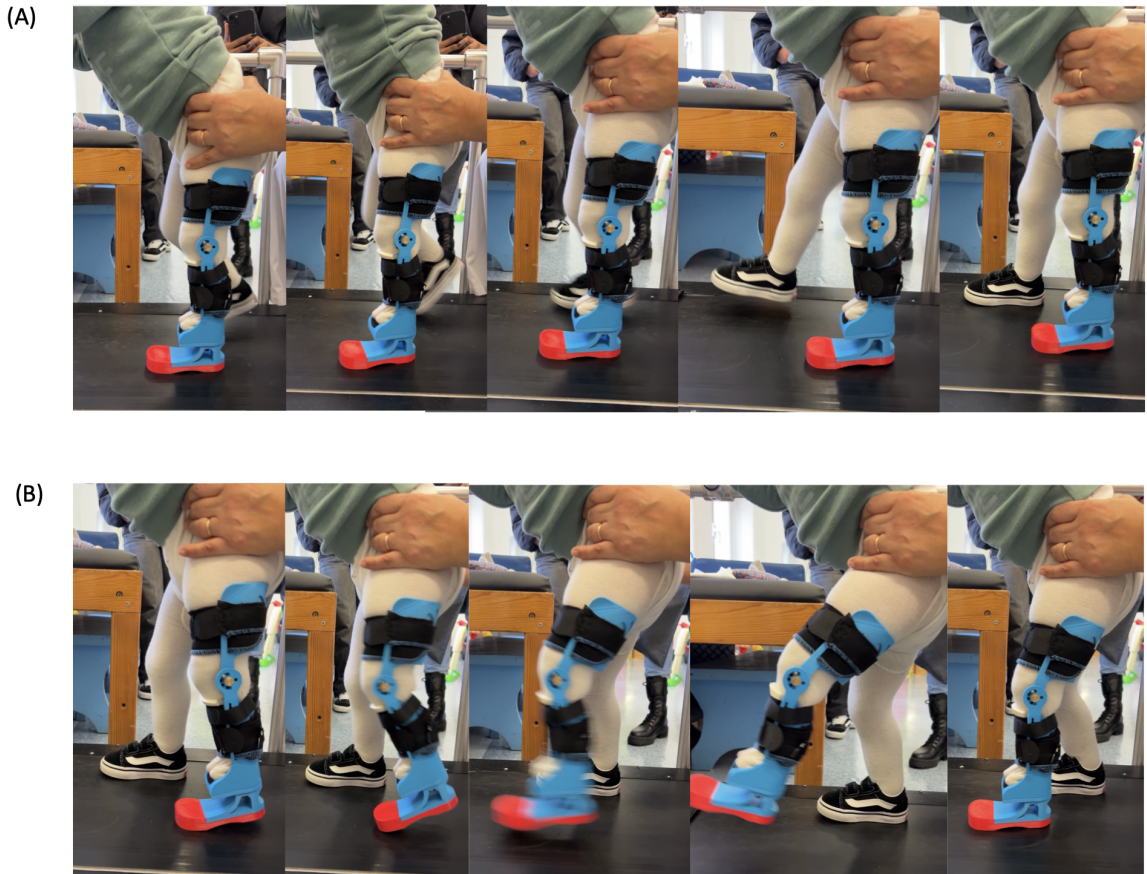


**Figure 6.5:** Comparison of gait patterns between the healthy limb (A) and the orthoprosthetic limb (B) during treadmill walking.

## 6.2 Data-Driven Validation

### 6.2.1 Preliminary Work for Data Acquisition

To better understand the child's gait and neuromuscular behavior, sEMG and FSR sensors were placed on the lower limb. Prior to data acquisition on the child, preliminary trials were conducted on a healthy adult subject to refine the methodology. These tests included determining optimal sensor placement, selecting relevant muscle groups, and verifying synchronized data acquisition using the biosignalplus<sup>1</sup> system, including its software, sensors, and connectors. The biosignalplus system is a biomedical data acquisition system developed by PLUX Wireless Biosignals, used primarily for recording and analyzing physiological signals. It is often used in clinical research, rehabilitation, and biomechanics. The results of these preliminary trials are provided in the Appendix B.

Data collection on the child was performed using the exact same setup and protocol as in the pre-

---

<sup>1</sup>See the biosignalplus user manual: [https://support.pluxbiosignals.com/wp-content/uploads/2021/11/biosignalplus\\_User\\_Manual.pdf](https://support.pluxbiosignals.com/wp-content/uploads/2021/11/biosignalplus_User_Manual.pdf)

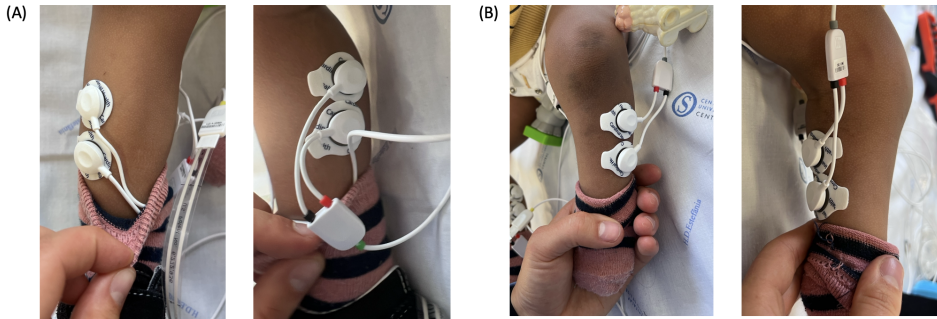


**Figure 6.6:** Sensor placement on both lower leg muscles TA and GC.

liminary trials. EMG signals were recorded from both legs, focusing on the TA and GC muscles; since the placing of the sensors of the child was uncomfortable, the number of electrodes was minimized. The analysis was therefore concentrated on the most functionally relevant muscles to ensure comfort while still capturing meaningful gait-related activity. As explained in Section 2.1, the GC is one of the most important muscles during early childhood. Aligning with the literature (Sec. 2.6.1), electrodes were also placed on the muscle belly with muscle fiber direction and spaced 2 cm apart for accurate signal capture. However, due to the child's small size, the sensor covered nearly the entire length of the leg (Fig. 6.6 A; B).

In this case study, the lower leg provided the most relevant data, as it is the region most affected by FH. As such, the focus was on understanding weight distribution, gait symmetry, and whether muscles were actively engaged. This is also important to know for future interventions such amputations or other treatments.

To complement the EMG data, FSR sensors were placed under the child's foot using the thru-mode described in Section 2.6.2. Due to the availability of only two sensors, they were positioned at the heel and the inner ball of the forefoot, which are the key pressure zones during walking (Fig. 6.7; B). The sensors were secured with adhesive tape.

All sensors were connected to the biosignalsplus hub, worn at the child's waist (Fig. 6.7; A), which digitized and transmitted all signals wirelessly to a laptop via Bluetooth. Cables were secured to the diaper, upper shell of the orthoprostheis, or under a tie to minimize distraction during movement (Fig. 6.7; C).

A reference EMG electrode was placed on the collarbone. Data was collected at a sampling rate of 1000 Hz with 16-bit resolution, allowing precise signal analysis. To analyse the CoP and ground reaction, the child was additionally standing on a force plate. The biosignalsplus system allowed for synchronized acquisition of EMG and FSR as well as the force plate data, capturing real-time muscle activity and load distribution during the child's first steps with the orthoprosthetic.

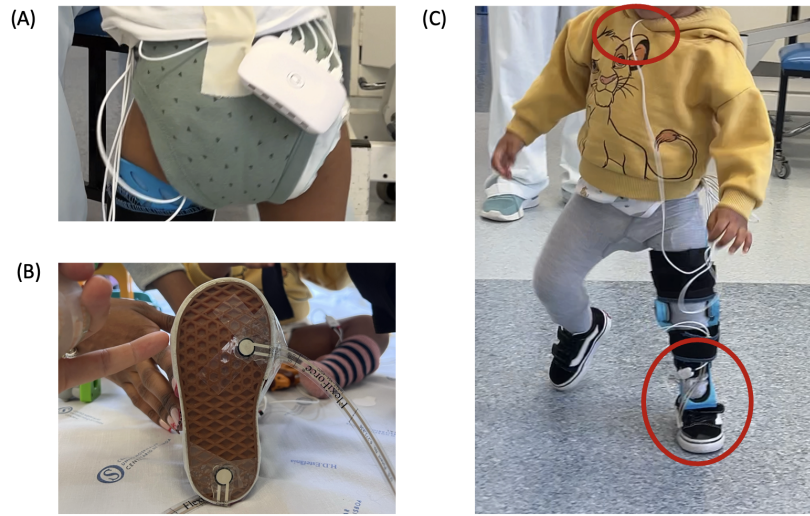


**Figure 6.7:** Remaining setup for data acquisition, showing:(A) biosignalsplus hub attached at the waist; (B) Reference electrode at the collarbone with fastened cables to avoid hindering smooth walking; and (C) FSR sensor placement under the foot.

### 6.2.2 CoP Assessment with Force Plates

In addition to the visual postural improvements, the CoP was further assessed using the biosignalsplus force plate, providing quantitative insights into weight distribution and balance behavior during quiet standing.

Figure 6.8 presents the pressure plate assessment in detail. Panel (A) illustrates the quadrant layout, divided into Q1–Q4, representing the forefoot and rearfoot of each foot. Panel (B) shows the child standing on the plate with the orthoprosthetic leg during a 60-second acquisition period. Bilateral foot contact is visible, allowing direct comparison between the affected and unaffected sides. Lastly, the prosthetic foot is positioned slightly more anteriorly and not fully aligned with the contralateral foot, which may partially explain the increased pressure in Q1 compared to Q4 (C). However, the child may also be

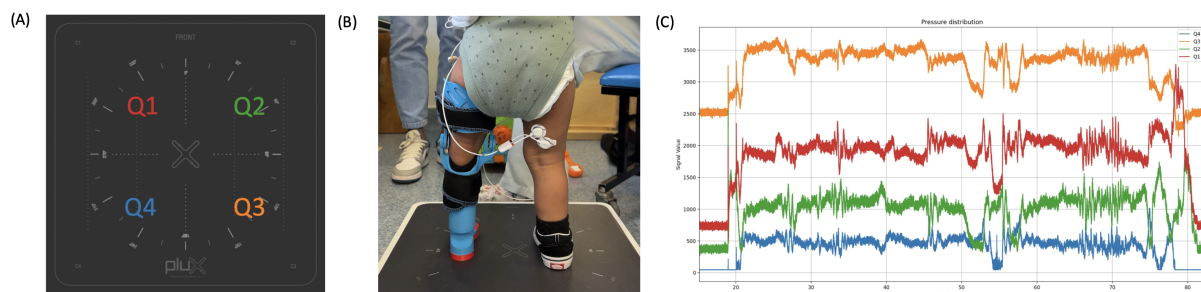


**Figure 6.8:** Plantar pressure distribution assessment using a quadrant-based pressure plate. (A) Top view of the pressure plate divided into four quadrants. (B) The child standing on the plate during testing. (C) Pressure data recorded across the four quadrants.

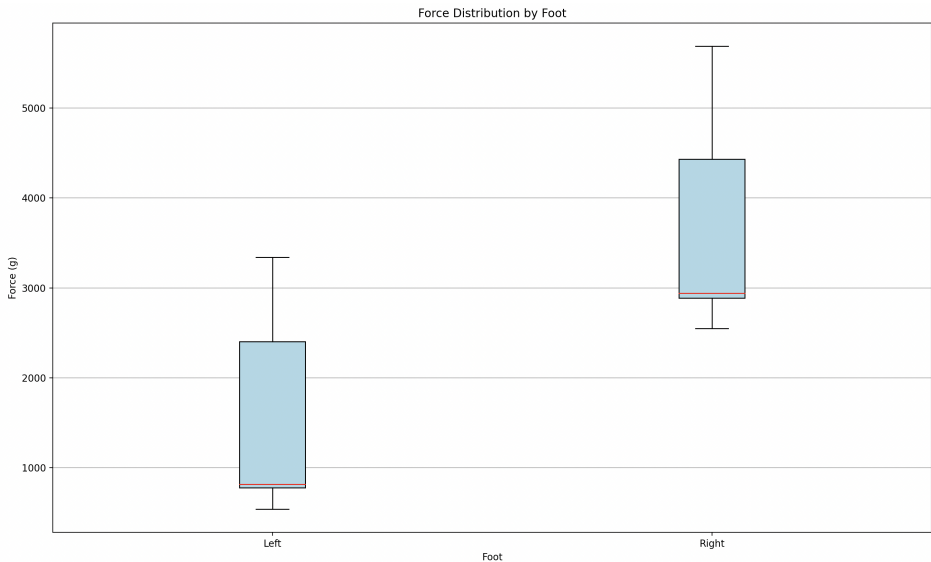


**Figure 6.9:** Distribution of vertical ground reaction forces under each foot during early standing (median in red).

actively shifting weight forward on the prosthetic limb to enhance stability, a compensatory strategy commonly observed in users lacking anatomical ankle function [82, 83].

Panel (C) displays the pressure signal across all quadrants over time; the similarity in temporal pattern is likely caused by postural sway, which is typical for early standing. Notably, the child appears to engage both legs to maintain posture, a promising indicator of developing balance control. This supports the observed transition from uncoordinated CoP and CoM dynamics toward more integrated postural control during early gait development [22].

Despite this engagement, the magnitude of pressure varies considerably between quadrants, pointing to uneven weight distribution. This is visualized in the box-and-whisker plot in Figure 6.9, which compares vertical ground reaction forces under each foot. The right leg bears significantly more force, as shown by its higher median and greater spread. This asymmetry likely reflects the child's compensatory strategy during quiet standing, it also aligns with known early postural behaviors in toddlers, who often show uneven weight distribution due to immature balance control and underdeveloped neuromuscular coordination [17, 22]. The broader interquartile range on the right side also suggests more active postural adjustment, while the lower and narrower range on the left reflects compensatory underuse.

Nevertheless, the presence of measurable loading on the affected side is encouraging, as it suggests early functional use of the prosthetic leg, which may promote recovery or neuromotor adaptation. This early activation is consistent with literature indicating that, as toddlers develop, increased sensory input and limb engagement help refine postural strategies [22, 24].

Figure 6.10; B shows the CoP trajectory in the X–Y plane; X = 0 cm marks the midline of the pressure plate, separating the left and right legs. The trajectory, shaded from light to dark blue to indicate time,

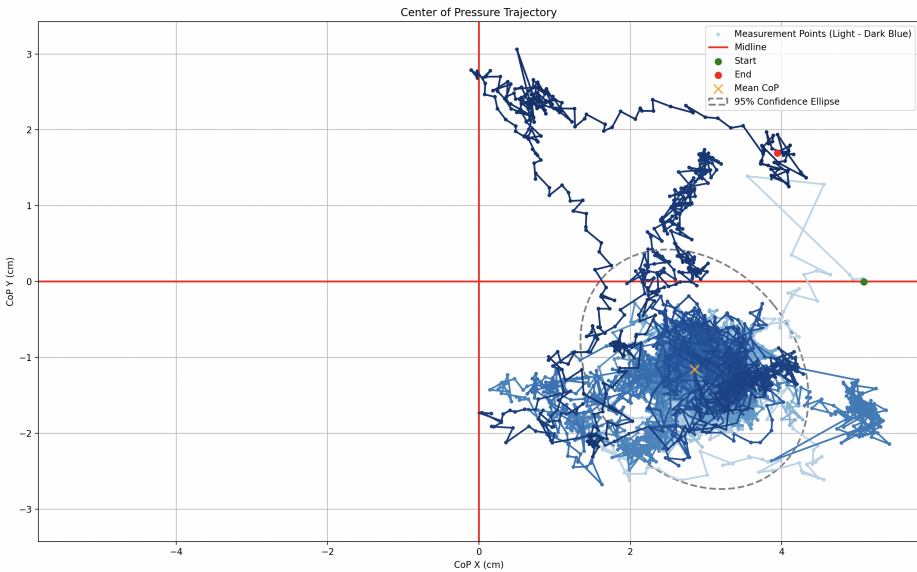


**Figure 6.10:** CoP trajectory in the X–Y plane, showing a rearfoot-biased, rightward stance with clustered movement and 95% confidence ellipse.

shows a rearfoot-biased pattern centered between -1 and -2 cm on the Y-axis. This corresponds to early postural development, where toddlers typically rely on the rearfoot for greater stability [84]. In this case, the CoP is clustered almost entirely over the right side, indicating asymmetrical support. This finding reinforces the child's reliance on the unaffected limb, and aligns with developmental observations that early CoP trajectories tend to stabilize around the dominant leg during unbalanced stance [22].

The X-axis data (clustered around 2–3 cm) further confirms a rightward weight shift, indicating that, although the left foot maintains ground contact, its contribution to load-bearing is limited, consistent with Figure 6.10. Occasional anterior CoP shifts are also present, reflecting transient forward corrections. These excursions likely represent early postural reactions, typical of toddlers who are just beginning to develop reactive balance control [17]. The mean CoP position and 95% confidence ellipse confirm that most of the movement remains localized in the rear-right quadrant, with only brief excursions away from this zone.

Overall, these results indicate that the orthoprosthetic contributes meaningfully to postural alignment and promotes partial weight-bearing through the affected limb. Although the child exhibits clear asymmetry, this early bilateral stance lays a crucial foundation for motor coordination and neural adaptation. These outcomes are supported by literature showing that improved CoM–CoP dynamics and progressive load sharing are key milestones in the development of stable, energy-efficient toddler gait [20, 22].

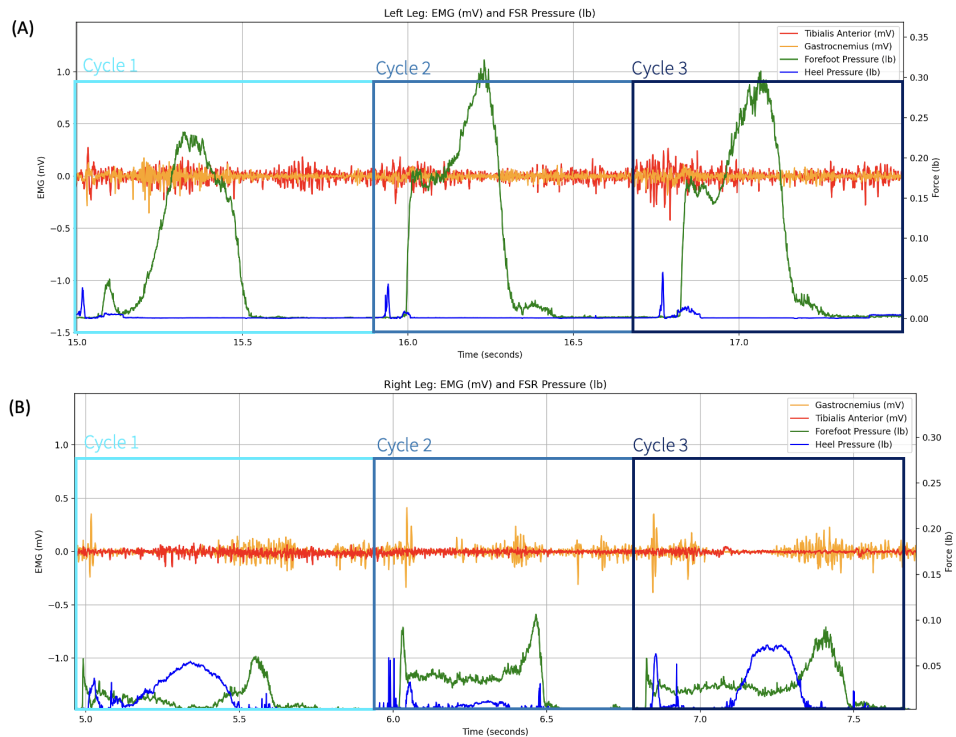


**Figure 6.11:** EMG and FSR pressure data across three gait cycles for the left (A) and right (B) legs during unassisted walking.

### 6.2.3 EMG & FSR Analysis

To further support and validate observational findings, synchronized surface EMG and FSR data were collected from both the affected left leg and the healthy right leg during early unassisted walking. The recordings captured muscle activation of the TA and GC, alongside foot-ground interaction through heel and forefoot pressure sensors.

To gain an initial overview of the gait dynamics, raw EMG and corresponding FSR signals were extracted from data collected in each leg over three representative gait cycles. These recordings provided synchronized data on muscle activity and foot-ground contact. The raw EMG and FSR signals (Fig. 6.11) revealed distinct differences in signal patterns between the affected and unaffected legs.

Since the cycles within each leg showed similar activation patterns, a single representative gait cycle was selected for detailed analysis. This allowed for a clearer comparison of the gait patterns between the affected and unaffected leg.

Figure 6.12 shows FSR sensor activation profiles and video stills for both the orthoprosthetic and healthy legs across a full gait cycle. The analysis focuses on the three key walking phases: heel strike; toe-off; and swing. The right leg (A), which has functioned as the dominant limb, shows a relatively mature gait pattern for a toddler. Heel strike is smooth and controlled, with a gradual force increase

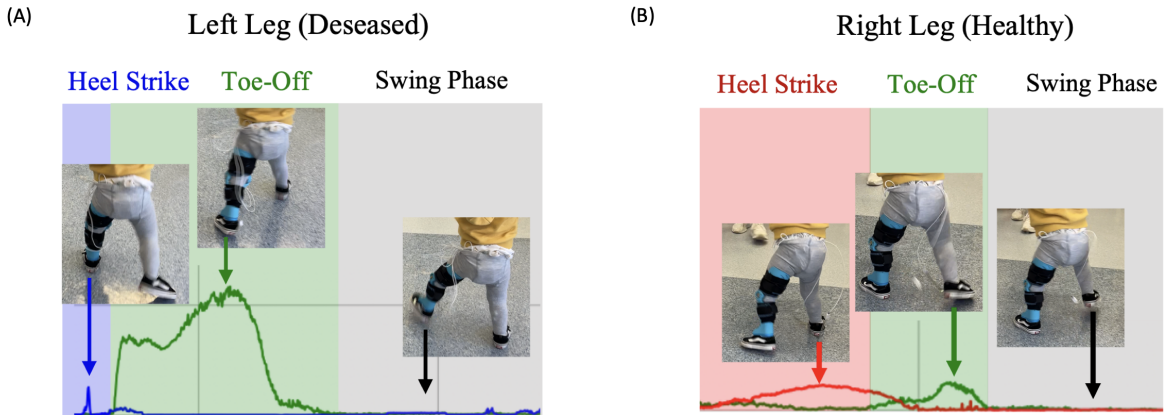


**Figure 6.12:** Gait analysis including heel strike, toe-off, and swing phase of both legs.

indicating stable weight acceptance. Toe-off is sharp and well-defined, suggesting effective propulsion. During the swing phase, the leg unloads completely with minimal force signal, reflecting coordinated movement.

In contrast, the left leg (B), affected by FH, still completes a full gait cycle but with altered dynamics. Heel strike is brief, producing only a small force peak, which indicates limited heel contact and increased forefoot loading. This reduced ground contact is expected, as the leg had not been previously used and corresponds to the early-stage gait features discussed in Section 2.2. Toe-off is broader and longer in duration, pointing to a more effortful push-off, likely due to reduced strength or control. The swing phase begins with a slight delay but is clearly present, showing proper unloading of the leg. Both legs have a longer stance phase of about 60%, matching what's reported in the literature. Overall, this walking pattern of the left leg is less efficient, puts more strain on the muscles, and likely causes the other leg to compensate. This interpretation is further supported by EMG results shown in Figure 6.11, which reveal asymmetrical muscle activation. It is also likely that the right leg, having compensated during early development, exhibits more advanced neuromuscular coordination and stability.

Both graphs show co-contraction in the muscles, which is typical in early motor development and may reflect an effort to stabilize and hold balance. Muscle activation patterns in the right leg were relatively stable, with the GC activating more than the TA, which aligns with literature findings. The relatively higher and more prolonged activation of the GC reflects its central role in propulsion and weight support, and is especially common in toddlers, who rely more on plantarflexors due to ongoing motor development. On the left side, the TA showed higher muscular activity comparatively to the GC. Given that the GC is typically one of the most affected and weakened muscles in cases of FH, it is likely that the TA is compensating for this muscular deficiency during gait.

To enable more meaningful comparisons across gait cycles and between limbs, EMG signals were

normalized in time to a standardized gait cycle length of 100%.

Initially, four cycles of each leg and muscle were plotted and overlaid (Appendix B). FSR sensor signals were used to identify discrete gait cycles based on heel strike and toe-off. For the right leg, the average duration of the four cycles was approximately 1.0 second. For the left leg, cycles were slightly longer and more variable in duration, ranging from 0.83 s to 1.07 s. The more variable cycle timing in the left leg and the shorter stride, can be due to the KFC, which can shorten the length (Sec.2.4.2).

Temporal normalization was used to align all gait cycles in time, allowing a more direct comparison and averaging; each cycle was adjusted to the same number of time steps, for example from 130 and 100 down to a common length. The time points were redistributed evenly across each cycle using downsampling:

$$x_{\text{normalized}}(i) = x \left( \frac{i \cdot L}{M} \right) \quad \text{for } i = 0, 1, \dots, M - 1$$

Where:

- $x(t)$  is the original signal of length  $L$ ,
- $M$  is the target number of steps (e.g. 100),
- $x_{\text{normalized}}(i)$  is the resampled signal.

Following normalization, RMS envelopes were computed from the EMG signals to estimate overall muscle effort. RMS smooths the raw signal and highlights amplitude changes over time:

$$\text{RMS} = \sqrt{\frac{1}{N} \sum_{i=1}^N x_i^2}$$

Where:

- $x_i$  is the  $i$ -th data point of the EMG signal,
- $N$  is the number of samples in the moving window.

To assess variability between cycles, standard deviation was also calculated across the normalized and averaged signals:

$$\sigma = \sqrt{\frac{1}{N} \sum_{i=1}^N (x_i - \mu)^2}$$

Where:

- $\mu$  is the mean activation across cycles at a given time point,

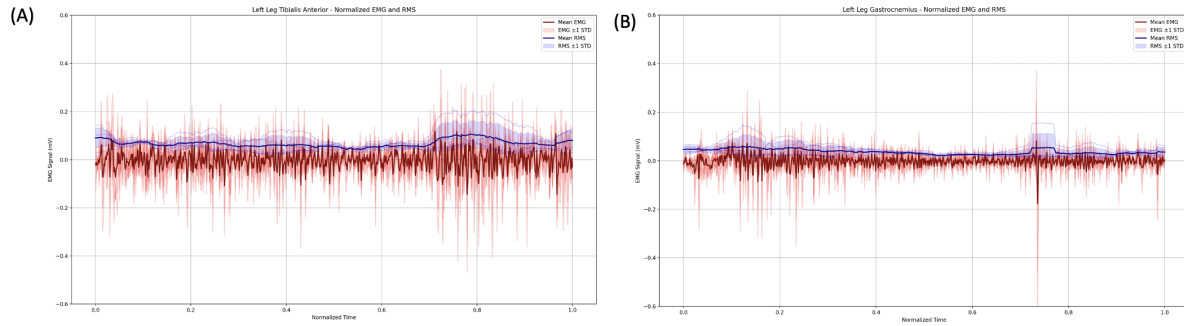


**Figure 6.13:** Temporally normalized surface of left leg.

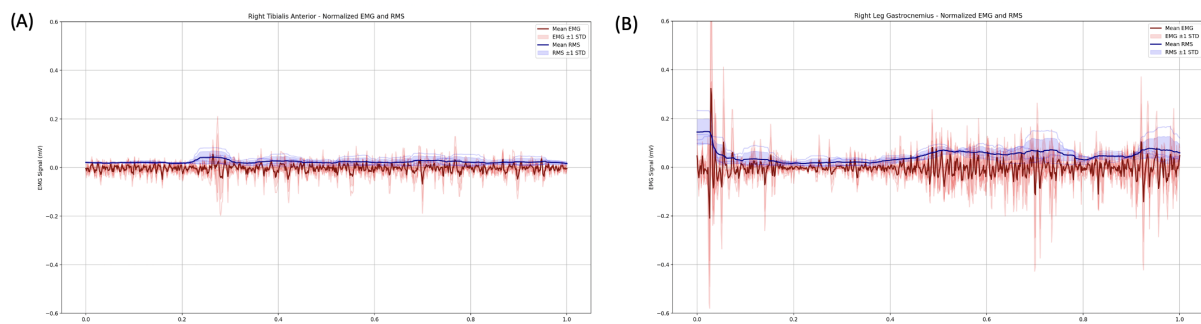
- $x_i$  are the values from individual cycles.

Figure 6.14 presents the temporally normalized EMG and RMS activity for the TA and GC muscles in both legs, averaged over four gait cycles. Shaded areas represent  $\pm 1$  standard deviation across cycles.

On the healthy right leg, both TA and GC displayed clear, phase-specific activation. The TA showed a distinct peak around initial contact and early swing, facilitating foot clearance, while the GC was strongly active during late stance and toe-off, reflecting effective push-off mechanics. The low standard deviation highlights consistent recruitment across cycles.

By contrast, the affected left leg showed broader, flatter RMS curves, particularly in the TA, with elevated EMG amplitudes and greater inter-cycle variability (Fig. 6.13). This pattern suggests compensatory overactivation and reduced phasic separation. The GC on the left leg exhibited minimal engagement and a near-flat RMS profile, indicating weak plantarflexion contribution. This imbalance suggests poor intermuscular coordination and underutilization of the posterior chain.

Together, these results reinforce earlier findings from raw and cycle-specific EMG analysis: the orthoprosthetic leg operates with greater muscular effort and reduced efficiency. The simultaneous activation of TA and GC on the left reflects immature motor control strategies such as co-contraction, however, the presence of coordinated muscle activity suggests that neuromuscular pathways remain intact. With



**Figure 6.14:** Temporally normalized surface of right leg.

continued orthotic use, therapy, and gait training, there is a strong foundation for improving control, efficiency, and gait symmetry over time.

## 6.3 Discussion

The findings herein described demonstrated that the 3D-printed orthoprosthetic was functionally effective and immediately usable upon initial application. The child was able to walk independently using the first working prototype, which provided adequate support for standing, balance, and weight-bearing. Despite evident motor asymmetries, distinct gait phases, including heel strike, stance, and toe-off, were observed in both limbs. Although the prosthetic knee joint was not fully engaged during walking, it contributed significantly to transitional movements, such as rising from the floor after a fall. This showed a potential for neuromuscular activation associated with prosthetic use, even during ambulation.

While there was no previous evidence found in literature on whether a leg affected by FH had any muscle function at all, the EMG analysis herein described showed that both the TA and GC were active on the affected leg. This muscular activity suggests that an amputation is not needed at this point. The TA was more active than usual and not clearly linked to gait phases, which likely means the TA was compensating for the weak GC. Still, both muscles showed a clear pattern, suggesting the nerves and muscles can work together; with more targeted training, the overcompensation may decrease. The child could then develop better control and make greater use of the GC. Also RMS and temporal normalization showed that the muscle activity on the affected leg was more variable, in particular, the TA had a wider and less consistent activation pattern.

CoP and force plate data showed that the child maintained bilateral stance with measurable pressure under both feet, even though the majority of the weight was shifted toward the unaffected limb. The CoP was clustered in the rear-right quadrant, indicating typical early standing posture and also confirming reliance on the healthy side. The prosthetic foot provided a stable platform that allowed partial weight bearing on the affected side, demonstrating its role in promoting postural symmetry and initiating functional balance training.

Despite encouraging outcomes, this evaluation had a few limitations. Only two FSR sensors were available, restricting simultaneous bilateral foot pressure analysis, and EMG channels were minimized for comfort, limiting a wider study across multiple muscle groups. The data reflected the very first steps taken with the device. Longitudinal studies are needed to assess sustained adaptation, motor learning, and functional progress.

The early activation of all measured muscles, including compensatory and coordinated patterns, highlights the neuromuscular potential of the affected limb. With structured gait training, the child is expected to improve control over the prosthetic knee and shift more weight onto the orthotic leg. While long-term

outcomes remain unknown, these first observations provide a strong foundation for continued development, clinical confidence, and future optimization of low-cost, individualized pediatric orthoprostheses.

# 7

## Conclusion

### Contents

---

7.1 Summary .....	74
7.2 Regulatory Outlook .....	75
7.3 Future Work .....	75

---

This chapter summarizes how the developed 3D-printed orthoprostheses met all project objectives by enabling walking, maintaining structural stability, and supporting muscle use in the affected leg (Sec.7.1). It also outlines regulatory considerations (Sec.7.2) and presents future research directions toward an adaptive pediatric exoskeleton with embedded sensing and feedback systems (Sec.7.3).

## 7.1 Summary

This project addresses a gap in pediatric assistive technology, where most existing studies focus on older children or rely on rigid, non-modular systems. The present findings contribute with novel clinical and technical evidence supporting the use of fully 3D-printed, modular orthoprosthetic solutions for toddlers with congenital limb differences.

The three objectives of this study mentioned in Section 1.3 could all be answered through the fulfillment of requirements, experimental and observational evaluation of the orthoprostheses.

First, the study confirmed that a low-cost, 3D-printed orthoprostheses can be effectively tailored to the anatomical and developmental needs of toddlers with FH. The custom-fitted device enabled immediate unassisted walking, improved postural alignment, and activated key lower limb muscles, indicating that the orthosis met both structural and neuromuscular requirements. Its modular design and digital fabrication approach ensured individualized fit while remaining lightweight, affordable, and adaptable.

Table 3.1 compared existing state-of-the-art solutions with the specific needs of toddlers, showing that these can be effectively addressed through a tailored design. The newly developed solution fulfills these general needs, and more specifically, all project-defined requirements and their associated KPIs were fully or partially met, as shown in Figure 5.2. The orthoprostheses combined rigid and flexible components to balance strength with comfort; TPU provided flexibility for the foot sole, while PLA offered sufficient structural support for the frame and knee joint. The device remained stable during early gait trials, including standing, walking, and falling, showing real-world robustness. However, the study also emphasized the importance of continued validation.

Third, results showed that the 3D-printed device significantly improved postural alignment and functional mobility in a toddler with lower limb deficiency. The orthoprostheses corrected leg length discrepancy and pelvic tilt, supported bilateral stance, and allowed active participation of the affected leg during walking. EMG and FSR data confirmed that the prosthetic leg was not passively carried but actively used, with signs of motor learning and neuromuscular coordination; CoP data further indicated partial weight-bearing and postural symmetry improvements.

Importantly, the divergence between simulation predictions and real-world outcomes highlights the need for dynamic validation under real-use conditions. While computational tools are valuable in early design, they must be paired with user-centered testing to ensure safety, comfort, and effectiveness.

The completed device remained functional and structurally intact during a now on going month of testing. All materials used are widely accepted for biomedical prototyping and are considered safe for noninvasive pediatric applications.

In addition, this work successfully explored the potential of AM for lower limb devices. It demonstrates how combining AM with participatory design and rapid prototyping can in the future lead to a scalable, low-cost solution. This integrated approach shows strong promise for improving pediatric orthotic care while particularly avoiding high costs.

## 7.2 Regulatory Outlook

The production of a 3D-printed orthotic leg and prosthetic foot for a pediatric patient in Portugal falls under the European Medical Device Regulation (MDR) (EU 2017/745). <sup>1</sup> As a custom-made medical device, it is regulated under Article 2(3) and Annex XIII of the MDR. These regulations apply to devices made specifically for an individual patient based on a healthcare professional's prescription, rather than for mass production. However, manufacturers must still meet the safety and performance requirements outlined in Annex I of the MDR. A written statement must be provided, confirming compliance with MDR regulations, which must include the device's identification and specifications, the manufacturer's name and address, and confirmation that the device is patient-specific. In addition, a risk analysis must be conducted according to ISO 14971 <sup>2</sup>, identifying potential risks related to the design, materials, and manufacturing process. Manufacturers must also maintain a technical file that documents the design specifications, material details, validation of the 3D-printing process, and records of biocompatibility testing in compliance with ISO 10993. The file must also include instructions for use and patient-specific labeling. Since the device is 3D-printed, the materials must meet ISO 10993 <sup>3</sup> standards for biocompatibility to ensure patient safety, and the printing process must be validated to guarantee consistency and reliability.

## 7.3 Future Work

Building upon the findings and technical foundations of this thesis, the next phase of research will continue in the context of a PhD project. This upcoming work aims to expand the current orthoprosthetic approach into the development of a 3D-printed pediatric exoskeleton equipped with embedded sensors and adaptive control mechanisms. The long-term goal is to support early gait rehabilitation in young children with lower-limb impairments, by creating a system that not only provides structural support but

---

<sup>1</sup>European Union. Medical Device Regulation (EU) 2017/745.

<sup>2</sup>ISO 14971:2019. Medical devices - Application of risk management to medical devices.

<sup>3</sup>ISO 10993-1:2018. Biological evaluation of medical devices-Part 1: Evaluation and testing within a risk management process.

also actively encourages muscle engagement and motor learning. The project will focus on three key research directions that emerged from the limitations and insights of this thesis.

First, the control and mechanical support of the knee joint will be further developed, which includes investigating how to increase joint stability and force transmission, potentially through the use of damping systems. These improvements aim to make the device suitable not only for toddlers but also for older children up to three years old.

Second, the project will address the integration of surface EMG sensors directly into the orthotic structure. The goal is to create a system that is comfortable and unobtrusive for children, while ensuring reliable signal quality. This includes considering factors like sensor placement, heat dissipation, and skin compatibility. Additionally, longitudinal EMG tracking will be implemented to monitor changes in muscle activation over time. The feasibility of mild feedback mechanisms such as vibrotactile or electrical cues will also be explored to promote active engagement of key muscles during gait training. Last, it will be interesting to explore the integration of real-time proprioceptive or tactile feedback to enhance the user's ability to perceive foot position during walking.

Lastly, the scalability and adaptability of the system will be a major focus, aiming to adapt this thesis design for broader pediatric use. The project aims to develop a modular, parametric design framework that allows rapid customization for individual users. Digital tools like 3D-scanning and parametric CAD modeling will be used to streamline clinical adaptation. Furthermore, the potential for remote updates and adjustments will be investigated to support wider clinical use, especially in underserved or low-resource environments.

Together, these research directions aim to answer the overarching question: "how can assistive technology be designed to enable safe, independent walking and early rehabilitation in young children with lower-limb deficiencies?" This project establishes a solid foundation by demonstrating the feasibility and clinical relevance of low-cost, child-specific orthotic solutions. Future developments will build on this groundwork to advance a more intelligent, functional, and scalable system to support pediatric mobility. The expected clinical impact includes improved access to personalized assistive technologies, enhanced rehabilitation outcomes, and greater autonomy for children with mobility impairments.

# Bibliography

- [1] K. E. Adolph and S. R. Robinson, "The road to walking: What learning to walk tells us about development," in *Advances in Child Development and Behavior*, J. Benson, Ed. Academic Press, 2015, vol. 48, pp. 1–40.
- [2] P. M. Navarro, D. Copaci, and D. B. Rojas, "Design and control of a soft knee exoskeleton for pediatric patients at early stages of the walking learning process," *Bioengineering*, vol. 11, no. 2, p. 188, 2024. [Online]. Available: <https://www.mdpi.com/2306-5354/11/2/188>
- [3] S. Tan, M. Ochieng, and L. Ahmed, "Limb reduction defects: Global patterns and trends based on WHO database analysis," *International Journal of Pediatric Research*, vol. 11, no. 1, pp. 12–19, 2023.
- [4] L. M. Hart, T. L. Miller, and T. Craig, "Lower limb loss in children: Epidemiology and health care utilization in the United States," *Physical Medicine and Rehabilitation*, vol. 12, no. 5, pp. 423–430, 2020.
- [5] H. Gerber, D. Cho, and N. Patel, "Neurodevelopmental outcomes and early intervention in children with limb deficiencies," *Developmental Medicine and Child Neurology*, vol. 62, no. 3, pp. 324–331, 2020.
- [6] N. Jones, P. Black, and L. Tran, "Incidence of congenital limb deficiencies: A systematic review," *Journal of Limb Loss Research*, vol. 4, no. 2, pp. 45–56, 2021.
- [7] M. Sarajchi, M. K. Al-Hares, and K. Sirlantzis, "Wearable lower-limb exoskeleton for children with cerebral palsy: A systematic review," *IEEE Transactions on Neural Systems and Rehabilitation Engineering*, 2021.
- [8] C. R. Danilo Calderone, Giuseppe Cesarelli, "3D printing application for orthopedic pediatric surgery – a systematic review," *Rapid Prototyping Journal*, vol. 30, no. 11, pp. 276–288, 2024. [Online]. Available: <https://www.emerald.com/insight/content/doi/10.1108/RPJ-05-2024-0222/full/html>

- [9] W. C. Cheung, H. Meadan, and H.-W. Yang, “Effects of powered mobility device interventions on social skills for children with disabilities: A systematic review,” *Journal of Developmental and Physical Disabilities*, vol. 32, no. 5, pp. 855–876, 2020. [Online]. Available: <https://link.springer.com/article/10.1007/s10882-020-09729-x>
- [10] R. Kosif and R. Kecialan, “Anatomical differences between children and adults,” *International Journal of Scientific Research and Management*, vol. 8, no. 5, pp. MP–2020–355–359, 2020. [Online]. Available: <http://www.ijsr.in>
- [11] S. Apibantaweesakul, S. Omura, W. Qi, H. Shiotani, P. E. Evangelidis, N. Sado, F. Tanaka, and Y. Kawakami, “Characteristics of inhomogeneous lower extremity growth and development in early childhood: a cross-sectional study,” *BMC Pediatrics*, vol. 21, p. 552, 2021. [Online]. Available: <https://doi.org/10.1186/s12887-021-02998-1>
- [12] B. V. Y. Chow, C. Morgan, C. Rae, D. I. Warton, I. Novak, S. Davies, A. Lancaster, G. C. Popovic, R. R. N. Rizzo, C. Y. Rizzo, M. Kyriagis, R. D. Herbert, and B. Bolsterlee, “Human lower leg muscles grow asynchronously,” *Journal of Anatomy*, vol. 244, pp. 476–485, 2024. [Online]. Available: <https://doi.org/10.1111/joa.13967>
- [13] S. Patrick, N. A. Kumar, and P. Hur, “Evaluating knee mechanisms for assistive devices,” *Frontiers in Neurorobotics*, vol. 16, 2022. [Online]. Available: <https://www.frontiersin.org/articles/10.3389/fnbot.2022.790070/full>
- [14] C. Price, J. McClymont, F. Hashmi, S. C. Morrison, and C. Nester, “Development of the infant foot as a load bearing structure: study protocol for a longitudinal evaluation (the small steps study),” *Journal of Foot and Ankle Research*, vol. 11, p. 33, 2018.
- [15] B. Fritz and M. Mauch, *Foot Development in Childhood and Adolescence*. Woodhead Publishing Limited, 2013, ch. 3, pp. 49–71.
- [16] H. Jiang, Q. Mei, Y. Wang, J. He, E. Shao, J. Fernandez, and Y. Gu, “Understanding foot conditions, morphologies and functions in children: a current review,” *Frontiers in Bioengineering and Biotechnology*, vol. 11, p. 1192524, 2023. [Online]. Available: <https://www.frontiersin.org/articles/10.3389/fbioe.2023.1192524/full>
- [17] A. Hallemans, P. Aerts, B. Otten, P. P. D. Deyn, and D. D. Clercq, “Mechanical energy in toddler gait: A trade-off between economy and stability?” *Journal of Experimental Biology*, vol. 207, pp. 2417–2431, 2004.
- [18] N. L. Greer, J. Hamill, and K. R. Campbell, “Ground reaction forces in children’s gait,” *Pediatric Exercise Science*, vol. 1, pp. 45–53, 1989.

- [19] C. N. Burnett and E. W. Johnson, "Development of gait in childhood: Part ii," *Developmental Medicine and Child Neurology*, vol. 13, pp. 207–215, 1971.
- [20] A. D. Kuo, J. M. Donelan, and A. Ruina, "Energetic consequences of walking like an inverted pendulum: Step-to-step transitions," *Exercise and Sport Sciences Reviews*, vol. 33, no. 2, pp. 88–97, 2005. [Online]. Available: [https://journals.lww.com/acsm-essr/Fulltext/2005/04000/Energetic\\_Consequences\\_of\\_Walking\\_Like\\_an.8.aspx](https://journals.lww.com/acsm-essr/Fulltext/2005/04000/Energetic_Consequences_of_Walking_Like_an.8.aspx)
- [21] L. Ye and X. Chen, "Understand human walking through a 2D inverted pendulum model," in *Proc. of the IEEE Int'l Conf. on Humanoid Robots (HUMANOIDS)*, 2018, pp. 340–346. [Online]. Available: <https://ieeexplore.ieee.org/document/8625057>
- [22] B. Bril, G. Dietrich, and D. Corbetta, "Learning to tune the antero-posterior propulsive forces during walking: A necessary skill for mastering upright locomotion in toddlers," *Experimental Brain Research*, vol. 233, pp. 1815–1827, 2015.
- [23] W. Liu *et al.*, "Biomechanical characteristics of the typically developing toddler: A narrative review," *Frontiers in Pediatrics*, vol. 10, p. 8946917, 2022.
- [24] A. P. Shortland, *Gait and Clinical Gait Analysis*. Elsevier, 2020.
- [25] M. A. Smith and T. R. Johnson, "A comparison of kinematic angles in toddler gait across different ages and genders," *Journal of Pediatric Biomechanics*, vol. 15, no. 4, pp. 210–220, 2021.
- [26] C. Williams, J. Kolic, W. Wu, and K. Paterson, "Soft soled footwear has limited impact on toddler gait," *PLoS ONE*, vol. 16, no. 5, p. e0251175, 2021. [Online]. Available: <https://journals.plos.org/plosone/article?id=10.1371/journal.pone.0251175>
- [27] C. Teulier, D.-K. Lee, and B. D. Ulrich, "Early gait development in human infants: Plasticity and clinical applications," *Developmental Psychobiology*, vol. 57, pp. 447–458, 2015.
- [28] W. Samson, A. V. Hamme, G. Desroches, B. Dohin, R. Dumas, and L. Chèze, "Biomechanical maturation of joint dynamics during early childhood: Updated conclusions," *Journal of Biomechanics*, vol. 46, pp. 2258–2263, 2013.
- [29] R. Gupta and A. Akkouch, "Biomechanical analysis of 3D-printed prosthetic feet: Current insights and applications," *Micromachines*, vol. 14, no. 12, p. 2345, 2023.
- [30] D. H. Sutherland, R. A. Olshen, E. N. Biden, and M. P. Wyatt, "The development of mature gait," *The Journal of Bone and Joint Surgery. American Volume*, vol. 70, no. 6, pp. 850–858, 1988.

- [31] L. A. Livingston, J. M. Stevenson, and S. J. Olney, "Stairclimbing kinematics on stairs of differing dimensions," *Archives of Physical Medicine and Rehabilitation*, vol. 72, no. 6, pp. 398–402, May 1991.
- [32] S. A. Butterfield, E. M. Loovis, and J. Lee, "Kicking development by children in grades K–8: A multi-cohort longitudinal study," *Research Quarterly for Exercise and Sport*, vol. 80, no. 2, pp. 247–254, 2009.
- [33] S. Gröble, H. J. A. van Hedel, J. W. Keller, and C. Ammann-Reiffer, "Differences in gait parameters when crossing real versus projected everyday life obstacles in healthy children and adolescents," *Scientific Reports*, vol. 13, no. 7848, 2023. [Online]. Available: <https://doi.org/10.1038/s41598-023-34276-8>
- [34] L. A. Fordham, K. E. Applegate, D. C. Wilkes, and C. J. Chung, "Fibular hemimelia: More than just an absent bone," *Seminars in Musculoskeletal Radiology*, vol. 3, no. 3, pp. 227–238, 1999.
- [35] M. Salimi, R. Sarallah, S. Javanshir, S. P. Mirghaderi, A. Salimi, and S. Khanzadeh, "Complication of lengthening and the role of post-operative care, physical and psychological rehabilitation among fibula hemimelia," *World Journal of Clinical Cases*, vol. 10, no. 24, pp. 8482–8489, 2022.
- [36] M. Lazović, S. S. Leonchuk, S. Ducić, S. A. Imomov, and D. A. Popkov, "Limb lengthening and deformity correction in patients with severe fibular hemimelia: experience of the children's university hospital in belgrade," *Genij Ortopedii*, vol. 30, no. 1, pp. 38–45, 2024.
- [37] C. B. Fuller, C. E. Shannon, and D. Paley, "Lengthening reconstruction surgery for fibular hemimelia: A review," *Children*, vol. 8, no. 6, p. 467, 2021. [Online]. Available: <https://www.mdpi.com/journal/children>
- [38] D. A. Crawford, B. J. Tompkins, G. O. Baird, and P. M. Caskey, "The long-term function of the knee in patients with fibular hemimelia and anterior cruciate ligament deficiency," *The Journal of Bone and Joint Surgery. British Volume*, vol. 94-B, pp. 328–333, 2012.
- [39] D. Figueroa, R. Calvo, I. E. Villalón, A. Schmidt-Hebbel, F. Figueroa, and A. Baar, "Single time angular deformity correction and treatment of knee instability in congenital fibular hemimelia: A case report," *The Knee*, vol. 19, pp. 504–507, 2012.
- [40] E. H. S. Pantzar-Castilla, P. Wretenberg, and J. Riad, "Knee flexion contracture impacts functional mobility in children with cerebral palsy with various degrees of involvement: A cross-sectional register study of 2,838 individuals," *Acta Orthopaedica*, vol. 92, pp. 472–478, 2021.
- [41] A. V. Campenhout and L. Bar-On, "Knee contracture in children with cerebral palsy: Association with muscle lengths," *Developmental Medicine & Child Neurology*, vol. 60, no. 4, pp. 391–396, 2018.

- [42] H. I. Balci, M. Kocaoglu, L. Eralp, and F. E. Bilen, "Knee flexion contracture in haemophilia: Treatment with circular external fixator," *Haemophilia*, vol. 20, pp. 879–883, 2014.
- [43] Y. Huang, M. C. Leu, J. Mazumder, and M. A. Donmez, "Additive manufacturing: current state, future potential, gaps and needs, and recommendations," *Journal of Manufacturing Science and Engineering*, vol. 137, no. 1, p. 014001, 2015.
- [44] O. Abdulhameed, M. J. Ghazali, N. S. Ahmad, and M. F. Arif, "Additive manufacturing: Challenges, trends, and applications," *Advances in Mechanical Engineering*, vol. 11, no. 2, p. 1687814018822880, 2019.
- [45] A. Verma, P. Vishnoi, V. Sukhotskiy, and E. P. Furlani, "Numerical simulation of extrusion additive manufacturing: Fused deposition modeling," in *TechConnect Briefs 2018*. TechConnect, 2018, pp. 118–121.
- [46] T. J. Gordelier, P. R. Thies, L. Turner, and L. Johanning, "Optimising the fdm additive manufacturing process to achieve maximum tensile strength: a state-of-the-art review," *Rapid Prototyping Journal*, vol. 25, no. 6, pp. 953–971, 2019.
- [47] S. Alqahtani, A. Alwaked, and G. Tosello, "A review of multi-material additive manufacturing: Progress, challenges, and applications," *Additive Manufacturing*, vol. 28, pp. 167–191, 2019.
- [48] C. Barrios, G. Romero, G. Smit, and A. A. Zadpoor, "Advances in additive manufacturing for biomedical applications: A review on materials, processes, and scaffolds," *Materials*, vol. 13, no. 20, p. 4563, 2020.
- [49] L. Beníček, M. Vašina, and P. Hrbáček, "Influence of 3D printing conditions on physical–mechanical properties of polymer materials," *Polymers*, vol. 17, no. 1, p. 43, 2025. [Online]. Available: <https://www.mdpi.com/2073-4360/17/1/43>
- [50] J. Rybarczyk, F. Górska, W. Kuczko, R. Wichniarek, S. Siwiec, N. Vitkovic, and R. Păcurar, "Mechanical properties of carbon fiber reinforced materials for 3D printing of ankle foot orthoses," *Advances in Science and Technology Research Journal*, vol. 18, no. 4, pp. 191–215, 2024. [Online]. Available: <https://doi.org/10.12913/22998624/188819>
- [51] P. Steck, D. Scherb, C. Witzgall, J. Miehling, and S. Wartzack, "Design and additive manufacturing of a passive ankle–foot orthosis incorporating material characterization for fiber-reinforced PETG-CF15," *Materials*, vol. 16, no. 9, p. 3503, 2023. [Online]. Available: <https://www.mdpi.com/1996-1944/16/9/3503>

- [52] M. Pastorino, F. Galli, L. Gastaldi, and M. Vidoni, “Numerical and experimental mechanical analysis of additively manufactured ankle–foot orthoses,” *Applied Sciences*, vol. 12, no. 17, p. 8650, 2022. [Online]. Available: <https://www.mdpi.com/2076-3417/12/17/8650>
- [53] S. H. Mian, E. Abouel Nasr, K. Moiduddin, M. Saleh, and H. Alkhalefah, “An insight into the characteristics of 3D printed polymer materials for orthoses applications: Experimental study,” *Polymers*, vol. 16, no. 3, p. 403, 2024.
- [54] M. Daly, M. Tarfaoui, M. Bouali, and A. Bendarma, “Effects of infill density and pattern on the tensile mechanical behavior of 3D-printed glycolized polyethylene terephthalate reinforced with carbon-fiber composites by the FDM process,” *Journal of Composites Science*, vol. 8, no. 4, p. 115, 2024. [Online]. Available: <https://www.mdpi.com/2504-477X/8/4/115>
- [55] R. Shergill *et al.*, “Impact of printing parameters on tensile properties of PLA and PETG,” *Materials*, vol. 16, no. 11, p. 4820, 2023.
- [56] S. Rubashevskyi *et al.*, “Layer height effects on mechanical behavior of PLA composites,” *Materials Science Forum*, vol. 1052, pp. 123–131, 2022.
- [57] H. Gonabadi *et al.*, “Effects of layer parameters on tensile strength of PLA,” *Journal of Manufacturing Processes*, vol. 58, pp. 839–848, 2020.
- [58] J. Chacón *et al.*, “Additive manufacturing of PLA: Study of mechanical properties and printing parameters,” *Composites Part B*, vol. 124, pp. 143–152, 2017.
- [59] R. Hasan *et al.*, “Evaluation of infill density and layer thickness effects on PLA performance,” *International Journal of Advanced Manufacturing Technology*, vol. 124, pp. 4011–4020, 2024.
- [60] E. Abdelghany and et al., “An insight into the characteristics of 3D printed polymer materials for orthoses applications,” *Polymers*, vol. 16, no. 8, p. 2553, 2024.
- [61] A. Hund and et al., “3d-printed orthosis for paediatric lower limb deformities correction,” in *Proc. of the Int'l Conf. on Additive Manufacturing for Medical Applications*, 2022, pDF available via institutional repository.
- [62] S. Kim and et al., “Development and evaluation of 3D printed ankle-foot orthosis for pediatric patients,” *Journal of Prosthetics and Orthotics*, vol. 34, no. 1, pp. 10–17, 2022.
- [63] M. Pitt, “Update in electromyography,” *Current Opinion in Pediatrics*, vol. 25, no. 6, pp. 676–681, 2013.
- [64] Y. Wu, M. Á. M. Martínez, and P. O. Balaguer, *Overview of the Application of EMG Recording in the Diagnosis and Approach of Neurological Disorders*. InTechOpen, 2013.

- [65] Y. Yao, D. Shao, M. Tarabini, S. A. Moezi, K. Li, and P. Saccomandi, "Advancements in sensor technologies and control strategies for lower-limb rehabilitation exoskeletons: A comprehensive review," *Micromachines*, vol. 15, no. 4, p. 489, 2024.
- [66] Y. K. Kim, H. J. Kwon, and Y. T. Kim, "Flexible and wearable pressure sensors for smart human-machine interfaces," *Micromachines*, vol. 9, no. 11, p. 573, 2018.
- [67] G. S. Lakshmi and H. R., "Calibration of force sensitive resistor used in force controlled grippers," *International Journal of Engineering Research & Technology (IJERT)*, vol. 9, no. 8, pp. 356–360, 2020. [Online]. Available: <https://www.ijert.org/calibration-of-force-sensitive-resistor-used-in-force-controlled-grippers>
- [68] B. T. Smith, D. J. Coiro, R. Finson, R. R. Betz, and J. McCarthy, "Evaluation of force-sensing resistors for gait event detection to trigger electrical stimulation to improve walking in the child with cerebral palsy," *IEEE Transactions on Neural Systems and Rehabilitation Engineering*, vol. 10, no. 1, pp. 22–29, 2002.
- [69] Össur, "Össur - prosthetics & orthotics," 2025, accessed: 2025-01-14. [Online]. Available: <https://www.ossur.com/de-de>
- [70] F. Paradisi, A. S. Delussu, S. Brunelli, M. Iosa, R. Pellegrini, D. Zenardi, and M. Traballesi, "The conventional non-articulated sach or a multiaxial prosthetic foot for hypomobile transtibial amputees? a clinical comparison on mobility, balance, and quality of life," *The Scientific World Journal*, vol. 2015, pp. 1–10, 2015. [Online]. Available: <https://doi.org/10.1155/2015/261801>
- [71] E. Lathouwers, T. Ampe, M. A. Díaz, R. Meeusen, and K. D. Pauw, "Evaluation of an articulated passive ankle-foot prosthesis," *BioMedical Engineering OnLine*, vol. 21, p. 28, 2022. [Online]. Available: <https://doi.org/10.1186/s12938-022-00997-6>
- [72] Ottobock, "Ottobock - prosthetics & orthotics solutions," 2025, accessed: 2025-01-14. [Online]. Available: <https://www.ottobock.com/de-de/startseite>
- [73] P. Taboga and A. M. Grabowski, "Axial and torsional stiffness of pediatric prosthetic feet," *Clinical Biomechanics*, vol. 42, pp. 47–54, 2017. [Online]. Available: <https://doi.org/10.1016/j.clinbiomech.2017.01.005>
- [74] P. Yeung and K. Subburaj, "Patient-specific design and fabrication of ankle-foot orthosis using hybrid additive manufacturing," *3D Printing in Medicine*, vol. 8, no. 1, pp. 1–12, 2022.
- [75] L. Wojciechowski and S. Yates, "Replication and redesign of ankle-foot orthoses using 3D printing for pediatric patients with Charcot-Marie-Tooth disease," *Journal of Pediatric Orthotics*, vol. 15, pp. 12–24, 2022.

- [76] S. Rochlitz and L. Pammer, "Design and optimization of a low-cost 3D printed prosthetic foot based on ESAR principles," in *Procs. of the 3D Printing for Prosthetics Conf.*, 2017.
- [77] Y. A. Thammakornsuksiri and M. N. Algabri, "The efficacy of ortho-prosthesis and knee ankle foot orthosis on functional gait activities in pediatric congenital limb deficiency: A case report," *Journal of Pediatric Orthotics*, 2023. [Online]. Available: <https://www.researchgate.net/publication/374506746>
- [78] M. N. Ahmad, M. R. Ishak, M. Z. Zulkafle *et al.*, "The effect of Fused Deposition Modeling parameters (FDM) on the mechanical properties of Polylactic Acid (PLA) printed parts," *Journal of Advanced Research in Applied Mechanics*, vol. 123, no. 1, pp. 238–246, 2024.
- [79] H. Chokshi, D. B. Shah, K. M. Patel, and S. J. Joshi, "Experimental investigations of process parameters on mechanical properties for PLA during processing in FDM," *Advances in Materials and Processing Technologies*, vol. 8, no. sup2, pp. 696–709, 2021.
- [80] T. J. Coogan and D. O. Kazmer, "Infill effects in 3D printed parts under tensile and impact loads," *Additive Manufacturing*, vol. 16, pp. 172–179, 2017.
- [81] M. S. Chaudhry and A. Czekanski, "Evaluating FDM process parameter sensitive mechanical performance of elastomers at various strain rates of loading," *Materials*, vol. 13, no. 14, p. 3202, 2020.
- [82] F. Miller, J. Slade, R. Montgomery, G. Lipton, and R. Marks, "Weight distribution of below-knee amputee and able-bodied children during standing," *IEEE Transactions on Rehabilitation Engineering*, vol. 3, no. 4, pp. 366–370, 1995.
- [83] L. Brady, K. R. Kaufman, L. Vrbos, D. Fish, and D. Levinson, "Standing pressure distribution for normal and below-knee amputee children," *Journal of Prosthetics and Orthotics*, vol. 1, no. 3, pp. 152–157, 1989. [Online]. Available: [https://www.oandplibrary.org/poi/pdf/1989\\_03\\_152.pdf](https://www.oandplibrary.org/poi/pdf/1989_03_152.pdf)
- [84] E. Pourreza, S. Jalali, S. Ostadabbas, A. Aguiar, D. Barone, F. Silva, I. da Cunha, V. Zatsiorsky, and M. Latash, "Spatiotemporal evolution of toddlers' regional foot pressure distribution and center of pressure at antero-posterior axis during learning of standing," *Journal of Biomechanical Engineering*, vol. 146, no. 1, p. 011001, 2024.

# A

## Preliminary Design Attempts

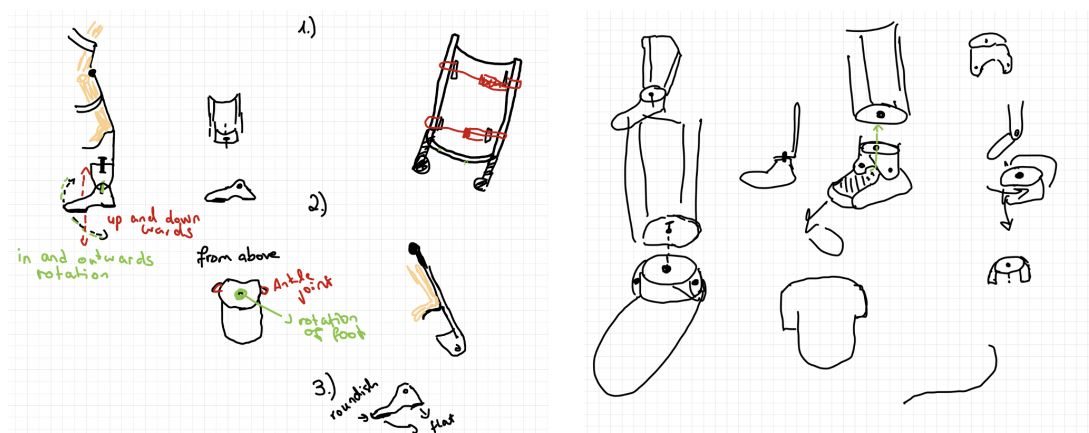


**Figure A.1:** Preliminary ideas.

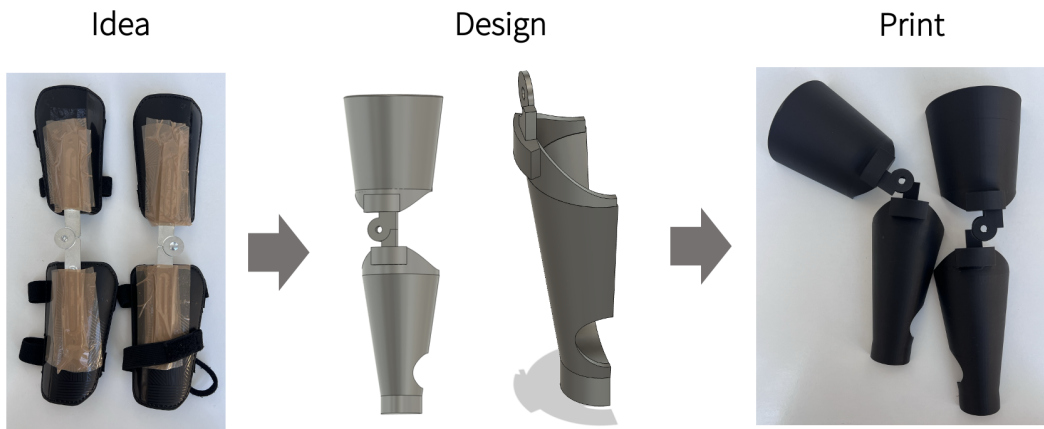


**Figure A.2:** Preliminary shell design.

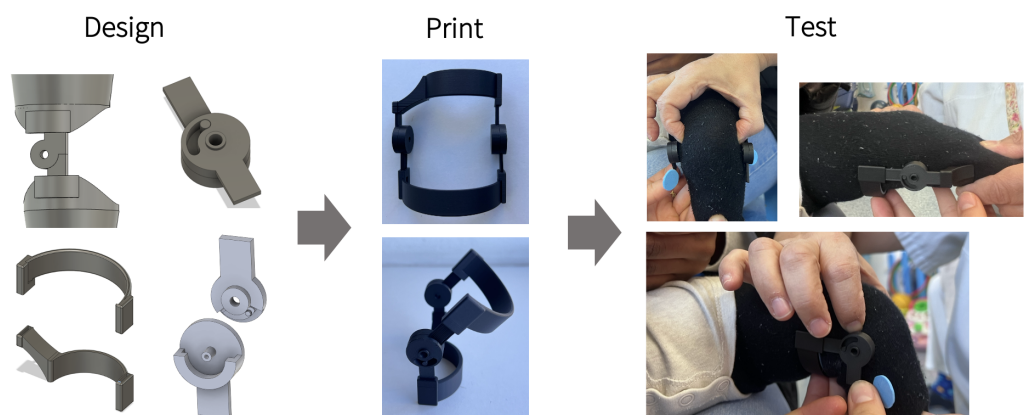


**Figure A.3:** Preliminary knee design.

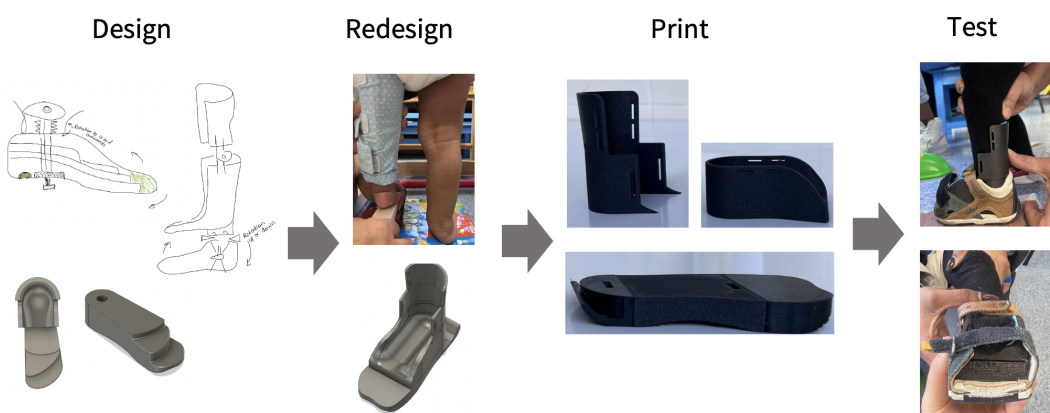


**Figure A.4:** Preliminary foot design.

**Table A.1:** Key parameters across prototypes.

#### Knee Joint

Prototype	Thickness	Circumference	Middle Hole	Stop Pin	Side Hole	Print Direction
PT1	4 mm	20 mm	4 mm	3 mm	3.5 mm	Vertical
PT2	5 mm	23 mm	6 mm	3.5 mm	3.5 mm	Vertical
PT3	5 mm	25 mm	5.2 mm	4 mm	4.1 mm	45° angled
PT4	5 mm	25 mm	5.2 mm	4 mm	4.1 mm	Asym. 45°
PT5	5 mm	30 mm	5.2 mm	4 mm	4.1 mm	45° angled
PT6	8 mm	32 mm	5.2 mm	4.1 mm	4.1 mm	Prioritized

#### Velcro Straps

Prototype	Strap Size	Openings Lower	Openings Upper
PT1	1.5 cm	3	2
PT2	1.5 cm	4	2
PT3	2.5 cm, 1 cm	2 + 1	3
PT4	2.5 cm	2	3
PT5	5 cm + 1.5 cm	1 + 1	1
PT6	5 cm, 2.5 cm	1 + 1	1 + 1

#### Shells

Prototypes	Wall Thickness
PT1–PT6	3 mm



# B

## Clinical Evaluation

---

<sup>0</sup>Electrode placement guidelines based on SENIAM recommendations: <http://www.seniam.org/>

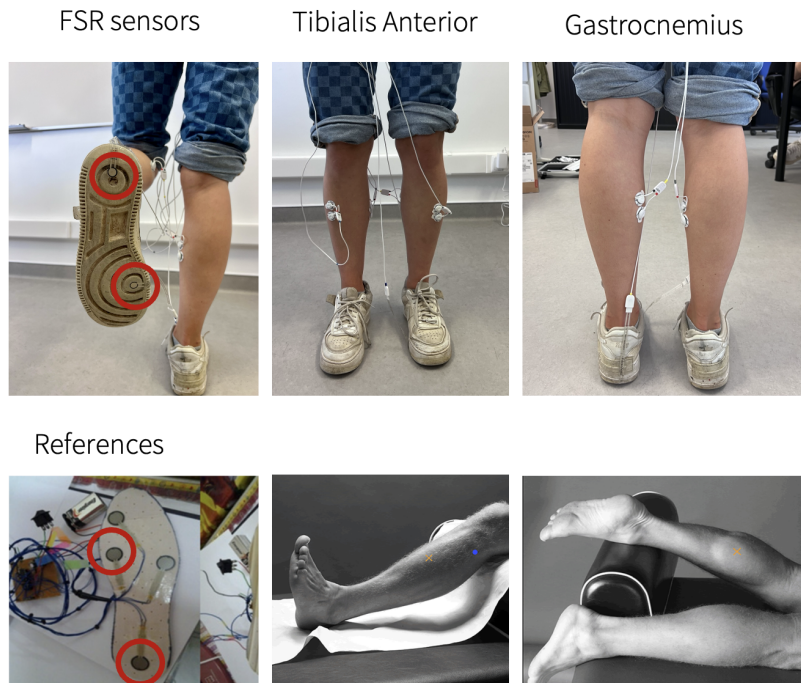


**Figure B.1:** Sensor placement on subject's own legs

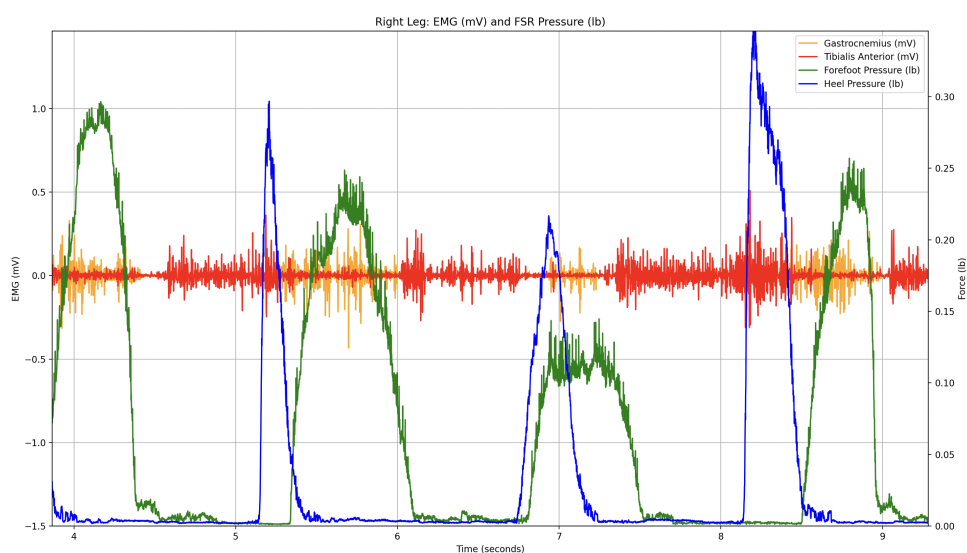


**Figure B.2:** Preliminary analysis of EMG activity and foot pressure (FSR) data recorded from the subject's own leg during gait.

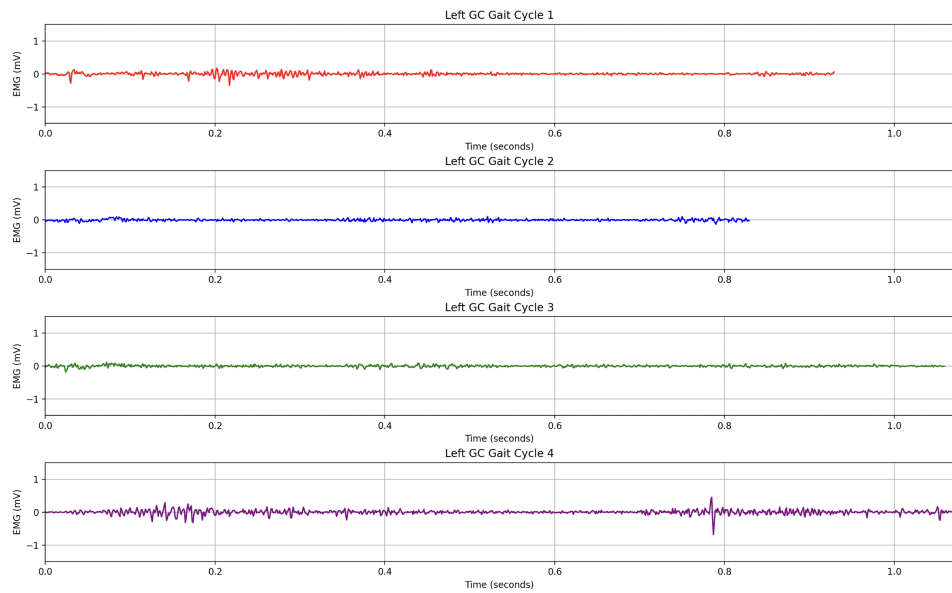


**Figure B.3:** Four cycles of the GC left leg.

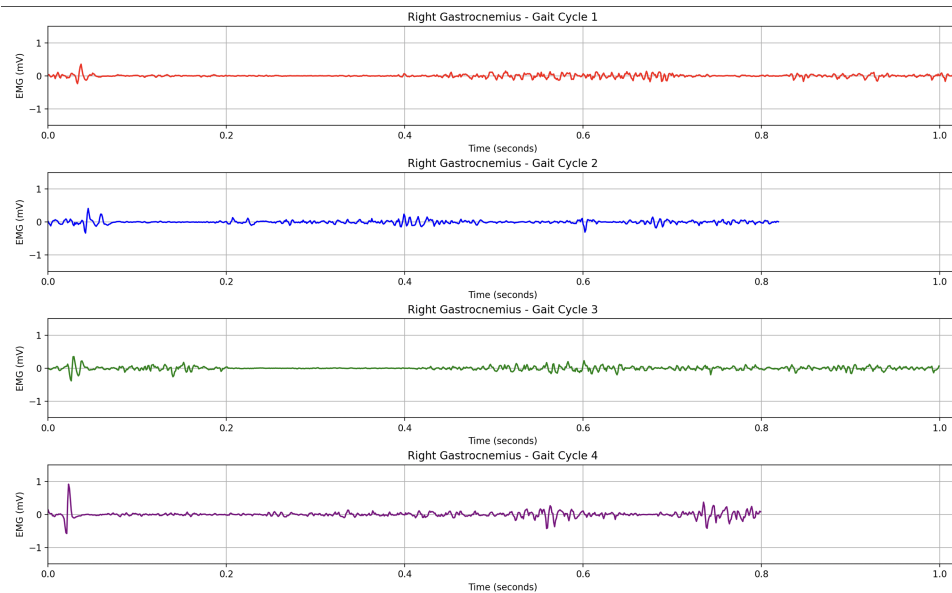


**Figure B.4:** Four cycles of the GC right leg.

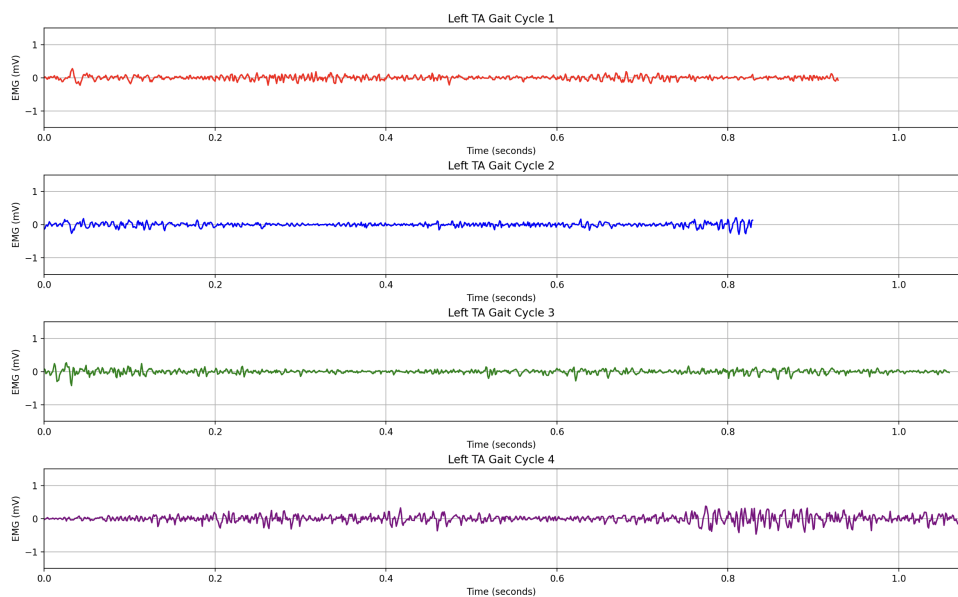


**Figure B.5:** Four cycles of the TA left leg.

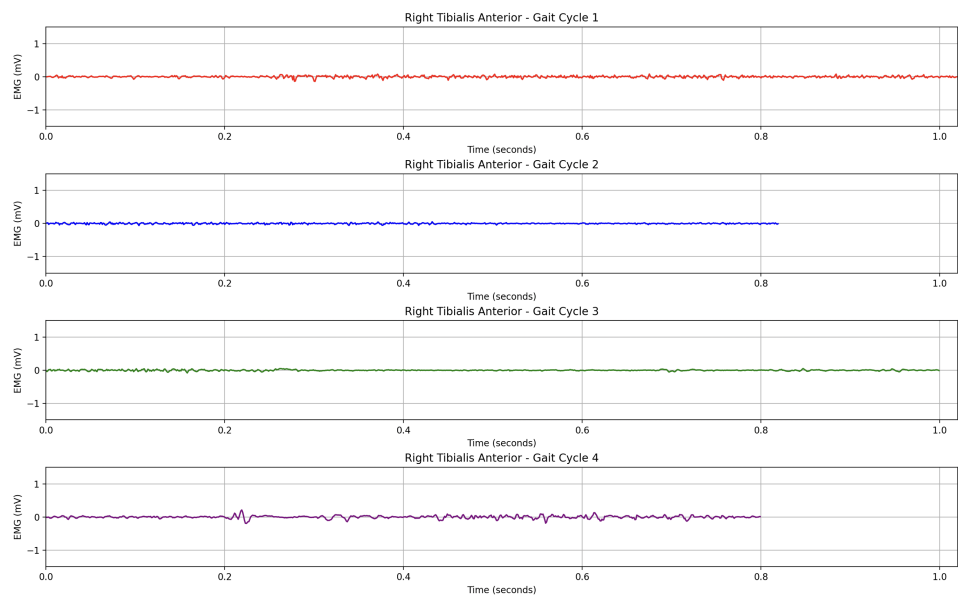


**Figure B.6:** Four cycles of the TA right leg.

